NUREG/CR-3936
SAND84-1122
R4
Printed October 1984

RELAP5 Assessment: Conclusions and User Guidelines

L. N. Kmetyk

Prepared by
Sandia National Laboratories
Albuquerque, New Mexico 87185 and Livermore, California 94550
for the United States Department of Energy
under Contract DE-AC04-76DP00789

Prepared for
U. S. NUCLEAR REGULATORY COMMISSION

Available from

GPO Sales Program
Division of Technical Information and Document Control
U.S. Nuclear Regulatory Commission
Washington, D.C. 20555

and

National Technical Information Service
Springfield, Virginia 22161

NUREG/CR-3936
SAND84-1122
R4

RELAP5 ASSESSMENT: CONCLUSIONS AND USER GUIDELINES

L. N. Kmetyk

Date Published: October 1984

Sandia National Laboratories
Albuquerque, NM 87185
Operated by
Sandia Corporation
for the
U. S. Department of Energy

Prepared for
Reactor Systems Research Branch
Division of Accident Evaluation
Office of Nuclear Regulatory Research
U. S. Nuclear Regulatory Commission
Washington, DC 20555
Under Memorandum of Understanding DOE 40-550-75
NRC FIN No. A-1205

ABSTRACT

The RELAP5 independent assessment project at Sandia National Laboratories is part of an overall effort funded by the NRC to determine the ability of various systems codes to predict the detailed thermal/hydraulic response of LWRs during accident and off-normal conditions. The RELAP5/MOD1 code has been assessed at Sandia against a variety of test data from both integral and separate effects test facilities. All these analyses have been documented in detail in individual topical reports; in this paper we attempt to evaluate the overall code performance by comparing results from many different calculations, and to offer other users some guidelines based on our experience to date.

All results show that good primary side steady state initial and/or operating conditions are readily obtained, given adequate facility descriptions and some user experience or guidelines, although problems are usually encountered in the steam generator secondary sides.

Results from a large number of integral test analyses show that the primary system response (e.g., pressure and break flow) is well-predicted in a wide variety of transients; most observed discrepancies can be attributed to known problems already being addressed by the code developers. Core heatup response (e.g., dryout and PCT) is generally also well-predicted, particularly during the blowdown phase of large break LOCAs. Given the lack of specific reflood algorithms in MOD1, it is not surprising that core quench is sometimes not calculated accurately; we have, however, seen a number of problems with the accumulator injection which would preclude calculating reflood correctly even when such a reflood package is implemented in later versions of RELAP5. The secondary system response (e.g., steam generator pressure and temperatures) is usually not correctly calculated in either integral or separate effects test analyses.

Several classes of unphysical oscillations (in temperature, mass flow and pressure) have been found that can often be eliminated by reducing the time step used, illustrating the inadequacy of the code time step control algorithm, and the quantum nature of the allowed time step in the code algorithm has been seen to result in inefficient run times. A number of MOD1 analyses indicate that calculated two-phase natural circulation flow rates are always high (although calculated subcooled natural circulation rates are in very good agreement with data), and that code mass and energy conservation problems can be encountered through improper user modelling of bypass and leakage flow paths. Both these last items are being addressed in new or altered code models for future versions of RELAP5.

The MOD1 code is not readily portable to computers other than the CYBER-176 on which it was originally developed, and significant amounts of programming time and effort are needed for any desired conversion. We have also found a number of errors and/or omissions in the code documentation which have not been corrected to date.

TABLE OF CONTENTS

Page

LIST OF FIGURES

Page

Page

Page

LIST OF TABLES

ACKNOWLEDGMENTS

I would like to express my appreciation to all the Sandia staff involved in the RELAP5 assessment project during its two-year extent, especially the following individuals:

-- Sam Thompson, Rupe Byers, John Orman, Randy Summers, Mike McGlaun, Channy Wong and Andy Peterson for doing many of the various calculations required,

-- John Orman for modifying and maintaining RELAP5/MOD1 on the Sandia computer system,

-- Katherine McFadden and Millie Elrick for both general graphics support and many individual plots used herein,

-- John Orman and Larry Buxton for contributing the appendix on code portability,

-- Jan Frey for the formal report assembly,

-- Larry Buxton, Rupe Byers and Randy Summers for constant and useful feedback during the preparation of this text,

-- Mr. R. A. Turner of Babcock and Wilcox for graciously releasing their OTSG data for inclusion in this report, and

-- BMFT for kindly allowing us to use their previously proprietary LOBI test data.

1.0 INTRODUCTION

Independent assessment of NRC-sponsored advanced best-estimate codes is underway at four national laboratories: Sandia National Laboratories in Albuquerque (SNLA), Los Alamos National Laboratory (LANL), Idaho National Engineering Laboratory (INEL) and Brookhaven National Laboratory (BNL). This assessment is performed in three ways:

-- a quantitative assessment, whereby the uncertainties in calculating selected key parameters are determined,

-- a phenomenological assessment through analyses of separate effects and other basic tests, whereby the capabilities of the code to predict details of two-phase flow phenomena are addressed, and

-- a qualitative assessment, whereby the overall predictive capabilities of the code are evaluated.

This report summarizes the results of the RELAP5/MOD1 independent assessment project at SNLA, concentrating primarily on the third assessment mode listed.

1.1 RELAP5 Code Evolution

RELAP5/MOD1 [1] is the latest formally released and documented code in the RELAP series developed at INEL for light water reactor safety analysis. RELAP5 is designed to be a generic code that can be used for simulation of a wide variety of hydraulic and thermal transients in both nuclear and non-nuclear systems involving steam-water-noncondensible fluid mixtures.

The RELAP5 code is based on a nonhomogeneous and non-equilibrium model for two-phase systems solved by a semi-implicit numerical scheme. The code contains many generic component models from which general systems can be modelled, such as pumps, valves, pipes, steam separators, heat structures, reactor point kinetics, electric heaters, accumulators and control system components; in addition, special process models are included for effects such as form losses and flow at abrupt area changes, branches, choked flow, boron tracking and noncondensible gases.

MOD1 represents a major revision of RELAP5/MOD0 [2], which was a pressurized water reactor (PWR) blowdown code. The MOD1 version extends the MOD0 applicabilities by including models unique to small break situations (such as stratified flow) and

by adding capabilities for modelling accumulators, noncondensible gas, nucleonics, control systems, steam separators and boron concentrations; the MOD1 code also contains improvements in the flow regime maps, choked flow models, code execution speed and output edits.

According to the current INEL program, only error correction is planned for MOD1, while major developmental efforts are being directed toward RELAP5/MOD2. An interim version of MOD2 (MOD1.5 [3]) has been created for use by the NRC and its contractors. New MOD1.5 models include reflood modelling (with nonequilibrium heat transfer, diabatic vapor generation, and both two-dimensional conduction and an axial conduction fine-mesh rezoning technique) and a jet mixer component (for modelling jet pumps, momentum transfer at ECC injection points and aspirators in once-through steam generators). Improvements in MOD1.5 to existing MOD1 models include a revised interfacial drag formulation, modifications to the heat transfer package, a more mechanistic steam separator model (with carryover and carryunder effects), the addition of boron feedback to the kinetics model and extensions to the horizontal stratified flow models for points of abrupt area changes (to model the connection of a smaller pipe at the top or bottom of a large pipe in addition to a concentric connection). The existence of such new and improved models in later versions of a code must be kept in mind during any code assessment.

1.2 Sandia Assessment Matrix

The RELAP5/MOD1 code is being assessed at SNLA against experimental data from various separate effects and integral effects test facilities, listed in Table 1.1. The MOD1 version used in our FY82 assessment project [4,5,6,7] was cycle 14, the latest publicly released version available at the time this project was begun. Cycle 18 with some additional recommended updates (most of which were later released as part of cycle 19) was used in FY82 to determine if problems found with cycle 14 had already been found and corrected by INEL, and was used as the MOD1 assessment code for calculations started during FY83. [8,9,10,11] The FY83 project completes the RELAP5/MOD1 assessment at Sandia.

Results from our MOD1 analyses are described in detail in topical reports. Completed analyses include:

-- three LOBI large break tests [12],
-- a PKL natural circulation test series [13],
-- a FLECHT SEASET steam generator separate effects test [14],
-- four Semiscale Mod-3 small break tests [15],
-- a LOFT turbine trip operational transient L6-7/L9-2 [16],

-- a LOFT loss-of-feedwater with recovery transient L9-1/L3-3 [17],
-- a LOFT small break test L3-6/L8-1 [18],
-- two LOFT intermediate break tests L5-1 and L8-2 [19],
-- two Semiscale Mod-2A steady state natural circulation tests [20],
-- B&W OTSG steady state and transient loss-of-feedwater tests [21],
-- a LOFT large break test L2-5 [22],
-- three Semiscale Mod-2A degraded heat transfer and transient natural circulation tests [23],
-- five Semiscale Mod-2A small break tests evaluating UHI [24],
-- two BCL ECC bypass/delivery tests [25], and
-- a UHI PWR plant analysis [26].

These analyses allow us to draw a number of conclusions about the code's performance, both individually and (perhaps more importantly) by comparison of code behavior in a wide variety of transients in a number of different facilities.

1.3 Nodalization Development

All of the nodalizations required for our RELAP5 assessment project were developed at Sandia, from original sources (e.g., facility descriptions, modelling workshop handouts, actual blueprints) whenever feasible. The exact configuration of any given input model is described in the topical report on the associated analysis, but the motivations and methodology were common to all the nodalizations being developed, facilitating comparisons for code assessment purposes.

We developed one basic nodalization for each facility, regardless of the number or variety of tests to be analyzed. Although various break assemblies, relief valves, etc. had to be added or modified to fully describe particular transients, the basic vessel, piping and steam generator modelling were seldom changed for individual transient calculations. As a consequence, every effort was made to include all known and potentially important features (e.g., bypass flow paths and structural metal mass) in the baseline nodalizations. The vessel was usually finely noded, particularly in the core to resolve the axial power gradient. The steam generator secondaries were also finely noded with the secondary sides from downcomer to steam separator and steam dome being carefully modelled. Through these relatively detailed nodalizations (~200 cells per model), we hoped to ensure reliable results for the various assessment analyses, without being forced to perform the costly nodalization sensitivity studies required to validate coarser models.

1.4 Report Outline

This report summarizes the conclusions we have drawn and suggests guidelines on future code development and use. The guidelines and conclusions are closely coupled: if we concluded that the code gave good results under certain conditions with particular modelling assumptions, the guideline would be to expect similar good results in future plant applications with similar models; if we found problems with a given model or method, the guideline would be to not do it that way.

Our evaluation of the code performance is divided into sections meant to allow easy application to planned plant analyses. Section 2 discusses steady state calculations, either to match experimental initial conditions or plant nominal operating conditions, for both primary and secondary systems; although most of our analyses involved U-tube steam generators, the results from our once-through steam generator separate effects test calculations are also given, because they identify a number of code problems precluding correct steady state OTSG behavior. Section 3 explores the code global response under a number of postulated transients, and is divided into individual subsections on primary system pressure and break flow, core clad temperature, and secondary side pressure and temperature responses. This section also presents the results of a number of natural circulation test analyses evaluating the code's ability to correctly model this phenomenon when encountered in given transients.

Section 4 describes a number of time step and nodalization dependent effects which result in unphysical code behavior, including oscillations and code aborts. Several limitations in the code time step control algorithm, which could impact either steady state or transient calculations, are discussed, together with some mass and energy conservation problems uncovered through improper modelling of bypass and leakage flow paths, and the modelling guidelines eventually provided by the code developers. Section 5 presents a summary of the various conclusions we have drawn about the code and its use. Finally, Appendix I reviews the incorrect and/or incomplete documentation we encountered in the course of this project, for the code input and models, for the facility descriptions, and for test operation and experimental data. Suggested requirements for documenting completed analyses are also given. Code portability (or lack thereof) is discussed in Appendix II.

Some of our conclusions and guidelines are indeed applicable only to RELAP5/MOD1. Others, however, will be equally valid for MOD1.5 and MOD2, or perhaps even for any future thermal/hydraulic analyses. On the other hand, the material in this report is not meant to be either complete or exclusive; it merely represents the best of our knowledge at the current time.

Table 1.1 MOD1 Assessment Matrix

LOFT	
L6-7/L9-2	ANO-2 turbine trip with pump trip
L9-1/L3-3	loss-of-feedwater with recovery
L3-6/L8-1	2.5% small break with late pump trip
L5-1/L8-2	25% intermediate breaks
L2-5	large break with early pump trip
SEMISCALE Mod-3	
S-SB-P1	cold leg 2.5% small break with early pump trip
S-SB-P3	hot leg 2.5% small break with early pump trip
S-SB-P4	hot leg 2.5% small break with late pump trip
S-SB-P7	cold leg 2.5% small break with late pump trip
SEMISCALE Mod-2A	
S-NC-2	single loop steady state natural circulation
S-NC-3	single loop two-phase natural circulation with degraded heat transfer
S-NC-4	single loop reflux natural circulation with degraded heat transfer
S-NC-7	two loop steady state natural circulation
S-NC-8	two loop transient natural circulation
S-UT-1	10% small break
S-UT-2	10% small break with UHI
S-UT-6	5% small break
S-UT-7	5% small break with UHI
S-UT-8	5% small break with PWR bypass
PKL	
ID1-4	subcooled natural circulation
ID1-6 to 14	saturated natural circulation
LOBI	
A1-04R	large break with cold leg injection
A1-03	large break with combined hot and cold leg injection
A1-04	large break PREX
FLECHT SEASET SG	
23402	reverse heat transfer
B&W OTSG*	
28	steady state
29	loss-of-feedwater
BCL*	
26508	transient ECC delivery
29302	transient ECC delivery with hot walls
UHI PWR**	large break LOCA

* calculated with both MOD1 and MOD1.5
** started with MOD1, to be completed with MOD2

2.0 STEADY STATE CALCULATIONS

Our early efforts at steady state calculations (especially for our first LOFT transients) were greatly hampered by a lack of documentation, guidance and experience, particularly on the new control function features in RELAP5. With growing experience, we have found it relatively easy to generate acceptable steady state primary side initial/operating conditions, for most situations required, in a small number of iterations. The steady state initial conditions ultimately achieved for a number of different LOBI [12], LOFT [16-19,22] and Semiscale [15,24] analyses are summarized in Tables 2.1 through 2.3 for reference. The results of our experience -- the things that worked and the things that didn't -- are summarized in this section. Many of these comments are not specific to RELAP5/MOD1, but apply to steady state calculations in general.

2.1 Primary Side Steady States

A small number of standardized parameters are normally used to specify primary side steady state conditions. These global variables can include:

- -- core power
- -- primary side pressure
- -- hot leg temperature(s)
- -- cold leg temperature(s)
- -- core ΔT
- -- core flow
- -- loop mass flow(s)
- -- loop flow split(s)
- -- bypass flows (if any)
- -- pressurizer level or inventory
- -- pump speed(s)

The variables in this list are not all mutually independent, of course; for example, giving the core flow, any bypass flows and the loop flow split would also specify the individual loop flows.

The steady state "controllers" we have developed use

- -- an integral pump speed controller to set the loop mass flow, flow split, or loop or core temperature difference, as desired;

- -- either a time-dependent volume, pressurizer heaters and sprays, cooling lines, environmental heat losses, or any combination of the above, to control the system pressure;

-- the heated equivalent diameter for the secondary side of the U-tube heat slabs to adjust the primary-secondary ΔT; and

-- detailed geometric modelling to calculate the local pressure gradients around the system (rather than semi-arbitrary use of input form loss coefficients).

All of these will be discussed in detail in the following sections. (Some of these are, of course, not "controllers" in the sense of control functions; they are merely the methods we used to control the values of specified parameters.) Some examples will be given for a calculation being driven from a completed LOFT L6-7 steady state to the desired LOFT L2-5 steady state conditions. The two initial conditions are considerably different, as can be seen in Table 2.2; a single 200 second "transient" run (requiring ~600 CPU seconds on the CRAY-1) was sufficient to achieve an acceptable L2-5 steady state.

2.1.1 Primary Pressure

The absolute value of the primary pressure (as opposed to local pressure gradients) has been controlled in a number of different ways in our various steady state analyses, all equally successful. In the reactor system, of course, it is the pressurizer which controls the system pressure, as it ultimately does also in our calculations.

In most of our LOFT analyses [16-19] we explicitly modelled the pressurizer cycling and backup heaters and cooling spray system. The various heaters were modelled as heat slabs with associated power input tables; the spray cooling was modelled as a volume connecting the intact loop cold leg to the top of the pressurizer, with both a valve and a leakage junction. Simple pressure-dependent trips were used to turn the heaters and sprays on and off.

In our Semiscale Mod-3 analyses [15] we modelled the pressurizer heaters just as we did in LOFT; however, the Semiscale facility relies on environmental heat loss for its high-pressure control (i.e., reducing system pressure when it becomes too high) and has no system equivalent to the LOFT (or plant) spray cooling. Environmental heat loss is included in most of our input decks (in all of our Semiscale Mod-3 decks), with specified heat transfer coefficients and a constant temperature sink on the outside of wall heat slabs, and we found it easy to maintain pressure control this way.

In the LOBI calculations [12] low-pressure control (i.e., raising system pressure when required) also came from modelling the cycling and backup heaters present in the facility, but high-pressure control in both the facility and the analyses is maintained by cooling tubes running through the upper pressurizer. Rather than condensation of steam from the bubble by direct injection of subcooled primary system water, as with the LOFT spray cooling (a closed system), these cooling tubes simply provide a cold surface for condensation of the steam bubble; the cold water which periodically runs through them does not mix with the primary system water directly. Careful modelling of this system also allowed accurate pressure control.

In the PKL [13] and Semiscale Mod-2A [20] natural circulation analyses, the pressurizer was not modelled; pressure control came from a large time-dependent volume. In these calculations, since the pressurizer was valved out of the system in the test when the "transient" (inventory draining) was started, there was no problem in removing the time-dependent volume as required. In normal transient analyses the pressurizer is needed, and the transition from steady state to transient calculation is much smoother if the time-dependent volume (full of saturated steam at the desired pressure) is attached to the top of the pressurizer rather than if the time-dependent volume (full of saturated or subcooled water at the desired pressure and/or temperature) is attached to the pressurizer surge line or the hot leg itself. (In the Semiscale Mod-2A small break calculations [24], steady state pressure control did come from such a time-dependent volume attached to the top of the pressurizer.)

As already mentioned, all these methods are roughly equivalent in the pressure control provided during steady state analyses. Figure 2.1.1.1 shows the primary system pressure during the L2-5 initialization calculation; as in the PKL and Semiscale Mod-2A models, that run used a large steam-filled time-dependent volume to control the primary system pressure with no difficulty. [22]

Only two minor problems with any of the above-mentioned methods have been encountered to date. In one LOFT calculation [17], the heaters were not correctly disabled at the start of the transient, and they eventually "melted" (got hot enough to run off the material properties tables provided). In a few LOFT and LOBI calculations, the presence of the small-area spray line and cooling tubes caused a few time step reductions as a result of Courant limiting during the transients.

(No control of the associated pressurizer liquid level was attempted during these steady state analyses. After otherwise acceptable steady state initial conditions had been achieved, the

void fractions in the pressurizer were simply redefined to give the desired liquid inventory before beginning the transient, if necessary. If the change required was sufficiently small, the associated differential pressure did not visibly perturb the steady state results already obtained.)

2.1.2 Primary Temperature Differentials

The absolute values of the primary system temperatures are determined by the steam generator secondary side saturation temperature, as discussed below. The temperature differential (between hot and cold legs, across the core or across the steam generator U-tubes) is determined by the core power and loop mass flow, through a simple enthalpy balance. Since most test facilities use electrically-heated core rods whose power input is very well known, we do not normally use the core power as an adjustable parameter. (In plant analyses, of course, and in LOFT which has a nuclear core, there is a much wider uncertainty in the power input.) Given that the power is fixed, changing the mass flow(s) will directly change the primary temperature differences. In our assessment analyses, we have used integral pump speed controllers to adjust these closely-related variables.

The integral pump speed controller we use is always of the form:

$$\text{new speed} = \text{initial speed} \pm \text{constant} * \int (\text{desired value} - \text{current value})\, dt$$

The "+" is used if the controller operates on mass flow, and the "-" is used if the controller operates on ΔT. The constant is an adjustable parameter chosen by trial and error to prevent the pump from overreacting to small system perturbations, but still allow convergence on the desired setpoint value in a reasonable length of time. If mass flow is used as the controlling variable, the user must be careful to scale down this constant for larger integral facilities and particularly for full-scale plants; if ΔT is used as the controlling variable, the same constant can be expected to work at all scales.

Which variable is chosen as the controlling parameter in any given calculation depends in part on the experimental data available. In some of our LOFT analyses we used mass flow as the controlling variable for both (parallel) intact loop pumps, while in others we used loop ΔT. [16-19,22] In the Semiscale Mod-3 and Mod-2A small break analyses we used loop or core ΔT for the intact loop pump, and intact loop/broken loop flow split for the broken loop pump. [15,24] In the LOBI calculations we used the individual loop mass flows for both the intact and broken loop pumps. [12]

The pump speed controller described above has always worked smoothly and quickly. As an example, Figure 2.1.2.1a shows that this controller was able to reduce the flow smoothly from the initial L6-7 value of ~480 kg/s to the desired L2-5 value of ~195 kg/s in only one minute, by reducing the pump speed from ~334 rad/s to ~130 rad/s as shown in Figure 2.1.2.1b. In this calculation the pump speed was controlled by the loop (or vessel) temperature difference, shown in Figure 2.1.2.2. [22]

The only problem encountered with this pump speed controller is that, due to a code error uncorrected to date, any pump using the "refer-back" feature to reference homologous curves input for another pump in the nodalization is forced to run at a constant speed (ignoring whatever was specified in its input). This problem was found in our first LOFT analyses where, since there are two identical parallel pumps in the intact loop, we were using this "refer-back" option. The easiest way around the difficulty, which we have used ever since, is to always input a full set of homologous curves for each pump, even if there is duplication. [16]

2.1.3 Primary Pressure Differentials

The pump speed controller just discussed intentionally does not utilize the actual pump speeds measured in the facilities. Rather, comparison of the calculated and experimental pump speeds provides an excellent global check on the accuracy of calculated pressure gradients around the various flow paths.

Although most facilities whose tests are used for code assessment analyses may provide enough information on steady state pressure drops to allow the analyst to match them using input loss coefficients at various junctions, there are a number of potential problems with this approach. First and most obviously, it presupposes the existence and availability of such detailed steady state operating data. Further, it does not address the different behavior which will occur in reverse flow during transients, and it applies only to single-phase operating conditions.

The approach we chose, on the other hand, while it requires detailed facility descriptions (basically, blueprints), can be used even in the absence of any operating data and applies equally in either flow direction. It relies on and allows evaluation of code wall friction and abrupt area change loss coefficient models for single-phase (and limited two-phase) flow conditions. Any available steady state pressure drop data is used for verification, not for derivation.

All calculations to date indicate that proper, consistent, and complete geometric modelling is entirely adequate to represent system pressure drops, without any additional arbitrary loss coefficients input by the user to force-fit experimental data. Tables 2.1.3.1 through 2.1.3.3 show comparisons between measured and calculated mass flows, pump speeds and differential pressures for LOBI [12], LOFT [16-19,22] and Semiscale [15,24] analyses. Another check on this method of obtaining steady state pressure drops is the very good agreement found for subcooled natural circulation flow rates in both PKL [13] and Semiscale [20] steady state natural circulation tests, as shown in Table 2.1.3.4.

All the facilities in our assessment matrix were modelled using the same geometric approach described above. The various nodalizations are described in detail in the individual topical reports; the basic common modelling assumptions we used are described here.

Wall friction losses contribute significantly to system pressure drops. The associated loss coefficient is of the form f*L/D, with f a friction factor given by standard correlations, L the flow channel length and D its hydraulic diameter, defined as {4*flow area divided by wetted perimeter}. Correct geometric lengths and areas are needed to properly model the wall friction pressure drops for simple geometries such as single straight pipes, where the hydraulic diameter can be defaulted to the pipe diameter. When modelling individual channels is impractical and parallel flow paths are lumped together by retaining or averaging actual lengths and summing areas (as in steam generator tubes, for example), the proper hydraulic diameter for the individual flow path (such as the diameter of a single tube) must be input explicitly. For regions such as the core or steam generator secondary boiler, where multiple tube surfaces provide significant additional wall friction, a user-input hydraulic diameter calculated using the standard geometric definition is required. (This hydraulic diameter, specified for fluid volumes and used to calculate friction losses, should be distinguished from the hydraulic and heated equivalenc diameters specified for heat slabs adjacent to the volumes; these are used to calculate heat transfer coefficients and are discussed in the next section.)

Another significant contributor to the system pressure drops is the loss associated with pipe elbows, bends, tees, etc. User-input loss coefficients are supplied at junctions to account for any horizontal or vertical elbows, flow tees or pipe entrances and exits. All these form losses are calculated or estimated for the given pipe sizes and geometries using standard Crane [27] formulae; e.g., the loss coefficient used for a 30° elbow is assumed to be 1/3 that for a 90° elbow. Whenever possible, these

loss coefficients are applied, not all at a single junction, but spread over several junctions. For example, two junctions defining an elbow inlet and outlet are each given half the total loss coefficient. For a branch volume modelling a tee, half the loss coefficient through the primary ("the run") is applied at each of the primary inlet and outlet junctions; the input loss coefficient at the secondary junction is adjusted so that the total loss coefficient through the secondary and either primary junction equals the desired loss coefficient through the branch. For close-pattern return bends (180°) such as those at the top of U-tubes or at the bottom of pump suction legs, the total loss coefficient can be shared between two or three junctions, depending on the exact nodalization used. (If a horizontal volume is used to connect two vertical volumes, both its inlet and outlet junctions are available to share the form loss. If two inclined (~45°) volumes are used to represent the bend, three junctions are available; the middle junction is then usually defined to have twice the loss coefficient of the other two, inlet and outlet, junctions.) Pipe entrance (sharp-edged) and exit loss coefficients are used primarily at vessel inlets and outlets. The only "arbitrary" user-input loss coefficients we used in the nodalizations are K=1.6 for each core grid spacer (based on previous experience).

A final portion of the system pressure drops comes from losses at area changes (e.g., expansions, contractions, orifices). Besides hydraulic diameters and user-input loss coefficients, any changes in flow area are modelled explicitly whenever possible by flagging the appropriate junctions as "abrupt area changes". The code then automatically calculates additional form losses in the current direction of flow at these junctions using expansion and contraction formulae; simple geometric formulae are used for single-phase flow, while a more complex model producing separate and probably different liquid and vapor loss coefficients is used during two-phase flow. Changes in piping size (e.g., 16-in. to 14-in. to 10-in. Sch 160 piping in LOFT) are usually modelled as abrupt area changes (if the change occurs over a relatively short distance), as are the inlets and outlets for the pressurizer and accumulator surge lines, steam generator plena and U-tubes. (For the U-tubes, the area used in the abrupt area change is the lumped flow area.) Also, junctions between the vessel and the hot and cold legs are always flagged as abrupt area changes, as are junctions between the downcomer and lower plenum, and junctions representing core support or other vessel plates. (If enough facility information is available, the steam generator baffle plates are also explicitly modelled as abrupt area changes.)

Although we attempted to model most area changes explicitly, a rapid series of area changes in a small space (such as occurs in the lower core structure in LOFT, for example) is modelled as a representative flow area with a user-imposed geometrically-derived loss coefficient. Such form loss coefficients are calculated by applying single-phase formulae at each actual expansion and contraction and then adjusting during the summation to account for the difference between the actual individual areas and the average representative area that is input. Ideally, we would have liked to model losses due to instrumentation (i.e., turbine meters and drag discs) explicitly using the abrupt area change model also. This was in fact done for the LOFT intact loop Venturi meter and the PKL flowrate measuring orifices and downcomer turbine flowmeter, and could have been done for the drag-body plates in the LOBI facility, where the blockage factors for the various drag-body and turbine probes were given as part of the regular test documentation. In the available Semiscale documentation, on the other hand, very little information was given on instrumentation losses and they are neglected in our models for this facility. (Of course, well-designed instrumentation should not contribute significantly to the overall system pressure drops.)

At a few junctions in each of our nodalizations, both user-input loss coefficients and the code's internal form losses calculated for abrupt area changes are used. One place this occurs is at the vessel inlets and outlets (i.e., at the connections between upper plenum and hot leg, or downcomer and cold leg piping). Another location is at injection tees (e.g., at the connection between the pressurizer surge line and the hot leg). In such cases, the user-input loss coefficient is meant to account for some additional effect (such as a 90° change in flow direction) occurring before or after the area change.

The only difficulty (described in more detail in Section 4.2) we encountered with the above approach was in modelling small bypass and leakage flow paths geometrically. Our original LOFT nodalizations used the published controlling areas and hydraulic diameters for the various bypasses. Guidelines were developed later by the code developers (based largely on our problems) which recommended defaulting the junction area to the minimum adjacent volume flow area whenever the actual area change is greater than 1:10 to 1:100, flagging the leak junction as having a smooth area change and adjusting the user-input loss coefficient at this junction to match the desired flow, in order to smooth the calculated behavior. [16,17] (A new branch-type component is being developed for later versions of RELAP5 to specifically model such "pinhole leaks", without large user-input loss coefficients adjusted to limited available data.)

2.1.4 Primary Temperatures

The interrelated specification of loop (or core) temperature difference, mass flow and pump speed has already been discussed. In this section we turn to the "control" of the absolute values of the loop temperatures. These are determined by the secondary side saturation temperature and by the temperature profile across the steam generator U-tube walls. In our analyses we have usually adjusted both of these variables -- the secondary side saturation temperature by varying the secondary side pressure and the U-tube temperature drop by changing the secondary side heated equivalent diameter. (This equivalent diameter, specified for heat slabs and used in heat transfer correlations, should be distinguished from the hydraulic diameter input for volumes and used to calculate frictional pressure drops.)

Our early steady state calculations (for LOFT [16-18] and Semiscale Mod-3 [15]) consistently produced primary side hot and cold leg temperatures that were significantly higher (~5 K) than measured values (whose experimental uncertainties were on the order of 1-3 K). These primary side temperatures could be lowered somewhat by reducing the steam generator secondary side pressure and associated saturation temperature within its quoted uncertainty. The experimental uncertainties on the steam generator secondary pressure, however, are on the order of ~0.1 MPa, resulting in a maximum variation in secondary saturation temperature (and hence primary temperatures) of ~1 K, much less than the observed discrepancies in most cases.

Closer examination of the LOFT calculated results showed a peculiar temperature gradient from the primary to secondary systems across the steam generator U-tubes. An inordinately large temperature difference was observed between the secondary side fluid and the outside surface of the U-tube, resulting in an overall temperature difference between primary and secondary that is too high. Given that the correct power is being transferred to the secondary (which is required to achieve any steady state), the only way to decrease this temperature difference is to increase either the heat transfer area or the heat transfer coefficient (since $Q = h*A*\Delta T$). Increasing the heat transfer area would require fouling factors of >100%, which is clearly unphysical; therefore, we concluded that the heat transfer coefficient must be too low. A cursory look at the heat transfer correlation used in the code (the Chen correlation for saturated nucleate boiling) shows, among a number of other parameters involving fluid properties, an inverse dependence on equivalent diameter. This geometric parameter can either be user-input for each heat slab or be defaulted to the hydraulic diameter of the adjacent fluid volume.

In these early LOFT [16-18] and Semiscale Mod-3 [15] steady state analyses, we had input an equivalent diameter on the outside surface of the U-tube heat slabs which was equal to the secondary side heated equivalent diameter (using the standard definition of 4*flow area/heated perimeter), as opposed to the secondary side hydraulic equivalent diameter (defined as 4*flow area/wetted perimeter) which we had input as hydraulic diameter for the secondary side fluid volumes. (The same approach was taken for the core volumes and heat slabs.) The heated equivalent diameter calculated was usually larger than the hydraulic equivalent diameter (by ~50%), since the heated perimeter consists of only the tube surface while the wetted perimeter includes the shroud as well. (For the inside of the U-tubes, both definitions default to the tube inner diameter.) The use of this characteristic length in the circular tube correlations applied to the outside of a tube bundle is questionable, to say the least. Equally reasonable characteristic distances in the tube bundle are the pitch and the wall-to-wall separation. The latter is the smallest characteristic length in the bundle, and we chose to input it as the equivalent diameter to maximize the heat transfer coefficient (and thus reduce the overall temperature drop across the U-tubes) in these and all later nodalizations.

This change in equivalent diameter and hence in primary-to-secondary ΔT allowed us to match both primary and secondary side steady state conditions within the specified experimental uncertainties in most cases (the exceptions being two of the Semiscale Mod-3 small break tests, as shown in Table 2.2). The smaller equivalent diameter, equal to the minimum tube-to-tube spacing, was always used in our later facility nodalizations (PKL [13], LOBI [12], and Semiscale Mod-2A [24]); Table 2.1.4.1 summarizes the changes required in the equivalent diameter for the various experimental facilities and for a full-scale Westinghouse Type 51 steam generator [26].

This problem of matching primary and secondary side conditions simultaneously is not unique to RELAP5; the same heat transfer correlations are used in the TRAC code being developed at Los Alamos National Laboratory (LANL) and the same problems are encountered with that code. Sensitivity studies were done there to investigate the consistent underprediction of secondary pressure at steady state when the desired primary conditions have been achieved. The wall conduction and material properties were verified, and the effect of coarse vs fine nodalization was analyzed. Sensitivity studies were also done on the equivalent diameter, since a strong inverse relation exists between the equivalent diameter used and the Chen nucleate boiling heat transfer coefficient as the diameter becomes small. As a result of such a sensitivity study, the published TRAC user guideline is to reduce the secondary side U-tube heated equivalent diameter to

the smallest value having a physical basis; since the baffle plates used to support the tubes tend to force some crossflow (in addition to the normal parallel flow along the tubes) and since cross flow results in an equivalent diameter proportional to the minimum wall-to-wall distance for the tubes, this minimum wall-to-wall distance is recommended. [28] This is the same conclusion we reached for RELAP5 steady state analyses.

2.2 Secondary Side Steady States

Just as in the primary system discussed above, a small number of standardized parameters normally specify secondary side steady state operating conditions. These global variables can include:

-- steam dome pressure
-- saturation temperature
-- downcomer temperature
-- feedwater temperature
-- feedwater flow
-- recirculation ratio
-- liquid level
-- liquid inventory

The variables in this list are not all mutually independent; e.g., giving the steam dome pressure would also specify the associated saturation temperature.

The required secondary "controllers" were much more difficult to develop and to use than were the primary side "controllers" discussed already. The difficulties were compounded by coupling between quantities with varying time constants, and by the lack of detailed information on the secondary side geometry (e.g., baffle plate location and flow area restriction). The steady state "controllers" we developed for the secondary side use

-- either a steam flow control valve or a time-dependent volume to control the steam dome pressure;

-- a time-dependent main feedwater junction or a feedwater control valve to set the liquid inventory/level;

-- the heat transfer to the secondary and the feedwater subcooling to adjust the downcomer/shroud differential liquid level; and

-- detailed geometric modelling to calculate the recirculation ratio by accounting for local pressure gradients around the flow path (rather than semi-arbitrary use of input form loss coefficients).

These will all be discussed in detail in the following sections. (Some of these are, of course, not "controllers" in the sense of control functions; they are merely the methods we used to control the values of specified parameters.)

2.2.1 Secondary Pressure

As already discussed in section 2.1.4, the secondary side pressure and associated saturation temperature directly determine the absolute values of the primary side temperatures. The secondary side pressure (normally given in the steam dome) is controlled by adjusting the steam outflow, either by using a steam flow control valve or (more simply) by connecting the steam dome to a large steam-filled time-dependent volume at the desired pressure and allowing the steam outlet junction mass flow to vary as required. This second alternative is exactly equivalent to using a steam-filled time-dependent volume connected to the top of the pressurizer to control the primary side pressure, as was discussed in section 2.1.1.

In most of the early LOFT steady state analyses [16,18-19], we depended on modelling the steam flow control valve explicitly (partially because the first test we analyzed required a steam flow control valve during the first part of the transient). The steam flow valve controller, which eventually emerged during the L6-7 study [16], is fairly simple conceptually: a combination of current, last-calculated and desired steam dome pressures was used in a scheme numerically equivalent to an exponential relaxation. It eventually worked well, but required much development and adjustment to produce stable results. Other LOFT steady state analyses [17,22] relied on a time-dependent volume, which proved easier to understand and use.

A steam-filled time-dependent volume was also used in the Semiscale Mod-3 [15] and LOBI [12] steady state calculations, and in the PKL [13] and Semiscale Mod-2A [20,23] natural circulation analyses. In contrast, the Semiscale Mod-2A small break initialization [24] returned to modelling servo valves in the steam outlet lines, but with much simpler integral controllers adjusting the areas to maintain a specified cold leg temperature in each loop (thus avoiding the intermediate stage of manually looking at the cold leg temperature resulting from a specified secondary pressure). These integral controllers have the same form as the primary pump speed controller discussed in section 2.1.3, and their gains must be based on the loop transit times and system masses to prevent overreaction to small perturbations. Such controllers could either directly use the secondary pressure or saturation temperature as the forcing function or use the primary side temperature (as we did), since the secondary pressure determines the cold leg temperature.

2.2.2 Secondary Liquid Level

The feedwater flow into the secondary side balances the steam outflow in normal steady state operation, with the magnitude of both determined by balancing the heat input to the secondary with the enthalpy difference between the saturated steam outflow and the subcooled feedwater inflow. Given such a balanced steady state, the liquid and steam inventories should remain constant (together with the downcomer and shroud liquid levels discussed in more detail in the next subsection). The liquid level/inventory can be increased or decreased by altering the feedwater flow relative to the steam outflow until the desired values are reached. In our various steady state calculations, the feedwater flow has been controlled both by modelling an actual flow control valve and by using a time-dependent junction whose flow rate was determined in various ways.

In most of our LOFT analyses, a feedwater valve was modelled explicitly. Early attempts controlled the valve using both the experimental liquid level and feedwater flow. [16,18-19] The controller first brought the liquid level to the desired value and then attempted to adjust the feedwater mass flow to its specified value; if the liquid level drifted outside the given limits (0.02 m in L6-7), the feedwater flow rate was then allowed to vary as needed to reestablish the desired level. Since no explicit effort was made to compare the resulting feedwater and steam flows (and because constant-rate motor valves can only occupy a discrete set of positions, depending on the size of the time step), a true steady state was not always achieved. In the L6-7 analysis [16] the resulting drift in liquid level (shown in Figure 2.2.2.1) extended for several hundred seconds before the level controller was reactivated (as would also likely occur in reality), so that reasonably quiescent initial conditions were available; in contrast, the same controller flopped back and forth between level and feedwater flow control every 20 seconds in the similar L5-1 analysis [19]. In the L9-1 analyses [17], the oscillations were so great that the level controller was removed entirely and only the feedwater controller remained; since the secondary dried out very early in that long transient the initial liquid level did not appear to be a critical parameter. In the L3-6 steady state calculations [18], we were not able to match the experimental feedwater flow and liquid level simultaneously; the resulting feedwater flow lay outside the experimental bounds, but since the main feed was to be stopped at the start of the transient we did not judge this to be a serious problem.

For the Semiscale Mod-3 analyses [15], the feedwater inflows were modelled as time-dependent junctions with mass flow rates controlled to maintain desired collapsed liquid levels in the steam generator downcomers. Each controller was of the form

feedwater flow rate = steam flow rate - constant *
(current level - desired level)

The constant was determined by trial and error; a value of 0.3 was found to give well-behaved results for both the intact and broken loop steam generators.

In the Semiscale Mod-2A natural circulation tests [20], the feedwater was also modelled as a time-dependent junction which maintained liquid covering the U-tubes (as was done with feed and bleed in the experiments). The feedwater flow rate was determined by a relation similar to that used in the Semiscale Mod-3 steady state, with

feedwater flow rate = constant *
(desired level - current level)

whenever the level dropped below a specified value (10 m); the constant was set equal to 0.2 in these calculations. For the Semiscale Mod-2A small break analyses [24], the feedwater flow rate was simply set equal to the steam flow in each generator.

The LOBI large break analyses [12] all used time-dependent junctions with constant feedwater flow rates equal to the experimental values during the steady state portions of the calculations. (Accurate secondary side initial conditions are less important in rapid large break transients than in most other, slower, transients.) Constant feedwater flow rates were also used in the PKL natural circulation runs [13], with values chosen to maintain adequate heat removal capability in the steam generator secondaries.

2.2.3 Secondary Liquid Level Differential

The previous section discussed balancing and adjusting the steam generator flows to maintain constant operating conditions, particularly constant liquid inventory and level. However, in addition to the amount of liquid present in the secondary side, the distribution of the liquid between the downcomer and shroud region must be correct if both the liquid inventory and the liquid (downcomer) level are to agree with experimental operating data. (Unfortunately, both numbers are seldom available for either test facilities or actual plants.) The level difference between the shroud and downcomer is directly controlled by the amount of steam generated in the boiler (shroud) region; this depends strongly on the power transferred from the primary side and weakly on the amount of feedwater subcooling. (This can be seen in the LOFT steady state results matrix, where the downcomer liquid level increases as the core power decreases.)

Although both these parameters are usually well-known for experimental facilities which rely on electrically-heated core rods, the power transferred from the primary side is much less well-known for nuclear plants, where it is hard to measure core power exactly. Thus, although in plant analyses it is possible to vary the core power somewhat in order to adjust the secondary side level difference, this cannot normally be done during most integral test analyses (except for LOFT, which has a nuclear core). The level difference can, however, be adjusted slightly in such experimental analyses by varying the relative resistances of the downcomer and shroud flow paths, and hence the recirculation ratio; because the relationship between hydraulic resistance, recirculation flow and level difference is complex and usually nonmonotonic, much trial and error is needed to obtain results desired.

2.2.4 Secondary Pressure Differentials

As just mentioned, the level difference between the shroud and downcomer and the relative flow path resistances in turn determine the natural convection in the steam generators, defined by the recirculation ratio. (This parameter is not known for many test facilities, although it is usually known in most plants.) Calculating the recirculation ratio requires modelling the secondary side geometry in detail, accounting for all pressure drops due to baffle plates, etc. (using the same methods already discussed for the primary side pressure drops in Section 2.1.3), and having the correct interface drag between the phases in the boiler region.

Although no great efforts were made to achieve a good secondary side steady state in the LOBI large break analyses [12], apparently the simple and well-documented geometry allowed calculation of the correct recirculation ratio. While visiting Sandia months after our calculations had been completed, Dr. Staedtke of LOBI mentioned [29] that the recirculation ratio in the intact loop steam generator was ~10, and when we checked our results we found that this large recirculation had in fact been calculated.

In contrast, we have to date been unable to match the recirculation ratio of 3.25 in a Westinghouse Type 51 steam generator [30] during steady state calculations initializing UHI plant analyses [26], although we have reasonably detailed information on the secondary side geometry for that steam generator and a correspondingly detailed nodalization. Any recirculation ratio much greater than 2 results in large flow oscillations; at recirculation ratios near 2 these can be substantially reduced by cutting the time step (as shown in

Figure 2.2.4.1), but reducing the shroud pressure drop further produces oscillations unaffected by any time step reductions. Increasing the pressure drop, of course, lowers the recirculation ratio which results in perfectly steady flow behavior.

Similar behavior was seen in the LOFT L2-5 initialization calculation. [22] A doubling of the code time step due to a small change in Courant limit resulted in mass flow and associated liquid level oscillations (shown in Figure 2.2.4.2); manual reduction of the time step on restart caused the oscillations to damp and disappear. Unfortunately we have no information on the recirculation ratio in the LOFT steam generator.

2.3 Once-Though Steam Generators

Although the vast majority of our analyses involve U-tube steam generators, we did analyze a loss-of-feedwater experiment performed at the Babcock & Wilcox (B&W) 19-tube once-through steam generator (OTSG) test facility. Although there are no similar or related analyses in our assessment matrix for comparison, the OTSG results (particularly from the steady state analyses) are quite interesting in themselves, identifying a number of code model problems and possible "fixes". [21]

In these calculations we automatically used the minimum tube-to-tube spacing as the equivalent diameter on the outside surface of the tube heat slabs, in keeping with the user guidelines developed for U-tube steam generators (as discussed above in Section 2.1.4). In response to questions raised at a code assessment review meeting [31], we investigated the effect of varying the heat structure equivalent diameters input for the secondary side of the OTSG tubes. Figure 2.3.1 compares the steady state axial temperature profiles obtained using the geometric value of 20.64 mm (4*flow area/heated perimeter of tubes) with the profiles obtained in the base calculation using the tube wall-to-wall spacing of 6.35 mm. The lower value used in the base calculation gives better agreement with the data, although there is no appreciable difference in the primary inlet-outlet ΔT.

The good agreement with experimental data is also the result of a number of code changes in the CHF and wall-vapor heat transfer calculations. Our analyses show that MOD1 cannot correctly calculate many important parameters for steady state OTSG conditions (e.g., steam superheat at the boiler outlet, CHF location, and primary ΔT). The principal problem we found is the low-flow CHF correlation used in MOD1, which underpredicts CHF at high qualities, as shown by the primary and secondary temperature profiles in Figure 2.3.2a.

After modifying the CHF correlation package, we found that the convective heat transfer from heat structures to single-phase superheated steam is not treated properly; the film boiling correlations used in MOD1 for this regime always use the saturation temperature as the fluid temperature for calculating the heat transfer rate, overpredicting the heat transfer as the (superheated) steam temperature approaches the primary inlet temperature, as shown in Figure 2.3.2b.

With some additional code updates to correct the fluid temperature used at these superheated vapor heat transfer conditions, excellent agreement was obtained with experimental conditions, as shown in Figure 2.3.2c and earlier in Figure 2.3.1. (We also changed the POOLNB subroutine to calculate the actual Chen suppression factor with subroutine SUPFAC instead of using the coded-in inaccurate approximation, as discussed below in Section AI.1.3.) Also, since our code changes were very similar to those subsequently implemented in MOD1.5, steady state calculations using MOD1.5 gave very similar results to those obtained with our modifications to MOD1, as shown in Figure 2.3.2d.

Table 2.3.1 summarizes the steady state parameters obtained using our modified version of MOD1 and compares these results with values calculated with the unmodified version of MOD1, with MOD1.5 and with experimental data. (The calculated secondary mass inventory is not as much higher than the data as first appears; the experimental value, derived by integrating the measured steam flow minus the feedwater flow, does not include the mass of steam left in the generator at the end of the transient, which amounts to ~4 kg at the operating pressure of the test.)

Calculations for the associated loss-of-feedwater transient were done using the same three versions of RELAP5. [21] The experimental behavior was predicted well using our MOD1 code modifications; transient calculations without the modifications showed fair agreement with the steam flow data but poor agreement with the primary and secondary temperature data, mainly due to initial condition errors. Transient calculations using MOD1.5 gave very similar results to those obtained with our modified version of MOD1.

Table 2.1 LOBI Measured and Calculated (in parentheses) Steady State Initial Conditions

PARAMETER	A1-03		A1-04R		A1-04	
	IL	BL	IL	BL	IL	BL
Primary System:						
Pressure (MPa)	15.2 (15.3)		15.3 (15.3)		15.2 (15.2)	
Core Power (MW)	5.22 (5.22)		5.12 (5.12)		5.38 (5.38)	
Mass Flow (kg/s)	21.7 (21.1)	7.1 (7.1)	21.1 (21.1)	7.0 (7.0)	19.7 (19.7)	5.9 (5.9)
Hot Leg Temperature (K)	592 (594)	599 (594)	600 (600)	606 (600)	601 (602)	605 (602)
Cold Leg Temperature (K)	562 (562)	562 (562)	571 (569)	571 (569)	566 (567)	563 (567)
Secondary System:						
Feedwater Flow (kg/s)	2.1 (2.1)	0.7 (0.7)	2.07 (2.1)	0.8 (0.6)	2.15 (2.15)	0.74 (0.74)
Feedwater Temperature (K)	473 (473)	473 (473)	493 (493)	501 (501)	490 (490)	485 (485)
Steam Temperature (K)	544 (545)	544 (545)	553 (553)	553 (553)	551 (551)	551 (551)
Pressure (MPa)	5.6 (5.7)		6.4 (6.4)		6.2 (6.2)	
Accumulators:						
Pressure (MPa)	2.7 (2.7)	2.7 (2.7)	2.7 (2.7)	---	2.7 (2.7)	---
Water Temperature (K)	305 (305)	305 (305)	305 (305)	---	305 (305)	---
Water Volume (liters)	224 (224)	75 (75)	224 (224)	---	224 (224)	---
Gas Volume (liters)	56 (56)	19 (19)	56 (56)	---	56 (56)	---

Table 2.2 LOFT Measured and Calculated (in parentheses)
Steady State Initial Conditions

Parameter	L6-7/L9-2	L9-1/L3-3	L3-6/L8-1	L5-1/L8-2	L2-5
Primary System					
Pressure (MPa)	14.75±0.11 (14.74)	14.9±0.1 (15.1)	14.87±0.14 (14.85)	14.93±0.08 (14.86)	14.94±0.06 (14.91)
Core Power (MW)	49.0±1.2 (49.0)	49.6±0.9 (48.7)	50.01±1.0 (50.0)	45.9±1.2 (45.9)	36.0±1.2 (36.0)
Mass Flow (kg/s)	483.7±2.6 (482.5)	479.1±2.6 (479.5)	483.0±2.6 (483.7)	308.2±4.0 (308.0)	192.4±7.8 (195.9)
Hot Leg Temperature (K)	576.4±0.3 (576.5)	578.9±1.3 (578.4)	577.1±1.8 (577.8)		589.7±1.6 (590.2)
Cold Leg Temperature (K)	556.7±1.0 (557.5)	558.9±1.3 (560.3)	557.9±1.1 (558.4)	552.3±0.9 (551.0)	556.6±4.0 (557.1)
Vessel ΔT(K)				26.8±1.3 (27.9)	33.1±4.3 (33.1)
SG Secondary					
Pressure (MPa)	5.51±0.08 (5.43)	5.67±.08 (5.67)	5.57±0.06 (5.51)	5.05±0.06 (5.06)	5.85±0.06 (5.85)
Feedwater Flow (kg/s)	25.0±0.6 (25.02)	27.01±1.0 (26.4)	27.8±0.1 (25.75)	25.3±0.6 (25.3)	19.1±0.4 (19.1)
Liquid Level (m)	3.09±0.08 (3.15)		3.17±0.03 (3.15)	3.22±0.02 (3.23)	

Table 2.3a Semiscale Mod-3 Measured and Calculated (in parentheses) Steady State Initial Conditions

Parameter	S-SB-P1	S-SB-P7	S-SB-P3	S-SB-P4
Core Power (MW)	1.96 (1.96)	1.97 (1.97)	1.965 (1.965)	1.968 (1.968)
System Pressure (MPa)	15.58 (15.58)	15.73 (15.73)	15.56 (15.56)	15.56 (15.56)
Intact Loop Hot Leg Temperature (K)	585.4 (584.7)	585.3 (583.8)	586.1 (585.3)	584.9 (584.7)
Intact Loop Cold Leg Temperature (K)	552.9 (550.3)	552.3 (547.9)	553.2 (552.0)	552.4 (551.3)
Broken Loop Hot Leg Temperature (K)	585.4 (582.6)	585.3 (581.0)	586.0 (584.9)	584.9 (582.7)
Broken Loop Cold Leg Temperature (K)	553.0 (550.6)	551.4 (549.8)	551.9 (550.0)	550.5 (549.5)
Core Inlet Mass Flow Rate (kg/s)	10.5 (10.6)	10.4 (10.3)	10.3 (10.1)	10.4 (10.5)
Intact Loop Pump Speed (rad/s)	247 (252)	243 (247)	243 (250)	244 (257)
Broken Loop Pump Speed (rad/s)	1629 (1287)	1599 (1272)	1592 (1249)	1645 (1300)
Intact Loop Pump Head (kPa)	460 (510)	450 (490)	440 (490)	450 (520)
Broken Loop Pump Head (kPa)	440 (540)	430 (520)	420 (490)	450 (540)
Intact Loop Steam Generator Pressure (MPa)	5.30 (5.50)	5.26 (5.46)	5.34 (5.42)	5.28 (5.36)
Broken Loop Steam Generator Pressure (MPa)	5.16 (5.24)	5.01 (5.09)	5.05 (5.13)	4.87 (4.95)

Table 2.3b Semiscale Mod-2A Measured and Calculated Steady State Initial Conditions

Parameter	S-UT-1	S-UT-2	RELAP	S-UT-6	S-UT-7	RELAP	S-UT-8	RELAP
Core Power (MW)	1.90	1.91	1.91	1.99	1.99	1.99	1.95	1.95
System Pressure (MPa)	15.5	15.5	15.5	15.8	15.6	15.8	15.6	15.5
Intact Loop Cold Leg Temperature (K)	557.9	557.8	559.0	557.0	558.0	557.2	559.5	559.5
Intact Loop ΔT (K)	32.7	32.9	33.0	41.0	41.0	41.0	35.1	35.2
Intact Loop Flow (ℓ/S)	10.7	10.5	11.0	9.4	9.4	8.7	10.3	10.0
Intact Loop Steam Generator Pressure (MPa)	6.03	5.74	5.82	5.70	5.70	5.58	5.71	5.75
Intact Loop Pump Speed (rad/s)	229.9	225.4	227.0	199.0	198.0	196.0	244.0	226.9
Broken Loop Cold Leg Temperature (K)	557.9	557.8	558.0	557.0	559.0	557.0	561.4	561.4
Broken Loop ΔT (K)	31.3	31.8	34.0	40.0	39.0	41.1	33.8	33.3
Broken Loop Flow (ℓ/S)	3.5	3.8	3.4	2.8	2.8	2.6	3.7	3.3
Broken Loop Steam Generator Pressure (MPa)	5.56	5.78	5.69	5.90	5.98	5.71	6.11	6.00
Broken Loop Pump Speed (rad/s)	1725	1714	1541	975	974	1200	1192	1491
Bypass Flow (ℓ/S)	0.43	0.43	0.43	0.37	0.33	0.36	NM*	NM*
Support Column Flow (ℓ/S)	0.10	0.10	0.10	0.09	0.09	0.09	--	--
Guide Tube Flow (ℓ/S)	0.31	0.31	0.31	0.03	0.26	0.27	0.09	0.09

*Not Measured

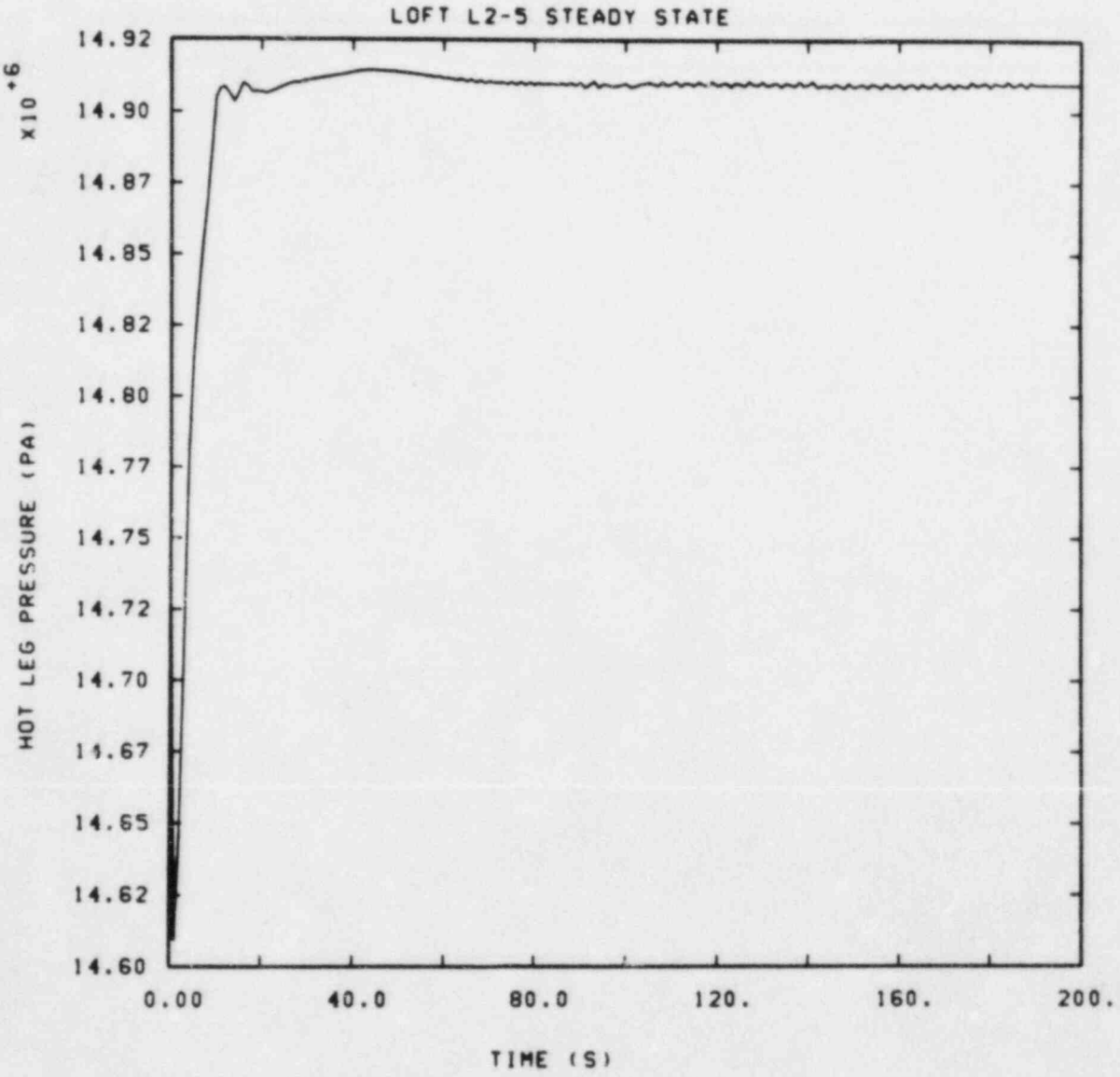

Figure 2.1.1.1 Primary System Pressure for LOFT L2-5 Steady State Initialization Calculation

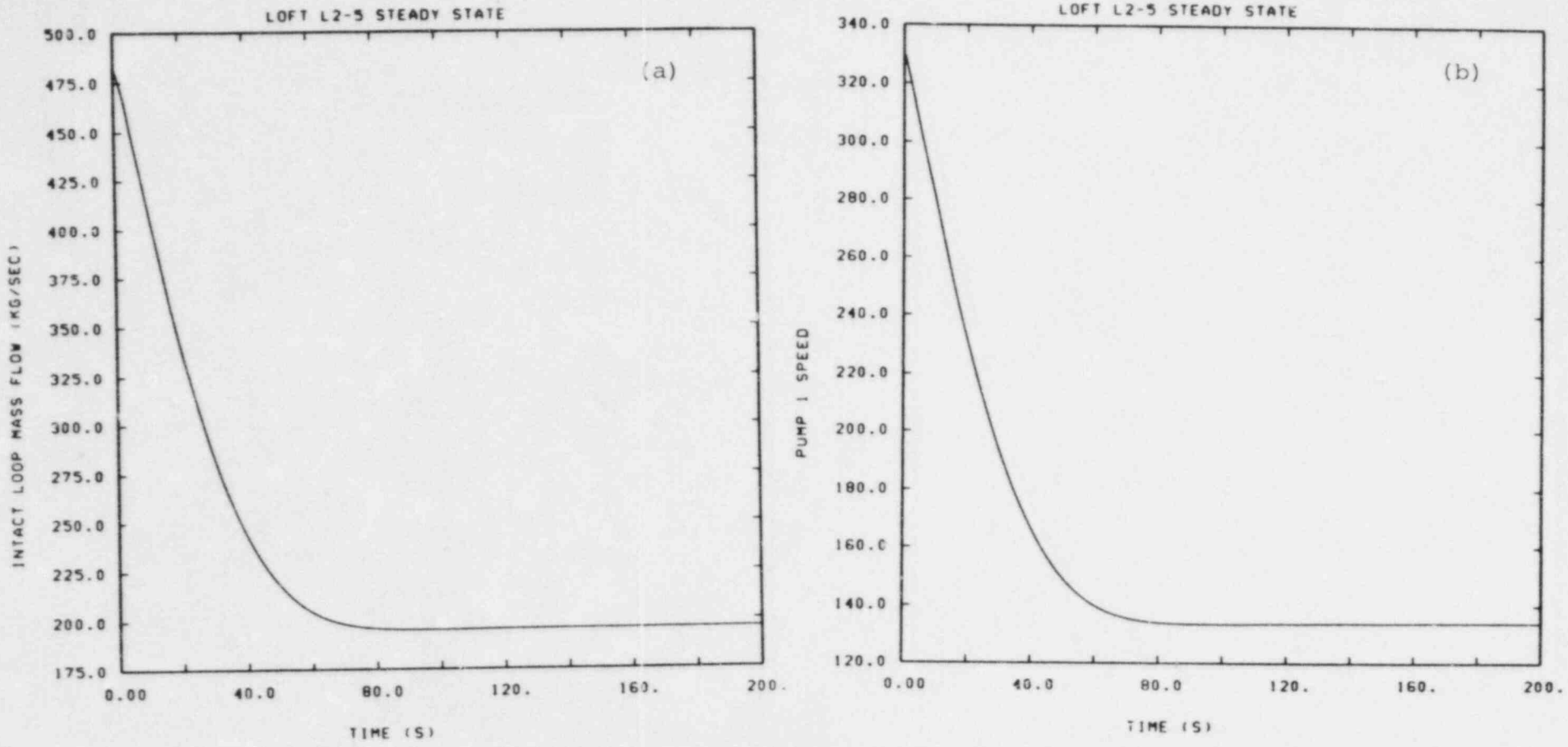

Figure 2.1.2.1 Primary System (a) Mass Flow and (b) Pump Speed for LOFT L2-5 Steady State Initialization Calculation

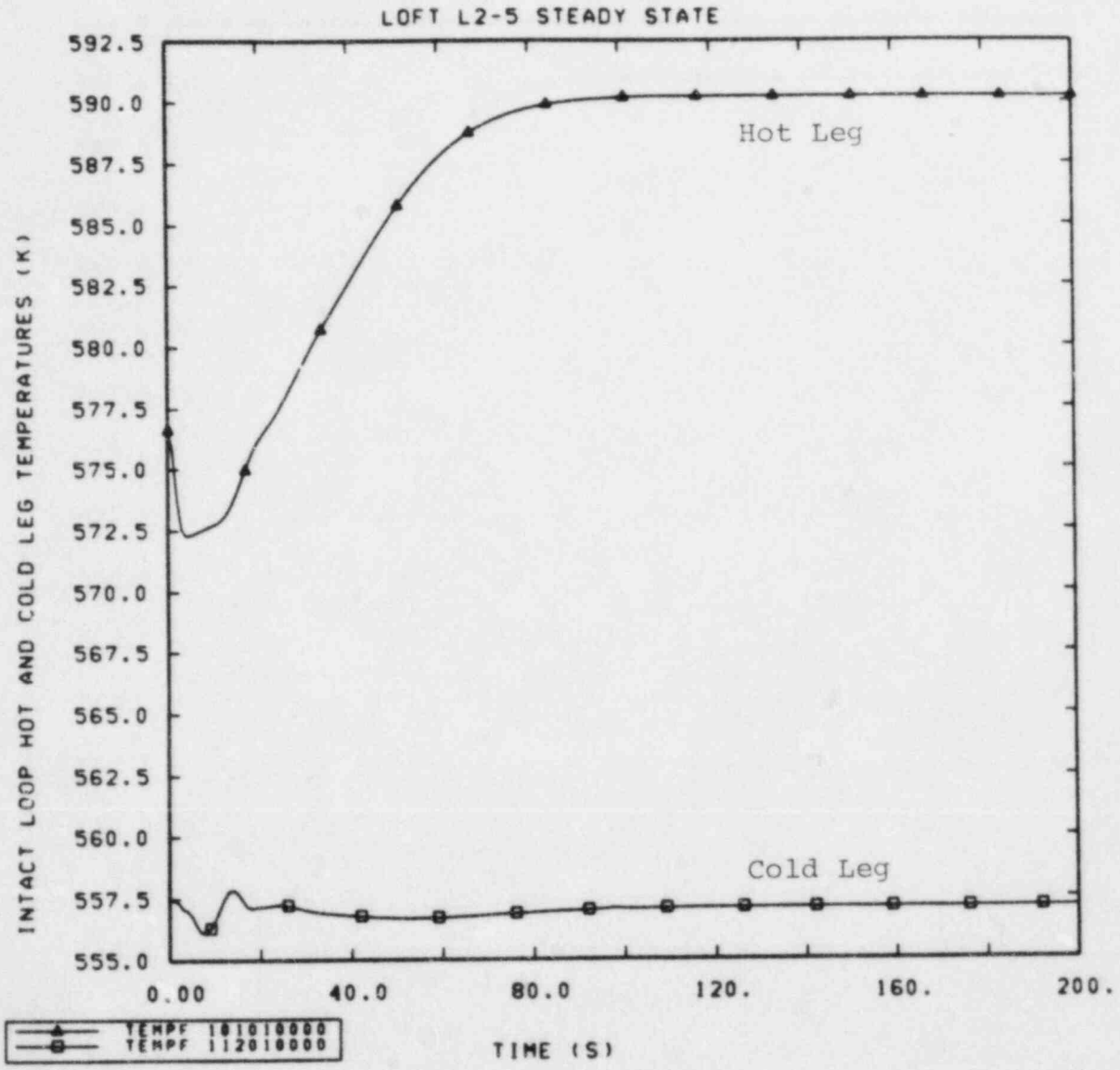

Figure 2.1.2.2 Primary System Loop Temperature Difference for LOFT L2-5 Steady State Initialization Calculation

Table 2.1.3.1 Measured* and Calculated (in parentheses) LOBI Initial Steady State Mass Flows, Pump Speeds and Differential Pressures

Parameter	A1-03	A1-04R	A1-04
IL Mass Flow (kg/s)	21.7(21.1)	21.1(21.1)	19.7(19.7)
IL Pump Speed (rad/s)	481.7(496.09)	476.5(497.90)	439.8(470.71)
BL Mass Flow (kg/s)	7.1(7.1)	7.0(7.0)	5.9(5.9)
BL Pump Speed (rad/s)	377.0(393.56)	377.0(396.77)	298.5(337.87)
PD121371 (kPad)	50(140.5)	110(144.3)	105(123.7)
PD151456 (kPad)	290(297.4)	260(306.1)	220(261.1)
PD222317 (kPad)	140(139.4)	---(140.2)	100(98.8)
PD252451 (kPad)	290(293.1)	---(295.7)	190(211.5)
PD161137 (kPad)	100(110.6	102(113.5)	---(97.1)
PD262133 (kPad)	100(92.0)	110(93.5)	---(71.6
PD163133 (kPad)	≲10(20.5)	≲10(21.2)	≲10(18.1)
PD263137 (kPad)	≲10(13.3)	≲10(13.6)	≲10(8.5)
PD313333 (kPad)	57(45.5)	52(44.6)	---(45.0)
PD313770 (kPad)	45(45.5)	50(44.6)	---(45.0)
PD363711 (kPad)	100(91.0)	95(91.1)	85(83.3)
PD381147 (kPad)	40(44.1)	40(45.3)	29(40.3)
PD382143 (kPad)	30(32.7)	30(32.9)	20(24.4)
PD383940 (kPad)	34(47.4)	32(36.9)	---(48.1)

*Estimated from small plots in Experimental Data Reports

Table 2.1.3.2 Measured and Calculated (in parentheses) LOFT Initial Steady State Mass Flows, Pump Speeds and Differential Pressures*

Parameter	L6-7/L9-2	L9-1/L3-3	L3-6/L8-1	L5-1/L8-2	L2-5
Mass Flow (kg/s)	483.7±2.6 (482.5)	479.1±2.6 (479.5)	483.0±2.6 (483.7)	308.2±4.0 (308.0)	192.4±7.8 (195.9)
Pump Speed (rad/s)	336.7±1.3 (330.5)	335.1±1.2 (331.2)	336.1±1.2 (332.9)	209.4±2.9 (208.7)	131±3.3 (134)
PdE-PC-001 (kPad)	473±10 (458)	462±5 (460)	470±10 (465)	195±10 (187)	73±2 (75)
PdE-PC-002 (kPad)**	249±5 (280)	242±5 (277)	252±5 (282)	104±3 (112)	38.5±2 (46)
PdE-PC-003 (kPad)	24±2 (33)	25±2 (31)	23±2 (33)	7.5±2.5 (12)	3±2 (6)
PdE-PC-005 (kPad)	24±2 (26)	24±2 (23)	24±2 (25)	10±3 (9)	5.5±2 (4)
PdE-PC-006 (kPad)	---	---	---	---	28±2 (19.5)
PdE-PC-008 (kPad)	---	---	---	4±2 (2.5)	---
PdE-PC-009 (kPad)	---	480±5 (478)	485±10 (484)	---	---
PdE-PC-010 (kPad)	505±5 (476)	488±5 (478)	495±8 (484)	208±8 (195)	70±3 (78)
PdE-PC-027 (kPad)	---	34.6±2 (34)	---	20±5 (8)	---
PdE-PC-028 (kPad)	---	-19±3 (-22)	-21±3 (-35)	-7.5±5 (-9)	---
PdE-RV-005 (kPad)	68±1 (58)	---	---	28±2 (25)	---
PdT-P139-030 (kPad)**	182±2 (118.5)	182±2 (129)	187±4 (124.6)	70±3 (54)	26±1 (19.5)

*Uncertainties on differential pressure represent range of oscillations ("hash") seen in data.

**Both these measurements involve one point at the hot leg density and the other at the cold leg density; we are not sure how the instrumentation was adjusted to zero out the gravity heads.

Table 2.1.3.3a Measured and Calculated (in parentheses) Semiscale Mod-3 Initial Steady State Mass Flows, Pump Speeds and Differential Pressures

Parameter	S-SB-P1	S-SB-P7	S-SB-P3	S-SB-P4
Vessel				
Core Flow (kg/s)	10.5(10.6)	10.4(10.3)	10.3(10.1)	10.4(10.5)
DD-DIA-13V (kPad)	175(158.4)	170(153.4)	180(152.8)	190(155.7)
DD-DIA-578 (kPad)	55(53.5)	55(52.2)	56(51.9)	58(52.7)
DV-578-501 (kPad)	13(14.1)	12(13.6)	13(13.5)	14(13.9)
DV-501-105 (kPad)	89(82.2)	85(79.3)	93(78.4)	97(80.6)
DV-105-13 (kPad)	18(8.6)	17(8.3)	19(8.2)	20(8.5)
Intact Loop				
Pump Speed (rad/s)	247(252)	243(247)	243(250)	244(257)
DI-13V-1A (kPad)	15(0.8)	14(0.8)	14(0.8)	15(0.7)
DI-1A-6 (kPad)	4(5.7)	4(5.4)	3.2(5.4)	3.6(5.4)
DI-6-7 (kPad)	290(284.1)	280(275.3)	265(271.7)	280(367*)
DI-7-13 (kPad)	11(13.2)	10(12.8)	9.6(13.8)	10.2(13.8*)
DI-13-15 (kPad)	-510(-464.2)	-490(-449.6)	-490(-445.6)	-520(-544.6*)
DI-15-17A (kPad)	9.5(2.2)	9.3(2.2)	8.7(2.1)	9.3(2.2)
DI-17A-DIA (kPad)	1.6(-0.2)	1.6(-0.3)	1.2(-0.2)	1.2(-0.3)
Broken Loop				
Pump Speed (rad/s)	1629(1287)	1599(1272)	1592(1249)	1645(1300)
DB-13V-20B (kPad)	14(10.2)	14(9.8)	14(9.7)	15(10.8)
DB-20B-21 (kPad)	10(4.3)	10(4.2)	---	---
DB-20B-26 (kPad)	---	---	29(7.6)	31(8.1)
DB-21-27A (kPad)	280(253.3)	280(245.1)	---	---
DB-26-27A (kPad)	---	---	250(239.2)	270(257.3)
DB-27A-28 (kPad)	14.5(11.5)	15(11.1)	8.3(11.1)	-(11.6)
DB-28-29 (kPad)	10(8.9)	7(8.5)	5(8.3)	1.4(9.5)
DB-29-40B (kPad)	-535(-457.2)	-520(-442.3)	---	---
DB-29-45A (kPad)	---	---	-490(-432.6)	-545(-458.1)
DB-40B-45A (kPad)	18(5.7)	18(5.5)	---	---
DB-45A-DIA (kPad)	0.5(4.9)	0.7(4.7)	0.9(4.7)	1.0(5.1)

*Not converged

Table 2.1.3.3b Measured and Calculated Semiscale Mod-2A Initial Steady State Mass Flows, Pump Speeds and Differential Pressures

	Parameter	S-UT-1	S-UT-2	RELAP	S-UT-6	S-UT-7	RELAP	S-UT-8	RELAP
IL	Mass Flow (ℓ/s)	10.7	10.5	10.0	9.4	9.4	8.7	10.3	9.9
	Pump Speed (rad/s)	229.9	225.4	227.0	199.0	198.0	196.0	244.0	226.0
	D-V13A*I1 (kPad)	---	---	---	14.37	14.22	2.9	16.72	3.3
	DPI*1*6 (kPad)	4.8	5.1	14.2	5.73	5.79	11.1	---	---
	DPI*1*3C (kPad)	---	---	---	---	---	---	7.45	9.0
	DPI*1*3C-G55E (kPad)	---	---	---	---	---	---	44.2	23.7
	DPI*6-IG55 (kPad)	---	---	---	failed	failed	17.0	---	---
	DIG-55E55X (kPad)	---	---	---	137.3	135.9	145.3	158.6	164.4
	DP*IG-55*7 (kPad)	---	---	---	-10.14	-10.14	-9.8	---	---
	DPI*6*7 (kPad)	158.4	169.9	208.4	---	---	---	---	---
	DPI*7*9 (kPad)	-15.5	-15.5	-16.6	-16.17	-16.21	-13.4	---	---
	D*IG55X-9D (kPad)	---	---	---	---	---	---	-2.33	5.4
	DPI*7*13 (kPad)	8.4	8.3	3.9	---	---	---	---	---
	DPI*9*13 (kPad)	23.6	25.1	20.5	23.94	23.88	18.2	---	---
	DPI*9*14 (kPad)	---	---	---	---	---	---	-22.46	-24.0
	DPI*13*15 (kPad)	-403.5	-392.0	-379.7	-303.16	-302.56	-279.2	---	---
	DPI*15*17 (kPad)	5.8	5.9	3.0	2.18	2.11	1.8	---	---
	DPI*18*21 (kPad)	---	---	---	---	---	---	-438.5	-376.8
	D*I17+VD29 (kPad)	---	---	---	18.9	18.74	-0.5	---	---
	D+29-13A (kPad)	---	---	---	133.9	133.4	106.3	---	---
	LI1112+90 (kPad)	36.1	29.0	58.1	---	---	---	---	---
BL	Mass Flow (ℓ/s)	3.48	3.77	3.42	2.8	2.8	2.63	3.3	3.3
	Pump Speed (rad/s)	1725.	1714.	1514.4	975.	974.	1200.	1192.	1486.
	D-V13A*B50 (kPad)	---	---	---	---	---	---	13.92	6.6
	DPB*50*55 (kPad)	---	---	---	---	---	---	7.44	6.9
	D-V13M*20B (kPad)	---	---	---	14.58	14.47	4.5	---	---
	DPB*20B*21 (kPad)	7.8	7.8	7.5	4.42	4.46	4.6	---	---
	DPB*21*27 (kPad)	248.8	242.4	234.7	---	---	---	---	---
	DPB*21*22 (kPad)	42.3	42.0	21.6	---	---	---	---	---
	DPB*22*26 (kPad)	321.9	325.2	215.6	---	---	---	---	---
	DPB*26*27 (kPad)	13.9	14.9	-1.1	---	---	---	---	---
	DPB*21BG55 (kPad)	---	---	---	26.24	28.93	19.8	---	---
	DPG-55E55X (kPad)	---	---	---	105.9	104.4	122.6	151.8	186.6
	DB-G55X*64 (kPad)	---	---	---	---	---	---	4.08	0.5
	D*BG-55*27 (kPad)	---	---	---	7.29	6.79	0.6	---	---
	DPB*27*28 (kPad)	-15.2	-14.8	-10.2	-17.74	-17.84	-16.7	---	---
	DPB*27*31B (kPad)	---	---	---	5.64	5.41	-1.1	---	---
	DPB*28*37B (kPad)	30.3	30.2	18.4	23.54	23.44	15.6	---	---
	DPB*37B*40B (kPad)	-477.0	-486.1	-413.8	-316.95	-308.55	-258.7	---	---
	DPB*40B*41D (kPad)	10.7	11.7	3.7	---	---	---	---	---
	DPB*40B*41U (kPad)	---	---	---	7.21	7.14	1.1	---	---
	DPB*41U*45 (kPad)	---	---	---	7.21	7.24	1.4	---	---
	DPB*65*73 (kPad)	---	---	---	---	---	---	---	---
	DPB*73*74 (kPad)	---	---	---	---	---	---	---	---
	D*B45+VD29 (kPad)	---	---	---	0.72	0.74	-1.4	---	---
	LB1112+90 (kPad)	30.4	---	47.0	---	---	---	---	---

Table 2.1.3.4 Measured and Calculated PKL and Semiscale MOD-2A Steady State Natural Circulation Mass Flows

Test Parameter	Measured	RELAP5
PKL ID1-4	4.55	4.555
S-SN-2		
30 kW	0.29	0.30
60 kW	0.36	0.40
100 kW	0.44	0.48
S-NC-7		
Intact Loop	0.447-0.43*	0.44
Broken Loop	0.123-0.14*	0.13
Downcomer	0.57	0.57
S-NC-8		
Intact Loop	0.396	0.411
Broken Loop	0.121	0.128
Total Loop	0.517	0.539
Downcomer	0.532	0.584
Bypass	?	-0.044

*Variation between S-NC-7B and S-NC-7C

Table 2.1.4.1 Secondary Side Equivalent Diameters Defined on the U-tube Outer Surface for Various Facilities

		Heated Equivalent Diameter	
	#Tubes	Geometric (m)	Reduced (m)
LOFT	1845	0.0187	0.0064
Semiscale Mod-3			
Intact Loop	53	0.0329	0.0064
Broken Loop	11	0.0706	0.0095
LOBI			
Intact Loop	18	0.0747	0.0080
Broken Loop	6	0.0758	0.0080
(for comparison) Westinghouse			
Type 51	3388	0.0495	0.0103

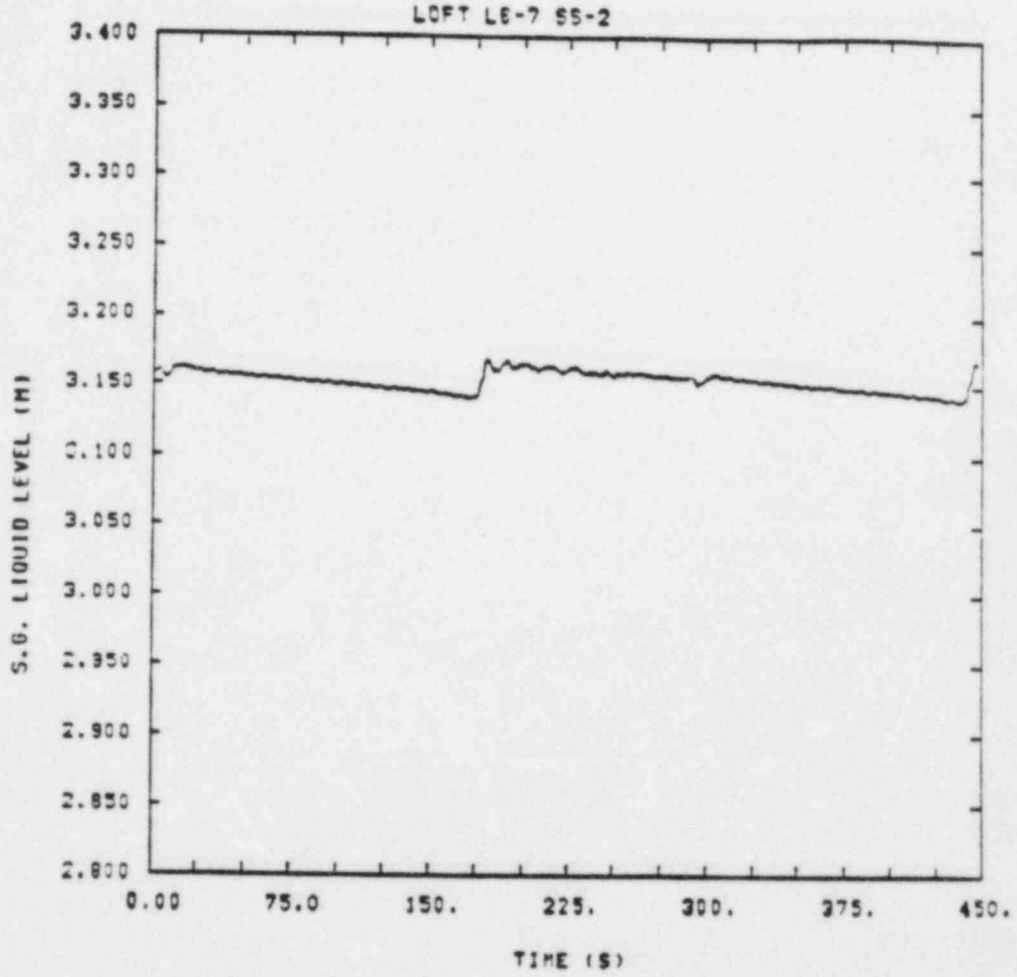

Figure 2.2.2.1 Secondary Side Downcomer Liquid Level for LOFT L6-7 Steady State Initialization Calculation

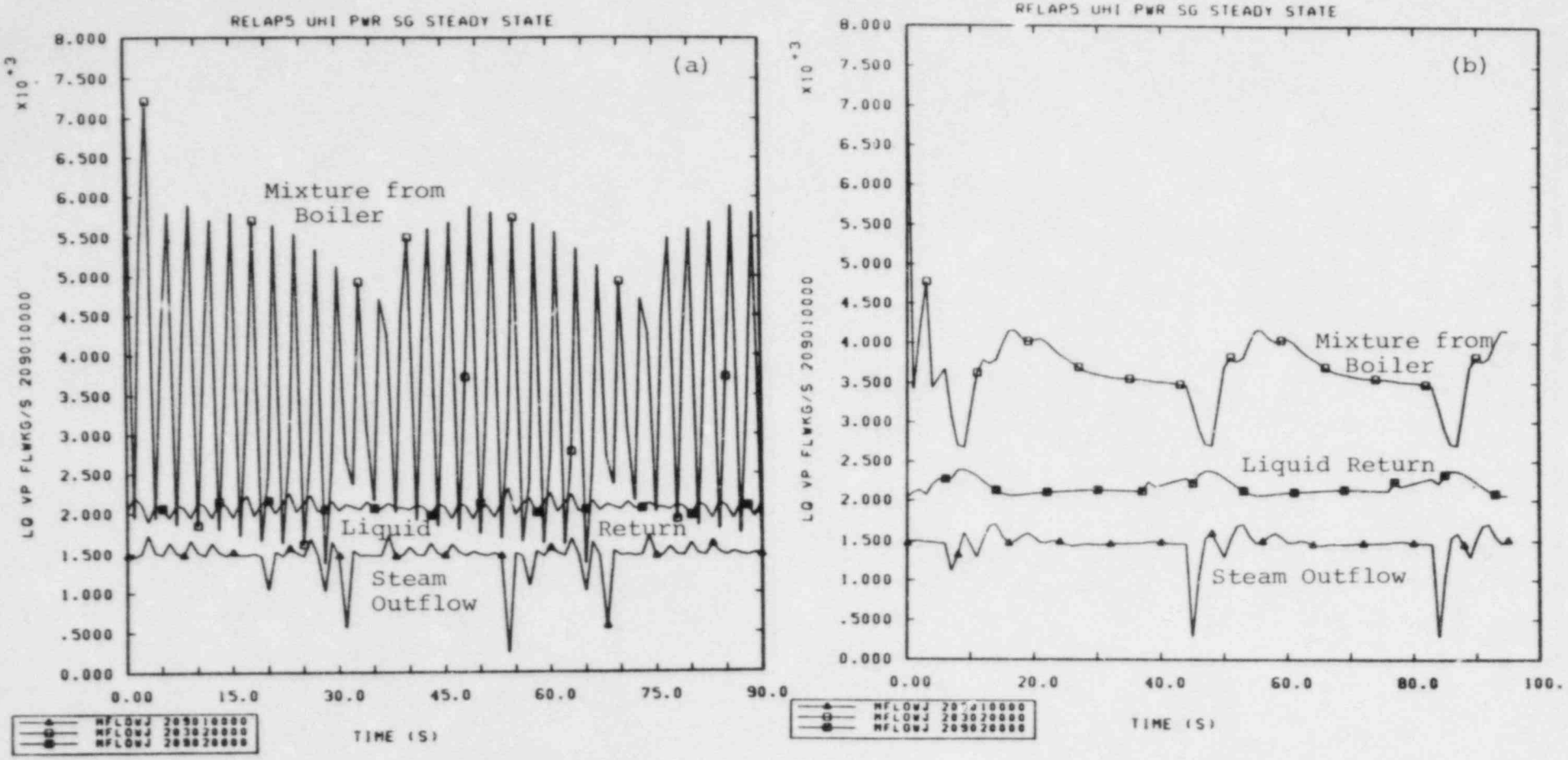

Figure 2.2.4.1 Recirculation Flow Oscillations Reduced by Lowering Time Step from (a) Δt = 5 ms to (b) Δt = 2.5 ms

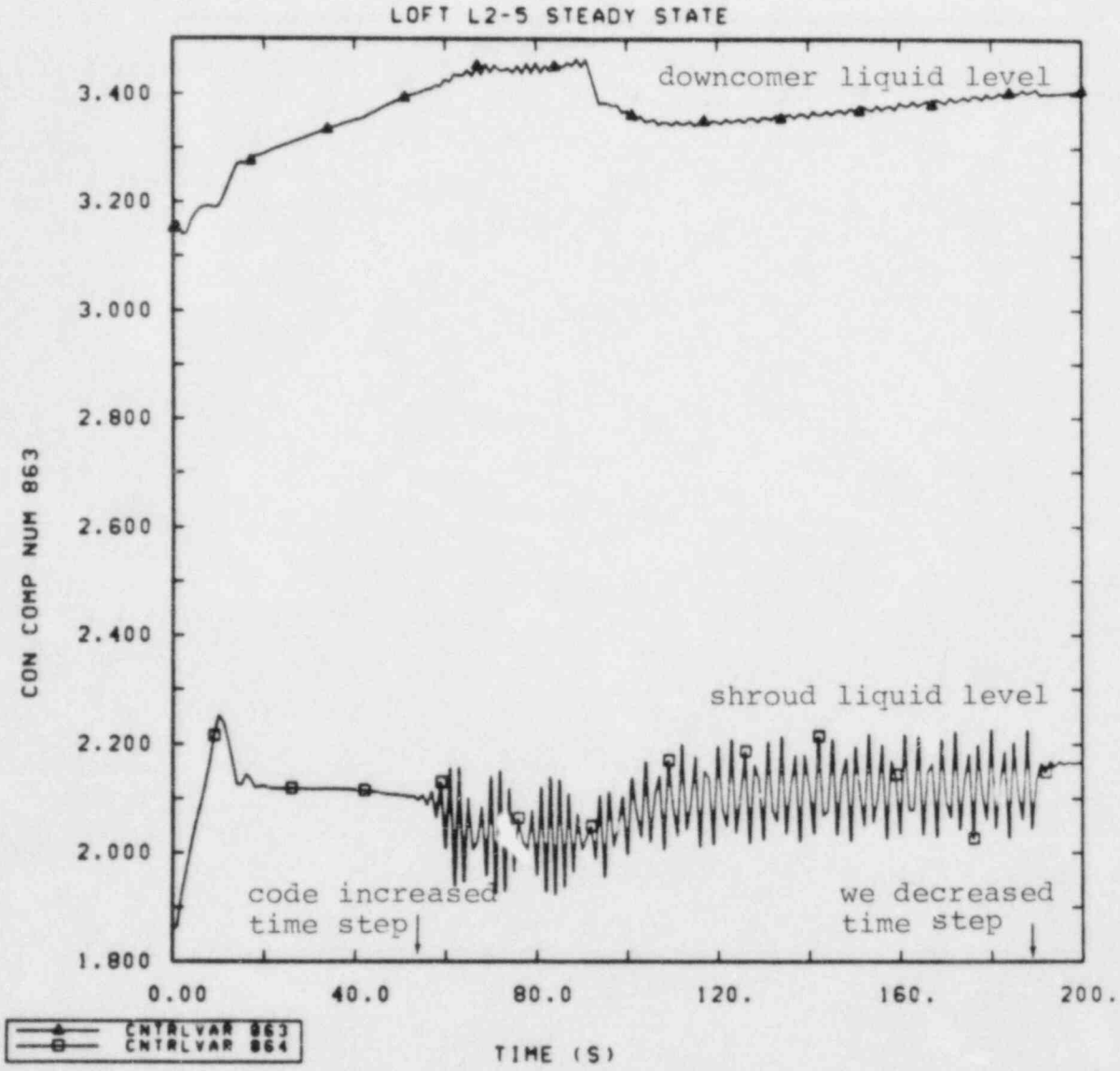

Figure 2.2.4.2 Secondary Side Downcomer and Shroud Liquid Levels for LOFT L2-5 Steady State Initialization Calculation

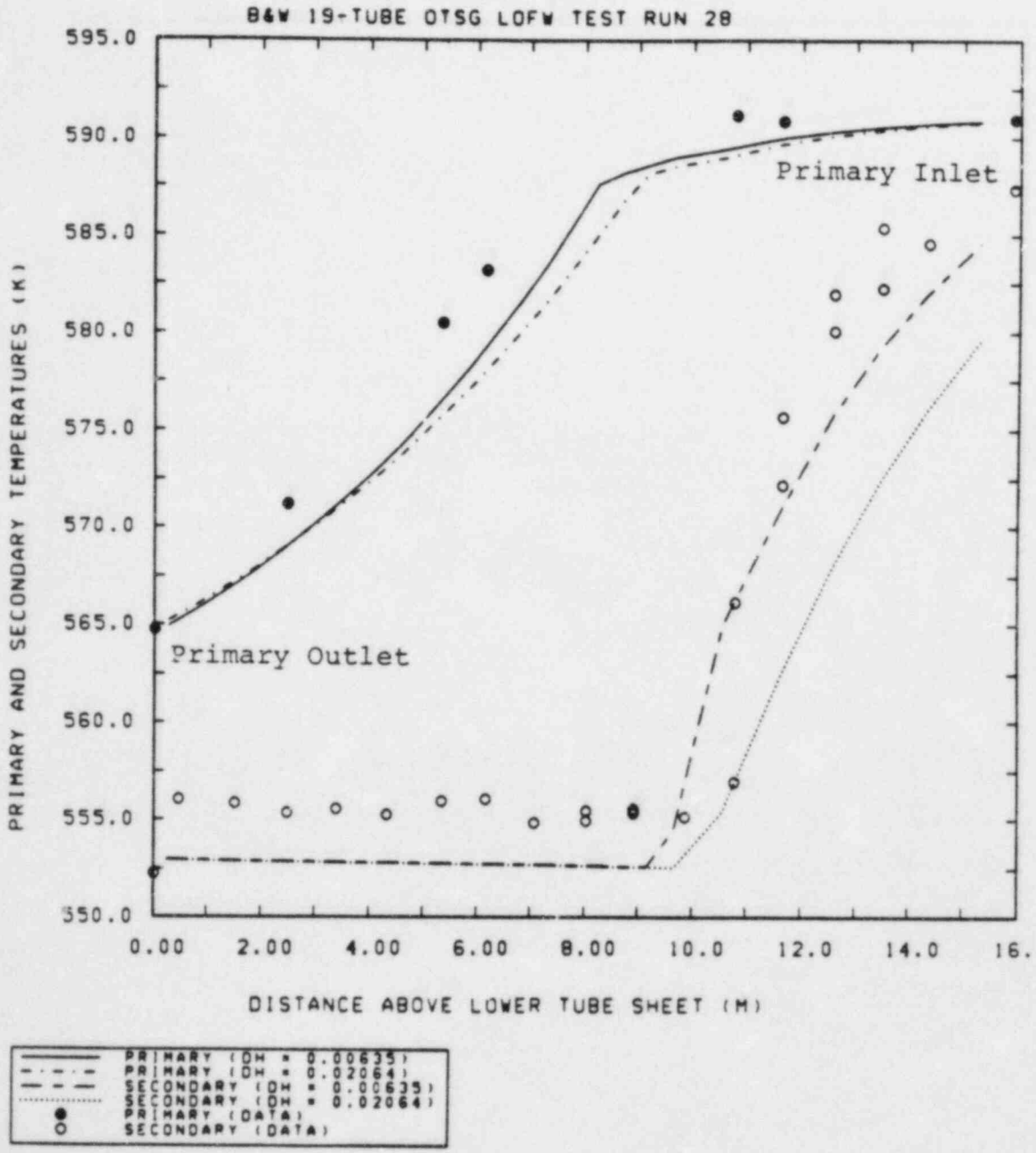

Figure 2.3.1 Primary and Secondary Temperature Profiles Using Geometric and Minimum Tube-to-Tube Spacing Equivalent Diameters for B&W Once-Through Steam Generator Steady State Test 28

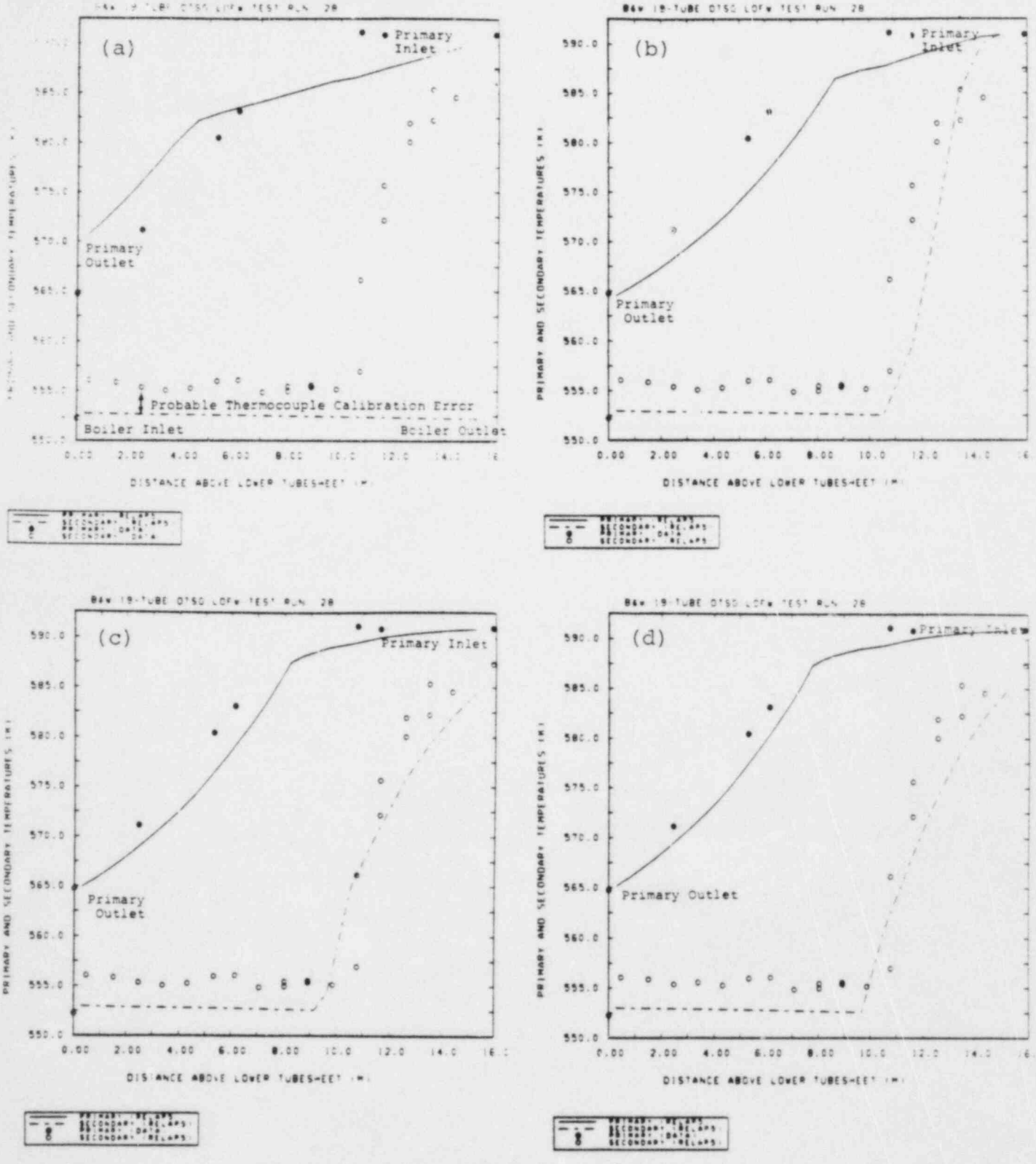

Figure 2.3.2 Primary and Secondary Temperature Profiles Using (a) MOD1 "as Released", (b) MOD1 With CHF Modifications, (c) MOD1 With CHF and Heat Transfer Modifications and (d) MOD1.5 for B&W Once-Through Steam Generator Steady State Test 28

Table 2.3.1 B&W Once-Through Steam Generator Test 28
Steady State Initial Conditions

	Exp.	Released MOD1	Modified MOD1	MOD1.5
Input Boundary Conditions:				
Primary Inlet Temp (K)	591	591	591	591
Primary Mass Flow (kg/s)	11.6	11.6	11.6	11.6
Primary Pressure (MPa)	14.7	14.7	14.7	14.7
FW Inlet Temp (K)	512 [a]	510	510	510
FW Mass Flow (kg/s)	0.9	0.9	0.9	0.9
Secondary Pressure (MPa)	6.3	6.3	6.3	6.3
Calculated Parameters:				
Primary Outlet Temp (K)	565	570	565	565
Primary ΔT (K)	26	21	26	26
Steam Discharge Temp (K)	587 [a]	553	584	585
Boiler ΔP (MPa)	72	55	74	76
Sec. Mass Inventory (kg)	21 [b]	26	27	26

[a] Measured by uncalibrated thermocouple; probably high by ~2 K.

[b] Integrated steam flow minus feedwater flow; does not include ~4 kg of steam left in steam generator at end of transient.

3.0 TRANSIENT CALCULATIONS

As mentioned in the introduction, we are attempting to summarize the results and conclusions of our RELAP5/MOD1 assessment project in a form permitting easy application to proposed future calculations, either for further experimental verification analyses or for required plant licensing analyses. This section represents the heart of this effort; while the results of individual assessment calculations are discussed in detail in the appropriate topical reports, here we concentrate on comparing similarities and differences in the various analyses done, hopefully allowing us to extrapolate the behavior that might be expected in later calculations.

The subsections are divided into three major classes:

-- primary side hydraulic response (such as system pressure, break flow and mass inventory behavior),

-- core thermal response (such as peak clad temperature, and core reflood and quench behavior), and

-- secondary side thermal/hydraulic response (such as steam pressure and downcomer temperatures).

Each subsection is further divided into the major recognized accident scenarios, i.e., large, intermediate and small breaks, and operational transients. In some cases (e.g., small breaks), we have a plenitude of assessment calculations for comparison purposes; in others (e.g., intermediate breaks and operational transients), we have only a few. However, since the same behavior is sometimes observed in more than one class of transients, even the relatively few intermediate break calculations done result in some surprisingly firm conclusions when combined with the results of large and/or small break analyses done.

3.1 Primary Side Hydraulic Response

For the purposes of this discussion, the major variables describing the primary side hydraulic response are considered to be the primary side system pressure and the break flow(s), if any. A number of closely-related variables can also be included. The primary temperatures are usually equal to the saturation temperature corresponding to the primary system pressure. The primary side mass inventory and density distribution throughout the system are closely related to the break flow. The density distribution determines the characteristics of any natural circulation occurring, which can determine the loop temperatures.

Results to date indicate that the RELAP5/MOD1 code generally does a good-to-excellent job predicting primary system pressure and break flow in large and intermediate break LOCAs, even when other features (such as pump coastdown and/or ECC injection) are not correctly calculated. The results for numerous small break analyses are usually not as good, largely because of known code errors and/or limitations, and because of increased dependence on not-well-known boundary and/or initial conditions. Qualitative behavior is often reproduced during small break analyses, but slow drifts away from the correct results (due for example to errors in core decay heat) and/or relatively constant offsets (due for example to errors in initial conditions) are observed quantitatively. Results from two operational transient analyses generally show poor quantitative agreement with data in early calculations, although in one case it proved possible to force good agreement after a number of "esoteric" model changes (where "esoteric" is taken to mean non-standard model changes which may work in one particular instance through hindsight, but are not recommended for general application).

3.1.1 Large and Intermediate Breaks

The results for the three LOBI large break tests analyzed [12] were all quite similar. Figure 3.1.1.1a shows the pressure in the intact loop cold leg and the broken loop upstream of the pump-side break for test A1-04R (the most similar to a design-basis cold leg break); the overall agreement between calculation and experiment is excellent. When the hot leg saturation pressure is reached, flashing starts and the depressurization rate decreases; flashing in the intact loop cold leg then begins, causing a further decrease in the depressurization rate (slightly underpredicted by the code). After ~25 s the accumulator activation pressure is reached and the accumulator injection starts. The saturated discharge coefficient applied at both break junctions was chosen by checking that this pressure is reached at the right time; we found a standard value of 0.85 gave good agreement with data in all three calculations.

Pressures near the break fall immediately to saturation and are then governed mainly by the break flows; during most of the blowdown, critical flow conditions exist at both discharge nozzle throats. Due to the large flow resistance of the pump and steam generator, the pump-side break flow (Figure 3.1.1.1b) is limited. However, subcooled water is supplied directly to the vessel-side break from the downcomer region, leading to prolonged subcooled conditions upstream of that break and consequently large initial vessel-side break flows (Figure 3.1.1.1c; the "truncated" peak flow in the data appears due to instrument problems since it is not observed in the other two tests). These peak break flows were

used to select the subcooled discharge coefficient; we found a standard value of 1.0 gave the best overall agreement for both pump-side and vessel-side peak flows in all three tests analyzed. The calculated break flows are generally in good agreement with data, although the pump-side flow is high around 5-15 s and the vessel-side flow is low over the same time, resulting in a net underprediction of system depressurization in this period, but no long-term deviations are visible.

Results of the two LOFT intermediate break tests analyzed [19] were also quite similar; the L5-1 results are discussed because the primary mass inventory data is available for comparison. Figure 3.1.1.2a shows measured and calculated primary pressures; the agreement is excellent throughout most of the transient, although there is a growing discrepancy at later times (125-175 s) with the experimental facility depressurizing more slowly than calculated. Since accumulator injection is initiated by a low pressure signal, we calculated it to begin ~18 seconds earlier than occurred in the experiment; this earlier injection in turn causes further pressure discrepancies. A possible reason for faster calculated depressurization could be overestimation of the break flow and underprediction of primary inventory at later times.

Overall agreement in break flow (Figure 3.1.1.2b) is quite good, with calculated subcooled break flow during the first ~20 s slightly lower than measured, and saturated break flow in the middle of the transient a bit high. Discharge coefficients of 1.0 were used for subcooled and saturated break flow; although no sensitivity studies were done, the results indicate a saturated discharge coefficient of 0.85, such as used in the LOBI analyses, might give better late time pressure and break flow agreement. Calculated and measured primary inventories (Figure 3.1.1.2c) are fairly close until ~80 s, when the calculated inventory begins falling below the experimental estimate, probably because of somewhat high calculated break flow between 70 and 150 s. By the time of accumulator injection, the calculated inventory is only 430 kg while the experimental estimate is 840 kg. Accumulator injection is visible as an increase in inventory, with analysis and experiment in good agreement except for timing and initial value, as expected with the flow being supplied as a boundary condition. (The HPIS flow is so low, ~0.5 kg/s, compared to the break flow, that small errors in the calculated value do not have a significant effect on the overall results.)

The intact loop cold leg pressure for the LOFT L2-5 large break transient [22] is shown in Figure 3.1.1.3a; despite slightly overpredicted depressurization around 5-10 s and later-time (~30-70 s) pressure oscillations traceable to the effects of ECC injection, overall agreement with data is very

good. The early-time calculated pressure agreed better with data when a double-downcomer nodalization with high crossflow resistance was tried, but the late-time pressure agreement with data did not change.

The vessel-side (cold leg) and pump-side (hot leg) break flows are shown in Figures 3.1.1.3b and 3.1.1.3c; again, the overall agreement between analysis and data is reasonably good, using standard subcooled and saturated discharge coefficients of 0.85. There are, however, some discrepancies in calculated and measured break flows (and in core response, discussed below in Section 3.2.1) due to excess ECC bypass being calculated, which prompted us to try the double-downcomer model. Figure 3.1.1.4 shows that, after the start of ECC injection at ~15 s, both analyses lose significantly more mass than occurred in the test, with the original single-downcomer calculation losing the most mass. However, the double-downcomer loses relatively more mass out the pump-side (hot leg) break, indicating that some ECC water is now being delivered to the lower plenum and being swept up the core before being lost from the system.

The excess ECC bypass being calculated is not particularly surprising; analyses of BCL 2/15th-scale vessel/ECC separate effects tests [9,11,25] indicate that a single-downcomer model will calculate prolonged ECC bypass, while a split-downcomer model is required to calculate any ECC penetration into the downcomer and delivery of liquid to the lower plenum. This was a known problem with the RELAP4 code [32], and has been reported by others for RELAP5 analyses [33], although it is rather surprising that the problem has not yet been formally resolved.

All of this is in dramatic contrast to claims often made (by others) that the break flow model is the major source of calculated discrepancies with experiment in many analyses. The results of our assessment project indicate that the break flow, and the associated primary pressure response, are well-predicted in large and intermediate break analyses even when many other features are not correctly calculated. In our analyses to date the major source of disagreement is probably the "condensation model" (more strictly, the interphase mass transfer and its possible nonequilibrium effects), and associated difficulties in calculating correct ECC bypass/delivery behavior.

3.1.2 Small Breaks

The small break assessment calculations show a marked sensitivity to code errors and/or modelling limitations, and to initial and/or boundary conditions specified. These analyses do not identify any major code difficulties not already being

addressed by the RELAP5 code developers; however, they do identify or verify a number of problems with the experimental data available for code assessment (discussed in more detail later in appendix I).

The LOFT L3-6/L8-1 small break analysis [18] was one of the earliest assessment calculations we did, using cycle 14. The results for the primary system hydraulic response appear to verify the existence of a code "reactor kinetics error", corrected by an update in cycle 18, that "makes decay heat too low" [34]. The calculation unfortunately was too long-running and expensive to repeat with cycle 18 to quantify the effect of this correction, although estimates based on other cycle 14/cycle 18 comparisons imply a cycle 18 rerun of the L3-6/L8-1 transient should be in much better agreement with data, since the decay heat calculated by cycle 18 seems to be generally ~10% higher than the decay heat calculated by cycle 14 (as discussed below in section 3.2.2).

Figure 3.1.2.1a shows the calculated and measured primary system pressures for the L3-6 transient. Agreement between data and analysis is excellent at early times but there is growing disagreement later in the test as the system depressurizes ~18% more slowly than calculated. (Since the L3-6 portion ends on a low pressure trip, it is thus calculated to end ~400 s earlier than actually occurred.) This discrepancy between calculated and measured depressurization rates could be caused by overprediction of steam generator heat transfer, overestimating break flow, overestimating environmental heat loss and/or underestimating core decay power; small errors in any or all of the above could lead to small errors in the depressurization rate and to significant cumulative errors in primary pressure at late times.

We believe the primary source of the pressure discrepancy to be the underprediction, by ~20% as shown in Figure 3.1.2.1b, of the core decay heat throughout most of this long transient. This error in decay heat is comparable in magnitude to the ~200 kW environmental heat loss modelled (although the large experimental bound quoted, of 200$\pm$100 kW, would also allow improved agreement between calculation and experiment if the heat loss were varied in sensitivity studies). The excellent agreement in primary side mass inventory during the transient, shown in Figure 3.1.2.1c, precludes any significant errors in break flow, although the comparison of calculated and experimental inventory does imply slightly high calculated break flow in the 200-600 s period and slightly low break flow later during 1500-2000 s, confirmed by the break mass flow rates shown in Figure 3.1.2.1d. (No break flow data is given for the first ~50 s of the L3-6 transient.)

The four Semiscale Mod-3 small break analyses [15] were also among the earlier calculations done in our assessment project. The results showed that qualitative aspects of the transients were described well, but a number of quantitative disagreements were seen. The pressure history, as shown in Figure 3.1.2.2a for test S-SB-P1, proved to be very sensitive to initial conditions (with constant offsets due to differences in saturation pressure between actual and calculated steady state temperatures) and to boundary conditions (with further offsets due to missing details of the secondary system response during and after steam generator isolation). Calculated steady state primary temperatures were 2-3 K higher than data, so the calculated saturation pressure was also high by ~0.25 MPa; further, the calculated secondary side temperatures during the first part of the transient were too high (discussed further in section 3.3.3) so the primary and secondary systems equalized at a correspondingly higher pressure. The resulting ~1 MPa offset is then maintained throughout the rest of the transient, since the long-term depressurization rate is correctly calculated.

The primary system mass inventory and break flow in these small break calculations verified known code problems modelling break flow through an uncovered orifice for stratified conditions in the pumps-off tests, and also a known facility problem modelling the broken loop pump with outdated and/or inapplicable homologous curves. Figure 3.1.2.2b shows the primary system inventory for a test with early pump trip resulting in natural circulation and stratified flow conditions. The agreement between calculation and experiment is very good until ~400 s, when the stratified liquid level drops below the break orifice (centered in the side of the pipe) and pure steam discharge begins; the MOD1 code has no capability to model this situation and continues discharging a two-phase mixture which corresponds to homogenizing the donor-cell stratified mixture, with the excess liquid loss resulting in a more rapid decline in primary inventory.

Figure 3.1.2.3a shows calculated and measured pressures for the corresponding pumps-on test. Early in the transient, the curves exhibit the constant pressure offset discussed above; later, the calculated depressurization rate is substantially greater than measured and the gap between the two curves narrows. During this period, the calculated broken loop mass flow shown in Figure 3.1.2.3b and, by inference, the break flow is also much higher than measured. (No actual break flow measurements are available.) This persists until ~1200 s, when the calculated depressurization rate begins to agree well with data. The cause of the high flow is shown in Figure 3.1.2.3c; during the time of interest, the calculated broken loop pump head is significantly higher than measured. The broken loop homologous pump curves contain two known "errors" than cannot be corrected by any

analyst; the single-phase curves were characterized before the venturi nozzle currently in place was substituted for the originally-present orifice, and the two-phase curves used are those which were developed for the (different) intact loop pump since the broken loop pump has only been characterized for single-phase conditions.

The five Semiscale Mod-2A small breaks analyzed [24] were among the last calculations done in this assessment project. As with our other small break analyses, much of the qualitative behavior was reproduced by the calculated results; however, a large number of discrepancies remain, and uncertainties in the facility geometry and measurements make drawing firm conclusions difficult. Primary depressurization was overpredicted throughout the two 10% breaks, and generally underpredicted in the three 5% breaks after loop seal clearing. The results for the 10% break tests are somewhat contradictory: the calculated primary side pressure and mass inventory are both low compared to data, particularly at later times, which is internally consistent; the calculated break flow and total mass lost out the break are also both low compared to data, which is again internally consistent, but not reconcilable with the pressure and inventory behavior.

The three 5% breaks analyzed show much more consistent behavior, possibly because new instrumentation was added to more accurately measure the break flow. Figure 3.1.2.4 shows measured and calculated primary side pressures and mass inventories for (the basecase) test S-UT-6. As seen in Figure 3.1.2.4a, early time pressure agreement is very good until the intact loop pump suction clears at ~200 s in both calculation and experiment, when the measured depressurization accelerated but the calculation did not. The recovery to data at late times allowed calculated accumulator injection to begin within 20 s of the observed time, and is probably due to slightly higher calculated break flows after ~400 s, as indicated by Figure 3.1.2.4b.

Very similar results were obtained for test S-UT-8, which was a counterpart test to S-UT-6 except for a different core bypass flow rate and different upper vessel geometry. The pressure in the S-UT-7 analysis (the UHI counterpart to S-UT-6) also showed excellent agreement with data at early times, as seen in Figure 3.1.2.5a; the calculated depressurization probably would have also slowed down compared to measurement when the intact loop pump suction cleared at ~200 s, but for the effect of a large surge of UHI accumulator water calculated to occur at ~225 s. The timing of several such flow surges can be seen in the discontinuous behavior of the UHI accumulator pressure shown in Figure 3.1.2.5b; such flow surges have been calculated in other assessment calculations (as discussed below in section 4.1.3).

The change in measured accumulator depressurization at ~300 s, on the other hand, represents the accumulator flow being valved off, and the later slow pressurization is due to heat transfer from the accumulator walls to the gas.

3.1.3 Operational Transients

LOFT turbine trip transient L6-7/L9-2 [16] was the first analysis done in our assessment project; we performed a number of calculations, which fall into three main categories. "Blind" analyses, using limited test data in initialization, were done first; actual experimental data, particularly for the secondary side boundary conditions, had to be used because the EOS was insufficient (for L6-7) or incorrect (for L9-2). The primary system pressure (shown in Figure 3.1.3.1a), intact loop hot and cold leg temperatures (Figure 3.1.3.2a) and mass flow (Figure 3.1.3.2b) are in good agreement with data through the L6-7 portion of the test, out to ~325 s, which is not surprising since the primary and secondary pressures are then closely coupled and the secondary pressure is used as a boundary condition. After the pump trip ending L6-7 and initiating L9-2, the calculated results deviate significantly from measured data, with greater primary depressurization and smaller loop temperature differences (the latter primarily caused by too-large natural circulation flows).

Our first normal posttest calculations concentrated on the long-term qualitative pressure discrepancies. With the stagnant broken loop isolated from the "cooldown" effects of unphysical oscillations in the bypass and leakage flow paths (discussed in detail in Section 4.2), the desired late-time pressure plateau was obtained, as shown in Figure 3.1.3.1b; this plateau correctly corresponds to the saturation pressure associated with the broken loop initial temperature, but is reached too early and does not persist long enough. The intact loop temperatures and mass flow did not visibly change from the "blind" calculations, as seen in Figures 3.1.3.2c and 3.1.3.2d. Our final posttest calculations showed excellent agreement with experimental data, but only after several more model changes. The most important were modifying the homologous pump curves to force the correct natural circulation flow (Figure 3.1.3.2f) and associated loop temperature difference (Figure 3.1.3.2e), and using the nonstandard equilibrium option in the broken loop at late times (also discussed in Section 4.2) to hold up the system pressure (Figure 3.1.3.1c); a minor change, adding a heat slab modelling the upper plenum internal structure, helped calculate the intermediate pressure plateau at ~9 MPa.

(Similar esoteric model changes and code updates were also used in the INEL posttest analysis [35], including increasing the pump "locked rotor hydraulic resistance" by modifying the pump homologous curves to match experimental flow data during natural circulation, and updating the code interphase drag model to change the magnitude of the nonequilibrium effects being calculated. These changes were not clearly identified in the main text of the posttest analysis report, but were alluded to within one of the appendices and included on the attached microfiche listing. No results from INEL posttest analyses with the unmodified MOD1 code were reported.)

LOFT loss-of-feedwater with recovery transient L9-1/L3-3 [17] was the second analysis begun in our code assessment project. The results were similar to the early results from the L6-7/L9-2 analyses, but the L9-1/L3-3 calculation was not pursued as far (in the sense of reruns and model changes) because of its greater cost. The measured secondary pressure was specified as a boundary condition, because undetermined leakage in the steam valve resulted in significant depressurization throughout L9-1. The first calculations showed the correct qualitative behavior, but occurring substantially earlier in time than measured, because of excessive system heatup; this excessive heatup prompted us to include ~200 kW environmental heat loss (steady state) in all our LOFT models. Subsequent calculations showed better agreement with data but significant discrepancies were still visible (as shown in Figure 3.1.3.3). The greater heatup, of course, directly causes the early onset of PORV cycling.

At this stage the L9-1 analysis was run to completion, at ~3250 s, and we began work on L3-3, despite the disagreements in the calculated and measured conditions at the end of L9-1; the L3-3 analysis was run through the (locked-open) PORV discharge period and the first steam generator refill period. Most of this calculation was plagued with recurrent code failures (discussed below in Section 4.2). The final L3-3 results show the correct qualitative pressure and temperature behavior calculated for the primary system, with constant offsets due to the difference in saturation pressure corresponding to calculated and measured temperatures at the end of L9-1 (as shown in Figure 3.1.3.4).

Through hindsight, we now know of some other model changes we should have tried in the L9-1 analysis (although the cost factor renders any reruns currently unfeasible). With more user experience, described in Section 4.2, we know that the PORV should probably have been modelled as a default smooth area change with large user-input loss coefficients, rather than as a geometrically-correct abrupt area change; such a change might have improved the mass and energy transport through the cycling and locked-open PORV, as might have modelling the top of the

pressurizer and the PORV piping in more detail. Also, the INEL posttest analysis report [36], which we later obtained, indicates that another ~100 kW could have been transferred from the primary system to the superheated secondary through wall condensation effects, which the code cannot currently model. However, our experience to date indicates that cycle 14 underpredicts the decay heat by ~10-20% (as discussed in Sections 3.1.2 and 3.2.2), which if corrected would be expected to cause more, not less, heatup. After a year's reflection, the results of the L9-1/L3-3 calculations are still not clearly understood; they are the most enigmatic encountered in the assessment project to date.

3.2 Core Thermal Response

In the discussion presented in this section, the major variable describing the core thermal response is taken to be the rod clad temperature. The peak clad temperature (PCT) occurring during a LOCA is a major measure of the accident severity, with the timing of initial rod heatup, PCT and eventual quench, and the PCT location (in terms of core elevation) also important. Additional related variables are the core liquid level and the thermal condition of the steam exiting the core.

RELAP5/MOD1 does very well (within ~30 K) calculating blowdown peak clad temperatures (PCTs) during large and intermediate break LOCAs after the update "fix" to the reactor kinetics in cycle 18, which results in a higher calculated decay heat. (This update can have a substantial effect on core thermal response, increasing PCTs from those calculated by cycle 14.) The core thermal response during small breaks is generally not as well predicted as for large and intermediate breaks, partly because of difficulties calculating the primary system hydraulic response driving the core thermal response. One cause of some of the discrepant core response seen in small and intermediate break analyses is due to intermittent rewets being calculated because of density oscillations corresponding to fluctuations around the simple MOD1 dryout/rewet criterion of $\alpha=0.96$.

However, even when the calculated PCT is in good agreement with data, its location is sometimes incorrect, with PCT usually calculated to occur in the highest-power core node and the data often showing PCT higher in the core. More generally, the clad temperature agreement is better in the lower half of the core and calculated rod temperatures fall progressively further below data with increasing core elevation. This is not due to any axial power shape uncertainty since the same behavior is seen with electrically heated rods (LOBI) as with nuclear fuel (LOFT). The main reason is that the expected mixture of superheated steam and

entrained saturated droplets (with the heat transfer from the rods to the steam) is not calculated by MOD1, which instead vaporizes all liquid before superheating any steam. Supporting evidence is that, while hot leg superheat is often seen experimentally, much less or no hot leg superheat is calculated.

Reflood and abrupt rod quench are not calculated correctly for large break LOCAs, as might be expected given MOD1's lack of a "reflood model", but rod quench is correctly calculated in intermediate and small break LOCAs, probably because these are less severe accidents.

3.2.1 Large Breaks

Comparisons of calculated rod clad temperatures for LOBI test A1-04R [12] with arithmetic mean values of selected measured heater rod temperatures are shown in Figure 3.2.1.1. DNB is both measured and calculated for the entire heated length at ~1 s. The maximum heater rod temperature of 823 K is measured in the high-powered middle section of the bundle at 3.2 s, just before the first power ramp; the calculated PCT (820 K) is in excellent agreement with the measured PCT, and is found at the top of the high-powered middle section of the bundle at the time of the first power step. The reduction in power and the improved cooling conditions beginning with flashing in the downcomer cause the early rod rewet measured at ~10 s, but a subsequent dryout occurs almost immediately in the middle and upper levels; rod quench due to accumulator ECC injection is seen at later times. The calculated rod temperatures also exhibit rewet after the early DNB, followed by a second dryout, in all core levels; however, the calculated rod temperatures do not then show the presence of a quench front, but gradually cool at approximately the same rate all through the core, resulting in large discrepancies at later times compared to experiment.

Although the calculated PCT is in excellent agreement with data, there is some disagreement in other early time rod behavior (perhaps due to the lack of nonequilibrium heat transfer models). The calculated rewet in all levels is earlier than observed, and the later dryout calculated in the lower levels is too early and the resulting temperatures too high. A possible source of this disagreement could be a low calculated fluid density at the core entrance which, combined with the pump-side break flow shown in Figure 3.1.1.1b and the core differential pressure, indicates that too much liquid was swept up from the lower plenum through the core and out the pump-side break very early in the transient (causing the too-rapid calculated rewet); the resulting relatively large amount of steam in the mixture moving up the core at later times reduces its heat removal capability (causing the early large dryout in the lower core).

The results for the LOFT L2-5 large break transient [22] are quite similar to those for the three LOBI large break tests analyzed. The rod clad temperatures are shown in Figure 3.2.1.2. The plotted experimental data includes all thermocouples at the elevation closest to the heat slab midpoint, to give an idea of the overall core response; considerable radial power variation in the facility, which we are not attempting to model, contributes to the different thermocouple readings throughout the core.

The early heatup is calculated well (especially in Figures 3.2.1.2a and 3.2.1.2c), except at the top of the core. The first total rewet in the upper core is also correctly calculated, as shown in Figure 3.2.1.2d. The calculated average PCT of 1105 K is in reasonably good agreement with data (noting that the measured PCT of 1077 K occurs at a core elevation not included in these plots, between those plotted in Figures 3.2.1.2b and 3.2.1.2c). However, the code predicts early blowdown PCT at ~10 s while the data shows PCT occurring at ~30 s, at the start of reflood. (The data does show a plateau in the higher-powered regions through these times, as seen in Figures 3.2.1.2a and 3.2.1.2b.)

The calculated core response after PCT occurs is similar to the behavior calculated in the LOBI analyses (cf. Figure 3.2.1.1b), a gradual cooldown calculated with roughly half the thermocouple readings showing significantly higher temperatures while the other half show quench to the saturation temperature. Although a sharp quench front progressing through the core is not being (and most likely cannot be) calculated by MOD1, the lower half of the core in particular is calculated to all be "quenched" by the correct time. However, due to the excess ECC bypass being calculated (already mentioned in Section 3.1.1), the calculation incorrectly shows the core beginning to heat up again after the end of accumulator injection at ~70 s.

The core response using a double-downcomer nodalization reflects the relatively greater amount of ECC water being swept through the core before being lost out the pump-side hot leg break; the PCT is a few (~5 K) degrees lower, the core nodes are calculated to cool somewhat faster, and the eventual core heatup after the accumulator empties is calculated to start somewhat later (by ~10 s). However, there are no significant qualitative differences in the results of the two analyses.

3.2.2 Intermediate Breaks

The core response in the two LOFT intermediate breaks we analyzed [19] was quite similar; we discuss L5-1 since it was used earlier in section 3.1.1. Figure 3.2.2.1 gives calculated and measured clad temperatures for core elevations of 0.64 m and

1.06 m, for both our final cycle 18+ and earlier cycle 14 runs. (The data shown include all thermocouples at approximately the same core heights as the RELAP5 heat structure midpoints.)

As shown in Figures 3.2.2.1a and 3.2.2.1b, using cycle 18+, the calculated dryout time is correct at the 1.06 m elevation but occurs ~20 s early at the 0.64 m elevation. Clad quench is calculated ~20 s earlier than occurred, because the accumulator pressure setpoint was reached 18 seconds early in the calculation (as discussed above in section 3.1.1). At 0.64 m elevation, the calculated clad temperature is, apart from a timing offset, in good agreement with thermocouples located at average radial power locations. However, the predicted rod heatup is repeatedly interrupted by partial rewets due to calculated density and void fraction fluctuations around the MOD1 dryout/rewet criterion of α=0.96, especially visible at the 1.06 m elevation; without these interruptions the calculated clad temperature would probably be in much better agreement with data, since the predicted heatup rate between rewets appears to be correct.

In comparison (in an otherwise identical calculation), as shown in Figures 3.2.2.1c and 3.2.2.1d, cycle 14 gave a later dryout and a peak temperature of 590 K at the 0.64 m height, while cycle 18 gave a peak temperature of 630 K; at the 1.06 m elevation, cycle 14 gave a peak temperature of 545 K with the same rewet oscillations predicted, while cycle 18 gave a peak temperature of 580 K. The obvious reason for the higher clad temperatures and earlier dryouts calculated by cycle 18 is the difference in decay heat predicted by the two cycles, already mentioned in section 3.1.3. The decay heat plots in Figure 3.2.2.2 show that, for the L5-1 transient, the cycle 18 decay heat was consistently ~10% higher than the cycle 14 decay heat, with the experimental decay heat lying between the two curves. (The early-time discrepancy is due to plotting total power for the calculation rather than just the gamma power term.)

3.2.3 Small Breaks

Results from the small break analyses we have done confirm some of the conclusions drawn from the intermediate break analyses, discussed above in Section 3.2.2. Lower clad temperatures were seen in the LOFT L3-6/L8-1 analysis because of the low decay heats calculated by cycle 14 of MOD1. Intermittent rewets due to density oscillations around the code dryout/rewet criterion prevented observed core heatup from being calculated, or caused calculated core heatup to be repeatedly interrupted; in spite of these calculated rewets, the nine Semiscale small break transients analyzed generally showed a more severe core transient being calculated than was measured to occur. Several calculations

predicted a sustained late-time core dryout and heatup which did not occur in the corresponding experiments; when late-time core dryout and heatup was observed experimentally, the calculations showed more of the core uncovering for a longer period of time.

The results for LOFT small break experiment L3-6/L8-1 [18] show that the MOD1 code correctly calculates the qualitative core behavior, both when the primary coolant pumps are running (L3-6) and when they have been tripped (L8-1). No core heatup is observed or calculated during L3-6, because the pumps maintain adequate residual core cooling; core heatup is both observed and calculated soon after pump trip, shown by the clad temperatures in Figure 3.2.3.1, where time zero marks the pump trip signifying the end of L3-6 and the start of L8-1. (The calculation reached the pump trip earlier than occurred experimentally as mentioned above in Section 3.1.2, but this discrepancy is not visible in Figure 3.2.3.1.) The two plots each compare the calculated clad temperature in a single core node (at 0.64 and 1.06 m core elevations, respectively) with all the thermocouple readings at the core elevation nearest the calculational node midpoint.

We have identified a number of reasons for the quantitative disagreements observed. The temperature rise starts from a lower (by ~10 K) value because of discrepancies between calculation and data at the "end" of L3-6; the subsequent heatup is slower due to the lower (by ~20%) decay heat calculated by cycle 14. The predicted quench is premature in the following sense: we tripped all events in the L8-1 calculation on time since pump trip, while in the experiment ECC injection was manually initiated when a thermocouple reading of 589 K was observed. This ECC injection signal of 589 K clad temperature would have been reached much later in the calculation than in the experiment if we had not tripped the accumulator on a time signal; however, the expected improvement in predicted PCT would have been counterbalanced by a significant disagreement in the measured and calculated times of accumulator injection. Besides these major causes, the primary mass inventory calculated is higher than that estimated from data, and the calculated pump coastdown is slower than recorded.

Of the four Semiscale Mod-3 2.5% small breaks analyzed [15], only one (S-SB-P1, a cold leg break scenario with early pump trip) exhibited core uncovery and heatup experimentally. As shown in Figure 3.2.3.2a, the calculation predicted core uncovery significantly later (~200 s) than occurred, as well as predicting more of the core being uncovered. In the experiment, the upper core began heating up as soon as it uncovered, as shown in Figure 3.2.3.2b, but in the analysis no sustained heatup was calculated in the upper core after uncovery because of constant rewet interruptions. (As in the intermediate breaks, these rewets

were caused by the fluid density and void fraction in the adjacent cell fluctuating around the α=0.96 criterion.) However, the middle of the core was calculated to heat up as it uncovered, due to the higher power level; this was not observed in the test since the core remained covered at this location.

Another of our Semiscale Mod-3 small break analyses (S-SB-P7, a cold leg break with late pump trip) predicted some uncovery near the top of the core at late times (~1300-2000 s), but no core heatup was calculated due to densities remaining at the dryout/rewet criterion. The analysis for a third Mod-3 small break (S-SB-P3, a hot leg break with early pump trip) showed large density fluctuations near the top of the core over the same time period, suggesting that the core may have been on the verge of uncovering. No core uncovery was visible in the experimental data in either case.

Of the five Semiscale Mod-2A small break transients analyzed [24], data from the two 10% break transients (S-UT-1 and S-UT-2) showed early-time core dryout and rewet while data from two of the 5% breaks (S-UT-6 and S-UT-7) showed late-time sustained core heatup and subsequent quench; the S-UT-8 transient showed both. Figure 3.2.3.3a shows that the analyses correctly calculate early-time core heatup and rewet when present, although the timing is shifted slightly and the heatup is interrupted by rewet oscillations. However, the analyses predict a sustained late-time core uncovery and heatup in the 10% break transients which did not occur experimentally; this heatup is caused by incorrectly calculated core densities, as shown in Figure 3.2.3.3b.

Such a late-time core heatup was measured in the 5% break transients; it was also calculated to occur, but beginning much earlier in the transient, with more of the core calculated to uncover and heatup than was observed, as shown in Figure 3.2.3.4. The combination of earlier calculated dryout and heatup with no corresponding early accumulator injection resulted in peak clad temperatures higher than measured.

In general, all our Semiscale Mod-3 and Mod-2A small break analyses showed less early-time core level depression and rod heatup due to liquid plugs in the pump seals, but showed more late-time core inventory boiloff and subsequent rod heatup. However, since this generalization is only based on results from a single facility (although at three different break sizes), it is not clear if such behavior is due to general code inadequacies or to specific modelling problems.

3.3 Secondary Side Thermal/Hydraulic Response

The last category of transient behavior to be considered is the secondary side thermal/hydraulic response, comprising the thermodynamic conditions existing in steam generator secondaries. The major variables describing this secondary system are the steam dome pressure and temperature, and downcomer temperatures. Related variables of interest include the steam generator liquid levels and the recirculation flow.

The results of various integral system small break and operational transient analyses and steam generator separate effects test analyses indicate that MOD1 generally does a poor job calculating the secondary side thermal/hydraulic response during many kinds of transients. The basic discrepancy observed is that the data usually shows significant global thermal nonequilibrium throughout the secondary side, with steam in the dome and subcooled liquid on the tube sheet, while the calculations consistently predict saturated conditions all through the secondary (usually resulting in greater secondary depressurization as energy required to maintain saturated liquid is pulled from the steam bubble).

The problem of saturated conditions throughout the secondary has been seen in both U-tube and once-through steam generator analyses. Although the major symptom appears the same, the causes are quite different. Only U-tube steam generator response, in both separate effects and integral tests, is discussed in this section; the once-through steam generator separate effects test analyses have already been discussed in Section 2.3.

3.3.1 Separate Effects Tests

The interpretation of the steam generator secondary side behavior calculated in the various small break transients analyzed in this assessment project rests heavily on the results of analyzing a FLECHT SEASET steam generator separate effects test; the whole point of such separate effects component testing is to isolate and highlight the physical phenomena also occurring, but harder to identify clearly, in integral tests. This analysis [14] verifies that MOD1 does a poor job calculating the detailed steam generator response in such a reverse heat transfer transient. Although the code calculates the correct average heat transfer rate throughout most of the test, as shown in Figure 3.3.1.1a, the resulting thermodynamic states of both the primary and secondary sides are quite different from those observed in the experiment; toward the end of the transient the deviation is so great that the correct heat transfer behavior could no longer be maintained.

Figure 3.3.1.1b shows that the code also correctly predicts the primary side flow mixture being superheated to almost the secondary temperature, with the amount of superheat slowly decreasing as the secondary cools down; however, the primary effluent incorrectly returns to saturation conditions at late times in the calculation. Although the calculated heat transfer rate and primary side outlet plenum temperature agree with data for more than a thousand seconds, throughout most of the transient, comparison of measured and calculated secondary side steam dome pressures in Figure 3.3.1.1c indicates that problems in the calculation began much earlier, within the first several hundred seconds.

The major source of these discrepancies is that RELAP5 is calculating overall equilibrium behavior while the experiment exhibits several nonequilibrium effects. Figure 3.3.1.2 shows the time evolution of the experimental and calculated secondary side temperature profiles seen by the primary side fluid travelling along the U-tubes. The experimental data in the upper figure (plotted at 144 s intervals) show a steep axial temperature gradient developing immediately and travelling slowly up the secondary side, with a subcooled layer growing in the lower part of the secondary and the upper region remaining at an elevated saturation temperature and pressure throughout the transient. In contrast, the calculated results shown in the lower figure (plotted at 145 s intervals) display a much shallower secondary side temperature gradient. With saturation conditions calculated throughout most of the secondary side, the correct total heat removal can lead to discrepant pressures and temperatures (as shown by the steam dome pressures in Figure 3.3.1.1c).

In the experiment, film boiling occurs on the tube walls as the two-phase mixture enters the steam generator tubes, and the heat transfer is from superheated tube wall to vapor (which then becomes superheated) to entrained liquid droplets. This observed nonequilibrium phenomenon of droplet carryover in superheated steam was not calculated to occur. The MOD1 mass transfer model produces vapor at such a rapid rate that any liquid droplets present evaporate much too quickly; superheated vapor cannot exist unless only pure vapor is present (as already noted in Section 3.2). The superheated steam was predicted to be perfectly dry and no liquid carryover was seen until the primary side superheat had entirely disappeared.

The phenomena of a "quench front" moving up the U-tubes and the resulting sharp secondary side axial temperature gradient, both present in the experiment, were not seen in the calculation (as shown in Figure 3.3.1.3). In the experiment the dispersed two-phase flow provides sufficient film boiling heat transfer and precursory cooling with intermittent liquid contact that the tube

is eventually quenched; the quench front advances up the tube with time, due to both precursory cooling and axial conduction effects which lower the local tube wall temperature. Given the resemblance to core reflood and quench phenomena, MOD1 should not be expected to calculate the correct behavior due to its recognized lack of a reflood model with nonequilibrium heat transfer and moving fine-mesh quench-front temperature profile resolution. Without this liquid film formation, the calculation spent significant portions of the transient in quite different heat transfer regimes than occurred in the experiment. The surprising thing is that the code managed to calculate the correct average heat transfer rate throughout most of the transient despite these local discrepancies.

3.3.2 Integral Tests without Aux Feed

Auxiliary feedwater injection was supposed to occur in all four of the Semiscale Mod-3 small break transients analyzed [15]; however, examination of the experimental data indicates that there was no aux feed to the broken loop steam generator in two of the tests (S-SB-P1 and S-SB-P3), and no aux feed injection to either the intact or broken loop steam generator in a third test (S-SB-P7). In all these Semiscale 2.5% break tests, the intact loop steam generator, being closely coupled to the primary system, clearly shows behavior characteristic of reverse heat transfer; the broken loop steam generator was not coupled to the primary either in the experiments or in the calculations, and thus responded quite differently.

The behavior of the intact loop steam generator in test S-SB-P7, shown in Figure 3.3.2.1, is qualitatively identical to the behavior seen in the FLECHT SEASET steam generator separate effects test analysis described in Section 3.3.1. The calculated secondary side depressurization rate is in good agreement with measurement during the first part of the transient but becomes progressively greater than the data indicates later in the test, as shown in Figure 3.3.2.1a. The calculated secondary side temperatures at the bottom of the downcomer and in the steam dome are both equal to the saturation temperature throughout the transient; the data shows a subcooled layer (whose temperature is closely coupled to the primary system saturation temperature) developing on the tube sheet while forced primary coolant circulation continues, and then remaining essentially constant after primary coolant pump trip, as shown in Figure 3.3.2.1b.

There was no auxiliary feedwater injection in any of the five Semiscale Mod-2A (10% and 5%) S-UT small break transients we analyzed [24]; neither the intact loop nor the broken loop steam generators were coupled to the primary either in the experiments

or in the calculations. (The Mod-2A 2.5% small break tests, which we did not analyze, showed the intact loop steam generator coupled to the primary system while the broken loop was not, as in the Semiscale Mod-3 small break tests we analyzed.) The behavior in these uncoupled steam generator secondaries was very similar to that calculated for the broken loop steam generator in similar (pumps-off) Semiscale Mod-3 small break analyses. The calculated pressures were generally higher than data, primarily because of too much pressurization very early in the transient, and the subsequent slight depressurization rate usually agreed well with data. The very-early-time behavior is quite sensitive to exactly how the secondaries are isolated at the start of the transient (e.g., valve closing rates and signal delays), which is usually not well-defined.

3.3.3 Integral Tests with Aux Feed

Auxiliary feedwater injection was supposed to occur in all four of the Semiscale Mod-3 small break transients analyzed [15]; however, as mentioned above in section 3.3.2, the experimental data indicates that intact loop steam generator aux feedwater injection occurred only in tests S-SB-P1, S-SB-P3 and S-SB-P4, while broken loop steam generator aux feed injection occurred in test S-SB-P4 only. Again, as with no aux feed, the intact loop steam generator response was closely coupled to the primary system while the broken loop steam generator was not, in these 2.5% break tests. Aux feed injection also occurred in two of the LOFT transients analyzed (during most of small break test L3-6 [18] and late in loss-of-feedwater recovery test L3-3 [17]).

One would expect the cold aux feedwater injected during such small break and/or recovery transients to collect at the bottom of the steam generator, forming a subcooled layer under a region of hotter saturated water, with steam in the dome; thus, a combination of forward heat transfer in the subcooled layer and reverse heat transfer in the saturated region could greatly reduce the net heat exchange with the primary system, holding up the secondary pressure. The experimental data examined tend to confirm this scenario, with the temperatures near the bottom of the steam generator downcomer and shroud progressively less than the saturation temperature, as measured in the steam dome. The calculations, on the other hand (except for brief periods of "correct" behavior in LOFT test L3-6), show the steam generator secondary at saturation conditions throughout. The subcooled auxiliary feedwater is in effect quickly and completely mixed and in equilibrium with the saturated liquid inventory, with the only possible source of the energy required to heat the subcooled liquid to saturation being condensation of steam in the dome; in the analyses, aux feed injection thus has a much larger overall depressurizing effect on the secondary side, contrary to data.

The same secondary side behavior was calculated in the three Semiscale Mod-3 small break tests with aux feed injection. The calculated primary and intact loop secondary pressures are very closely coupled throughout the period of aux feed injection, with the secondary depressurizing more rapidly than measured, as shown for test S-SB-P1 in Figure 3.3.3.1a. Secondary side temperatures are all calculated to be at saturation during this time, although the experimental data shows a growing subcooling in the lower regions of the secondary, as shown for the same test in Figure 3.3.3.1b. (After the end of aux feed injection, the calculation predicts approximately the correct secondary depressurization rate; however, the calculated temperatures show that the code is finally predicting some nonequilibrium behavior, but in the wrong way. Instead of showing the measured subcooled liquid layer at the bottom of the steam generator and near-saturated conditions in the steam dome, the calculation shows saturation conditions at the bottom and superheated steam in the dome.)

The same discrepancies in calculated and observed secondary side response are seen during reverse heat transfer in the later portions of LOFT small break transient L3-6 [18]. Figure 3.3.3.2a shows the calculated and measured pressures in the steam dome. While the calculation shows some quantitative disagreements with data during the first few hundred seconds (i.e., the relief valve cycling too early and the secondary repressurizing to too low a value), the calculated depressurization rate is then in excellent agreement with data for hundreds of seconds until the system enters a reverse heat transfer mode at ~1000 s. The measured and calculated pressures then diverge rapidly, although there are a few short periods late in the transient where the predicted depressurization rate agrees with that seen experimentally. The steam generator downcomer temperatures shown in Figure 3.3.3.2b indicate that these periods correspond closely to times when some saturated/subcooled temperature gradient is calculated on the secondary side. (The experimental steam dome temperature, which should represent the saturation temperature, was not reported.)

3.4 Natural Circulation

We have analyzed a number of natural circulation tests performed at the PKL and Semiscale test facilities. [13,20,23] Although natural circulation occurred in several of our small break transients, there it is coupled with other system phenomena which can mask the details of the code's performance; here we discuss the code's ability to model natural circulation without complicating factors.

The results of our natural circulation test analyses show that RELAP5/MOD1 qualitatively describes all modes of natural circulation correctly, but with quantitative disagreement on both the absolute magnitude of two-phase natural circulation (always overestimated), and on the mass inventories at which the peak flow and the various mode transitions (from single-phase to two-phase to reflux cooling) occur.

Such natural circulation analyses are stringent tests for the code two-phase entrainment models. We have already seen in Section 2.1.3 that the mass flows at 100% inventory are well matched by the code. At very reduced inventories, essentially all the core power is used in generating steam because there is little subcooling and the resulting natural circulation mass flow is very small; such mass flows at low inventories are also well calculated. The mass flow between these two limiting cases is governed by the entrained vapor or liquid. Our results indicate possible problems in the interphase drag model (determining the amount of steam or liquid entrained at any given inventory), and in the two-phase loss coefficients for abrupt area changes and/or two-phase wall friction factors (determining the flow magnitude in two-phase natural circulation). The code developers are redoing the two-phase pressure drop models in future versions of the code, and the interphase drag model is continuously being modified in attempts to improve code performance.

Much of the phenomena seen in these natural circulation tests is qualitatively reproduced in our calculations. Single phase, two-phase and reflux mass flows are calculated, and the maximum flow in a loop is predicted to occur when the upside of its steam generator U-tubes is two-phase and the downside is single-phase liquid, as observed in the experiments. Flow oscillations are calculated which are also observed in the experiments. As in the data, the primary pressure decreases as fluid is drained from the system; the hot leg temperature also decreases, because the hot leg is at saturation for all cases except for the initial liquid-full tests (when the primary system is still subcooled) and for some of the lowest inventory tests (where superheated steam is generated).

The code results are also in good quantitative agreement with much of the experimental data. The calculated temperatures and pressures generally compare well with measurement, with most discrepancies attributable to differences in the measured and calculated mass flow rates, shown for the steady state tests in Figures 3.4.1 through 3.4.3. (The "error bars" on the calculated flow rates correspond to calculated flow oscillations; some are numerical in origin, but others are long-period oscillations.) Single-phase and reflux mass flows are in excellent agreement with data, but calculated two-phase flows are always too high.

Transitions from one mode to another and the peak flow occur at different inventories than measured, but there is no consistent pattern to the inventory shifts. In the PKL IDI test series [13], the calculated flow curve is shifted toward lower inventories, as are the 60 kW and 100 kW experiments in S-NC-2; the 30 kW case for S-NC-2, on the other hand, shows calculated mass flows shifted toward higher inventories, as do both the intact and broken loop mass flows calculated for S-NC-7 (at 100 kW). [20]

The calculated intact loop mass flow curve for the S-NC-7 two-loop steady state test (Figure 3.4.3) resembles the measured curve shifted slightly in inventory; the broken loop mass flow quantitatively looks nothing like the experimental data, because of a relatively massive shift in the inventory dependence, but qualitative agreement is still visible on closer examination. Use of the one-velocity option at the junction between the vessel and the broken loop hot leg improves agreement for the broken loop tremendously, but worsens the intact loop agreement somewhat. In this case, more liquid is dragged along by steam going into the broken loop, resulting in correspondingly less hot leg void at any given system inventory. With more liquid removed from the upper plenum, there is less liquid left to be entrained by steam flowing into the intact loop, and the intact loop flow vs inventory curve is therefore shifted in the opposite direction from the broken loop curve. (The relative magnitudes of the two shifts represents the relative volume and flow area factor between the two loops.)

Measured and calculated downcomer, intact loop and broken loop mass flows for Semiscale transient natural circulation test S-NC-8 [23] are shown in Figure 3.4.4; the primary mass inventory used as the abcissa has been adjusted to allow for errors in calculated break flow. The behavior is somewhat similar to that seen in the equivalent steady state test S-NC-7. The calculated intact loop mass flow curve resembles the measured curve except for the high two-phase natural circulation flows at 65-75% inventories; the broken loop mass flow quantitatively looks nothing like the experimental data, because of a relatively massive shift in the inventory dependence, but qualitative agreement is still visible on closer examination. Differences between the steady state S-NC-7 and transient S-NC-8 results at higher (80-90%) inventories are due to the presence of the pressurizer in the latter test only.

Figure 3.4.5 compares the calculated and measured mass flow rates at different effective steam generator heat transfer areas for test S-NC-3 [23]. Qualitatively, the code correctly predicts two-phase natural circulation and the flow oscillations occurring in the experiment; quantitatively, the increased mass flow rate at high secondary inventories and the sharp decrease in mass flow

rate at low secondary inventories are not predicted. However, we know from our S-NC-2 analyses (Figure 3.4.2) that RELAP5 gives a higher peak two-phase natural circulation flow at a lower primary inventory than the experiment, at 60 kW power. We had initially set the S-NC-3 primary inventory at 91.8%, per data; draining the primary inventory to 84.8%, where the S-NC-2 calculation shows peak two-phase flow, results in better qualitative agreement during degraded heat transfer, although with a higher calculated mass flow rate, as expected. (Comparing the 100% secondary inventory data in S-NC-3 with corresponding data in S-NC-2, the S-NC-3 data appears wrong and the measured curve is probably flat for the higher secondary inventories.)

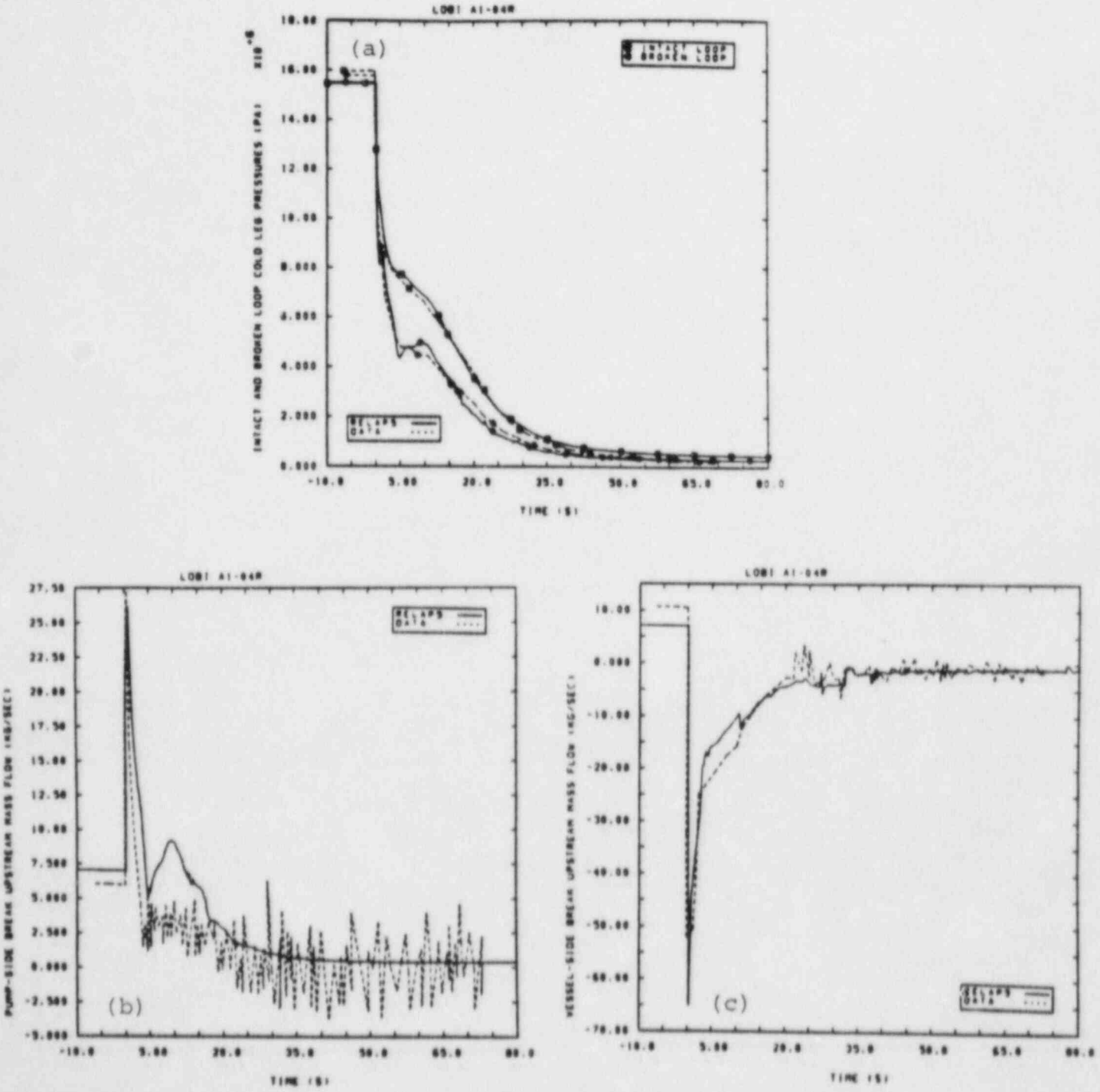

Figure 3.1.1.1 (a) Intact and Broken Loop Cold Leg Pressures, (b) Pump-side and (c) Vessel-side Break Mass Flow Rates for LOBI Large Break Transient A1-04R

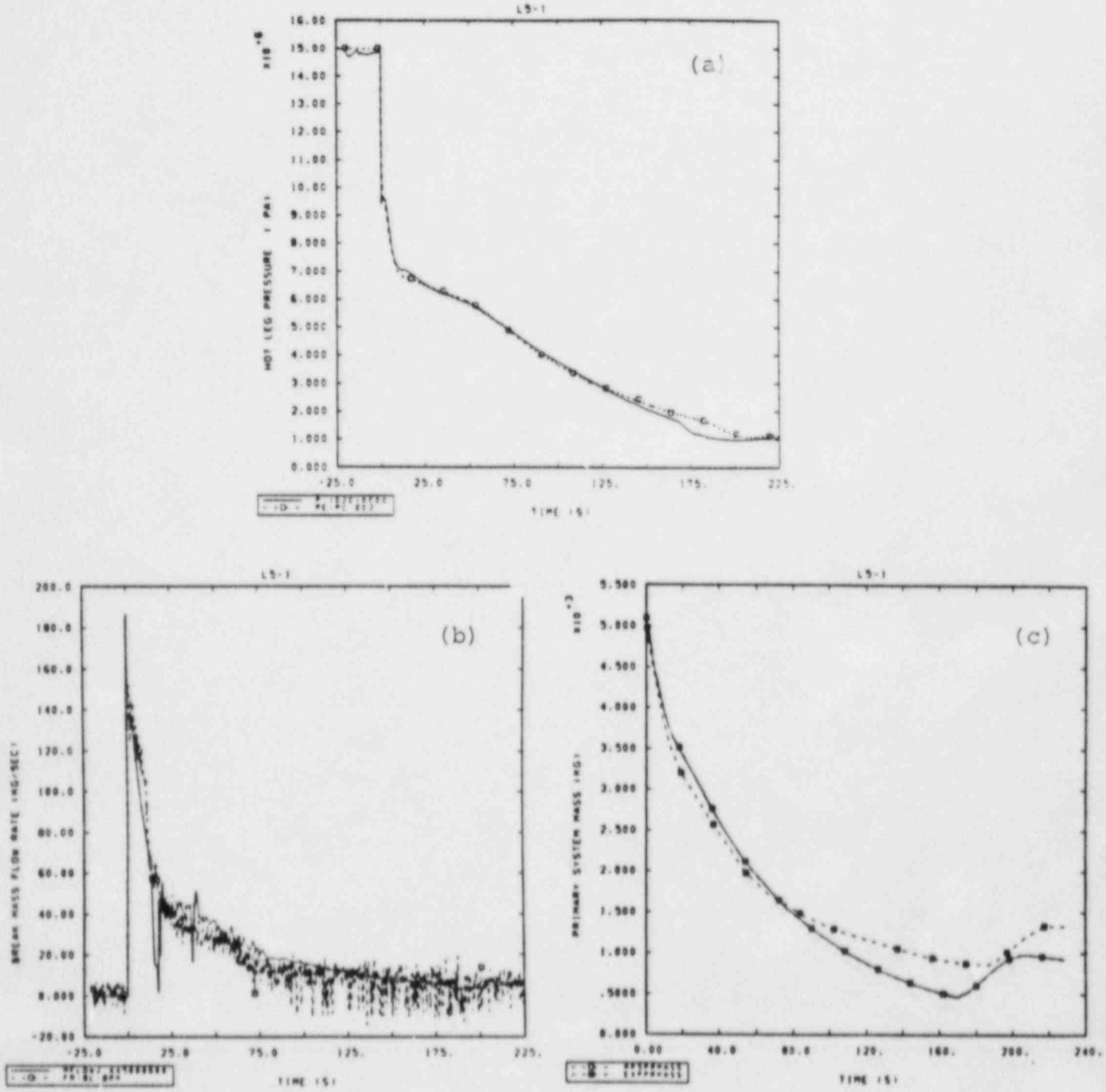

Figure 3.1.1.2 (a) Intact Loop Hot Leg Pressure, (b) Break Mass Flow Rate and (c) Primary System Mass Inventory for LOFT Intermediate Break Transient L5-1

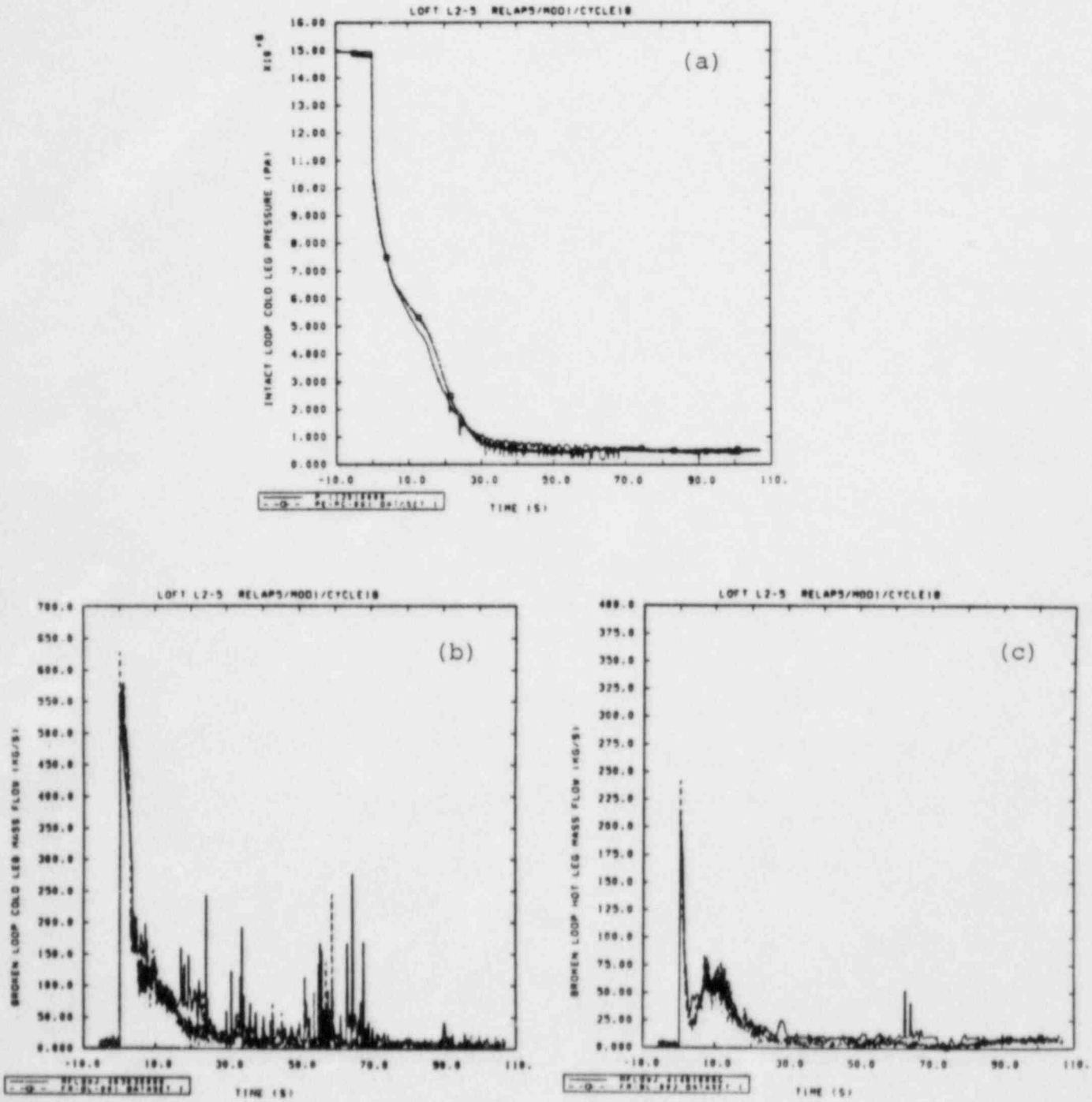

Figure 3.1.1.3 (a) Intact Loop Cold Leg Pressure, (b) Pump-side and (c) Vessel-side Break Mass Flow Rates for LOFT Large Break Transient L2-5

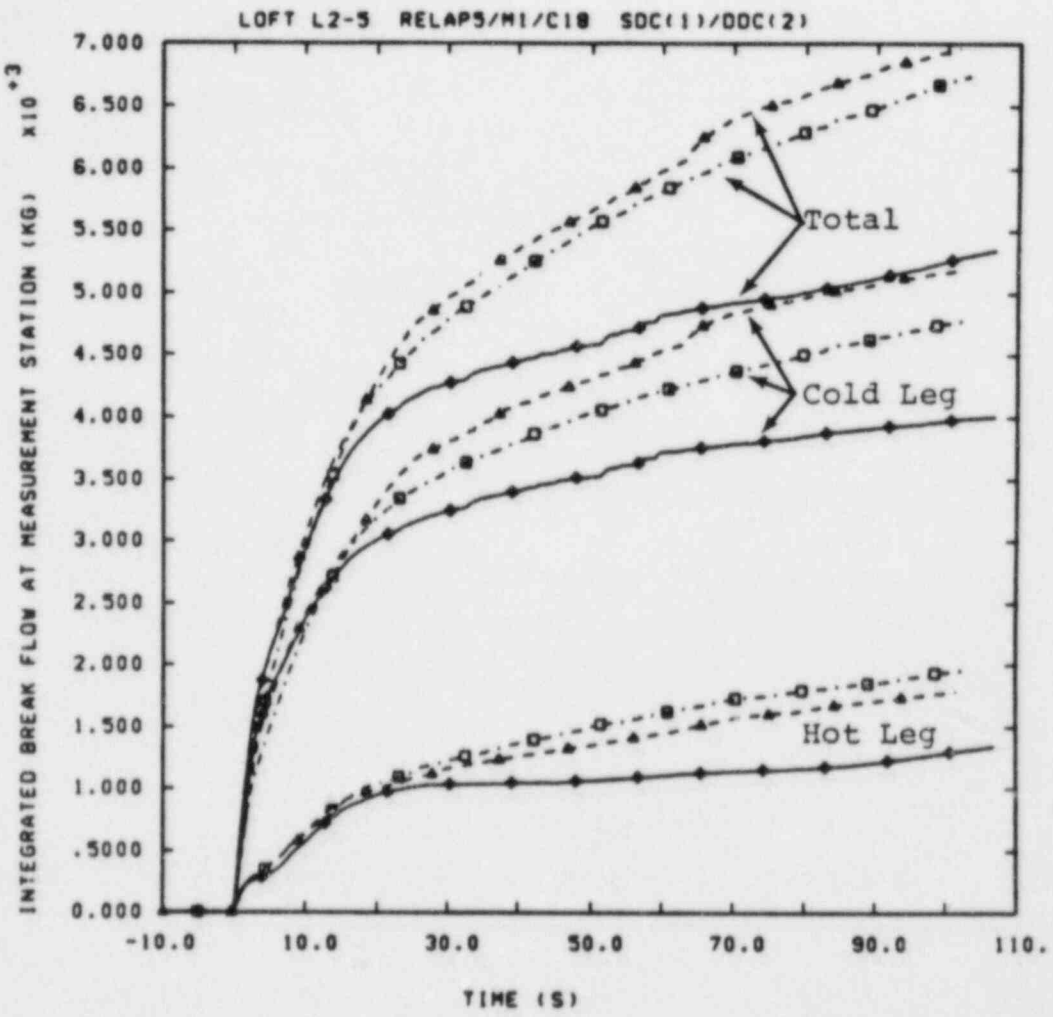

Figure 3.1.1.4 Integrated Break Flows using Single- and Double-Downcomer Nodalizations for LOFT Large Break Transient L2-5

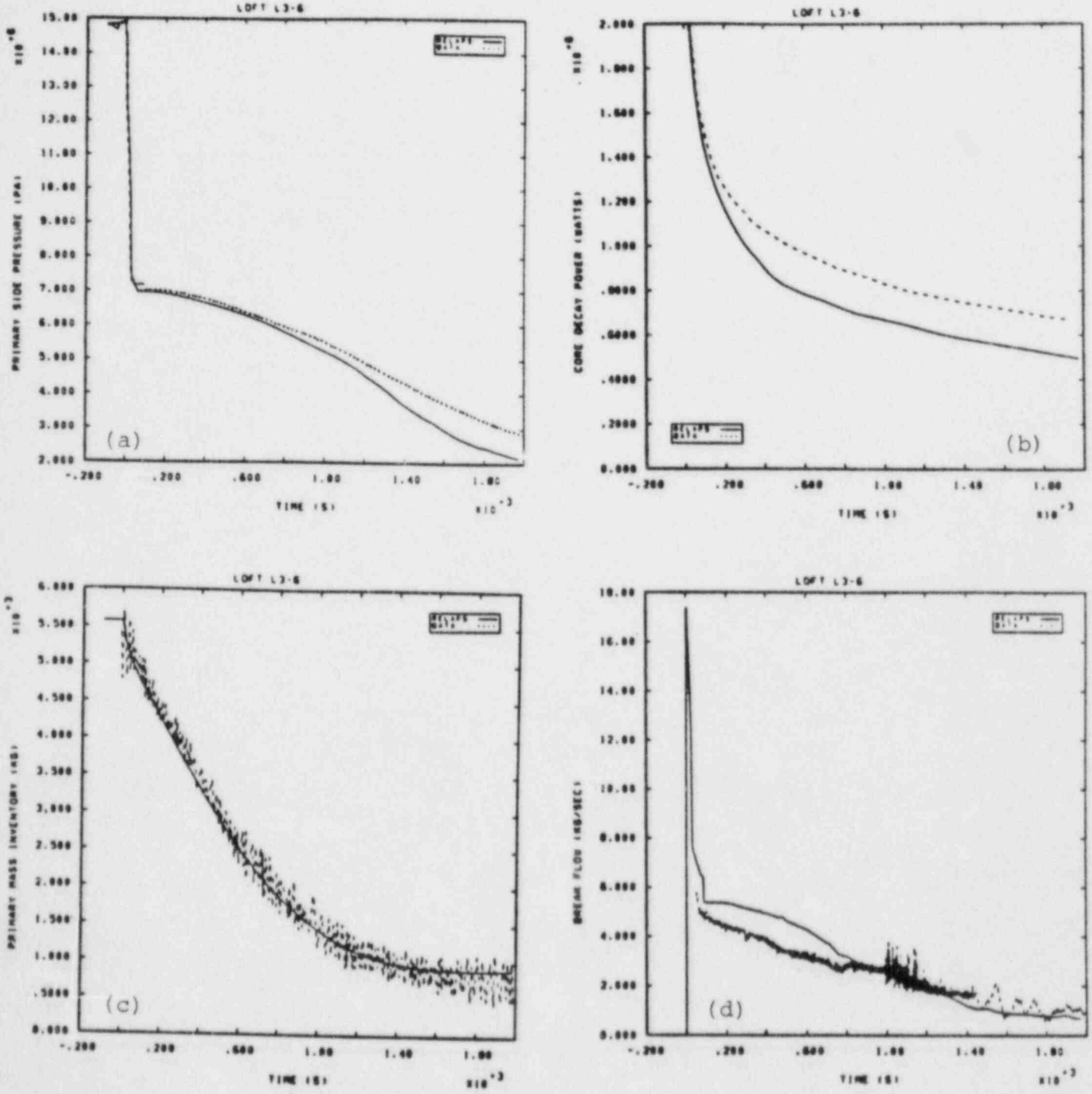

Figure 3.1.2.1 (c) Primary Side Pressure, (b) Core Decay Heat, (c) Primary System Mass Inventory and (d) Break Mass Flow Rate for LOFT Small Break Transient L3-6

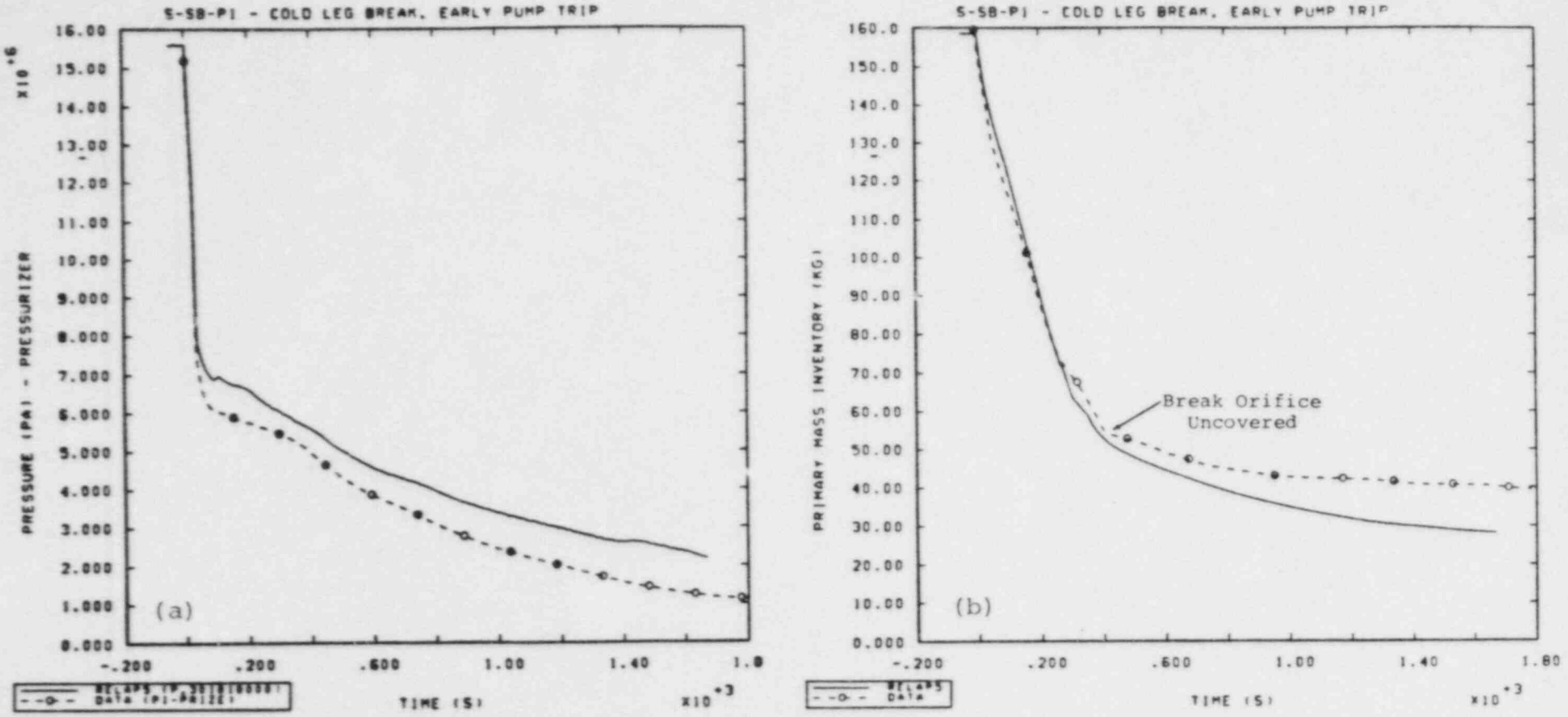

Figure 3.1.2.2 (a) Pressurizer Pressure and (b) Primary System Mass Inventory for Semiscale Small Break Transient S-SB-P1

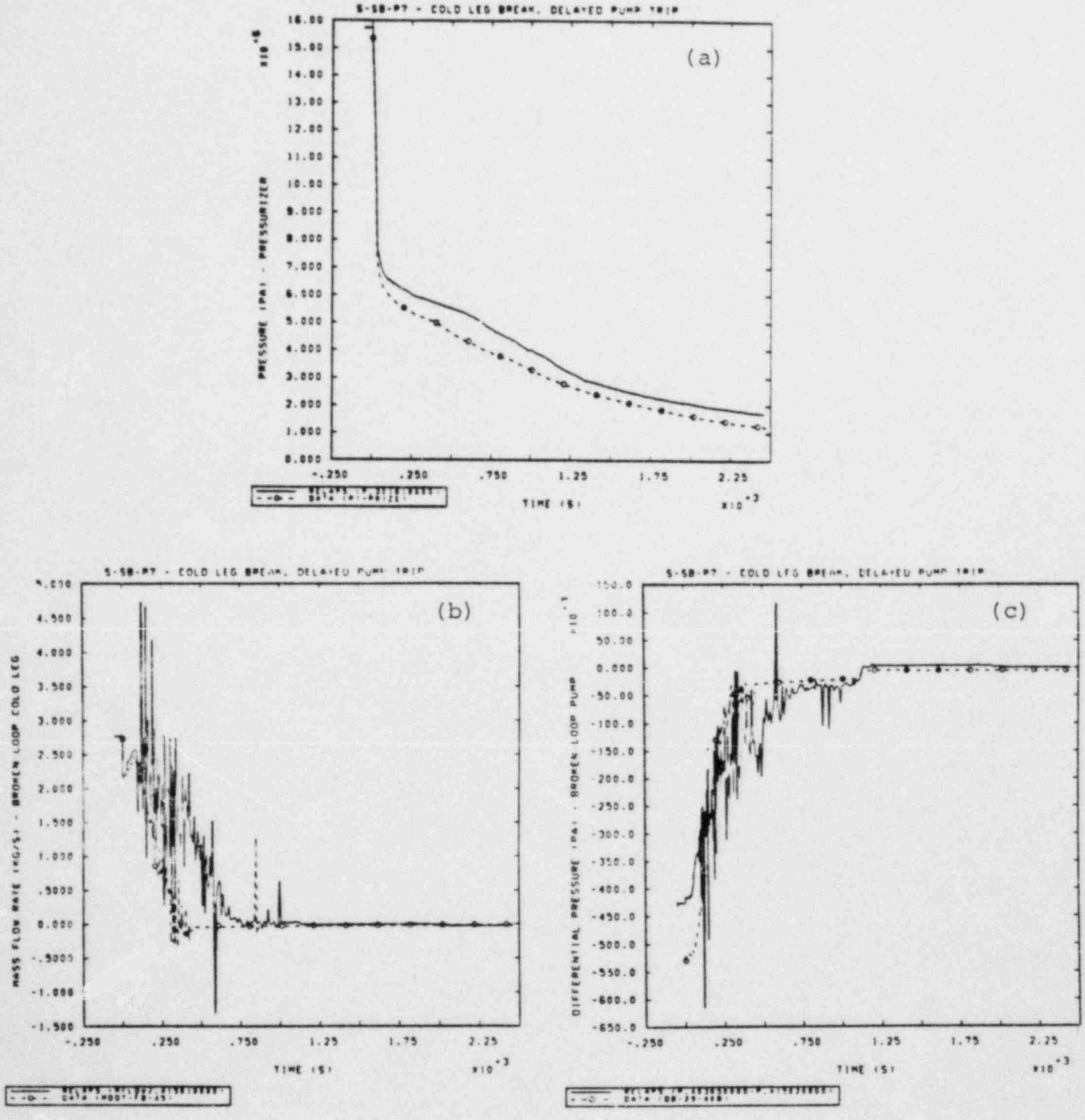

Figure 3.1.2.3 (a) Pressurizer Pressure and Broken Loop (b) Mass Flow Rate and (c) Pump Differential Pressure for Semiscale Small Break Transient S-SB-P7

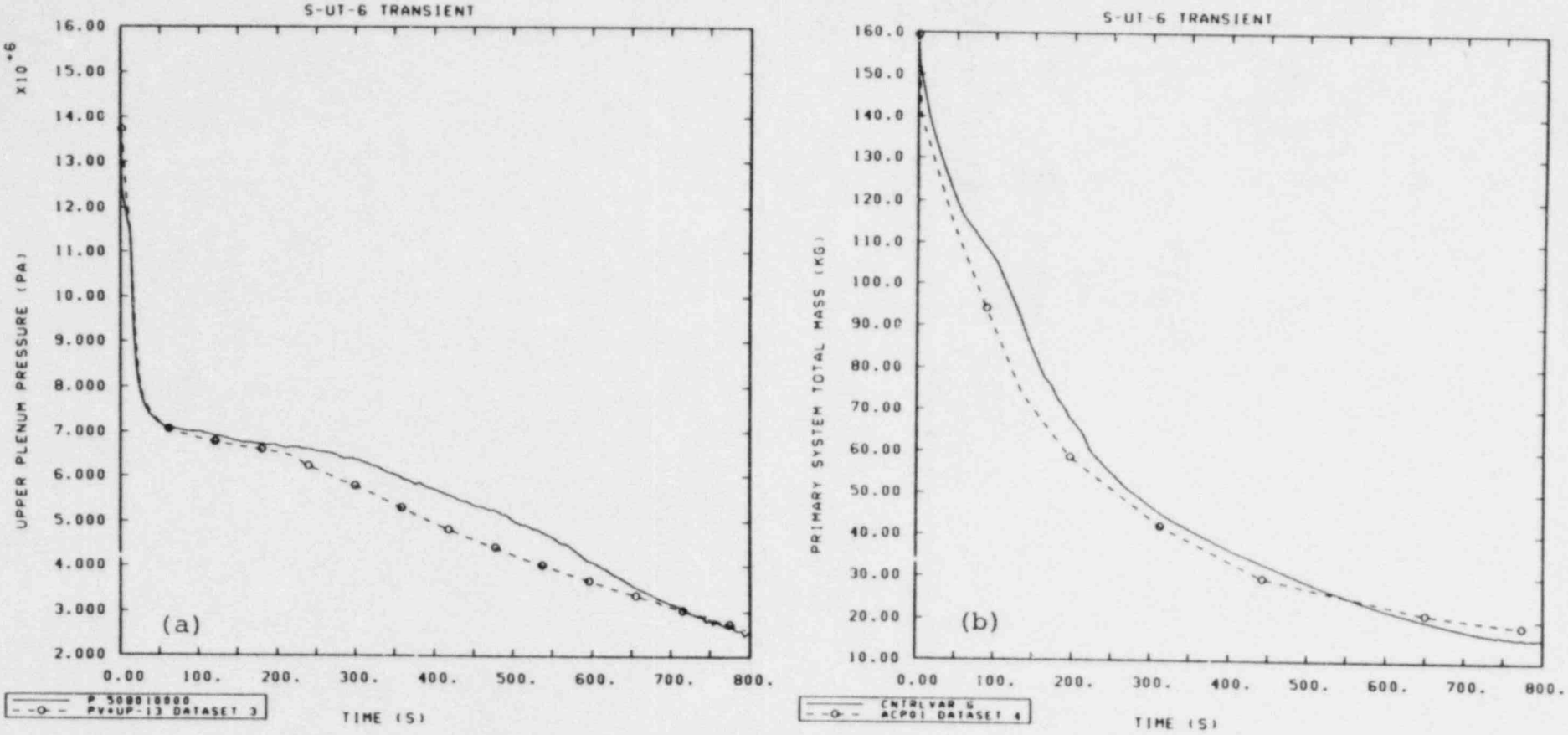

Figure 3.1.2.4 Primary Side (a) Pressure and (b) Mass Inventory for Semiscale Small Break Transient S-UT-6

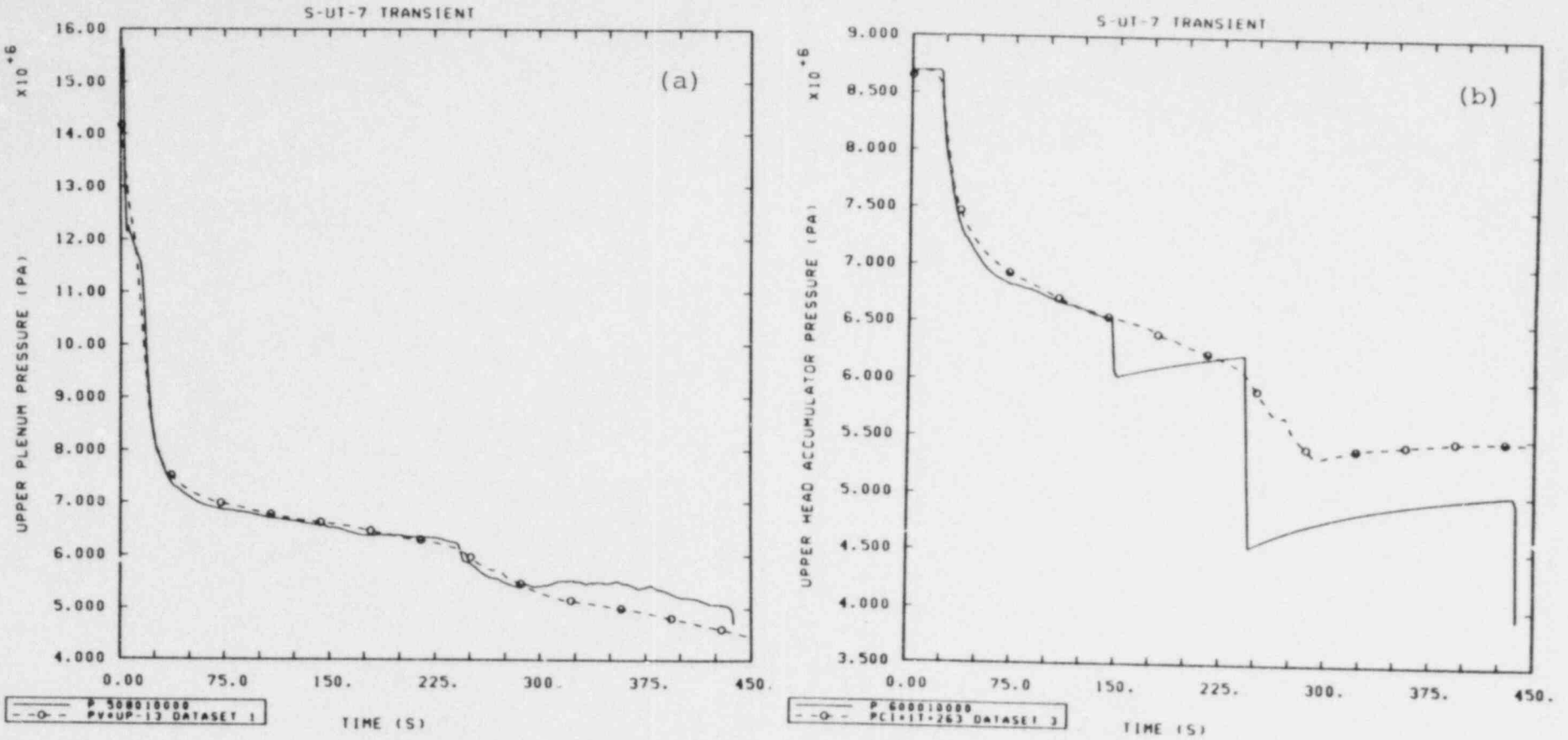

Figure 3.1.2.5 (a) Primary Side and (b) UHI Accumulator Pressures for Semiscale Small Break Transient S-UT-7

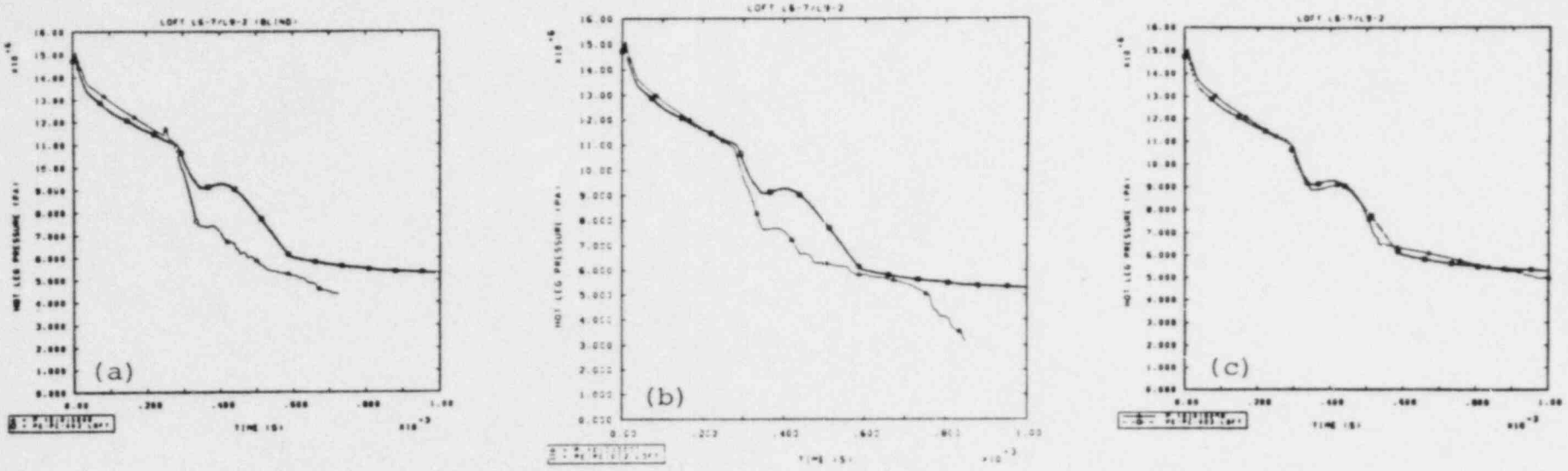

Figure 3.1.3.1 Intact Loop Pressure during (a) Initial "Blind", (b) Preliminary Posttest and (c) Final Posttest Calculations for LOFT Turbine Trip Transient L6-7/L9-2

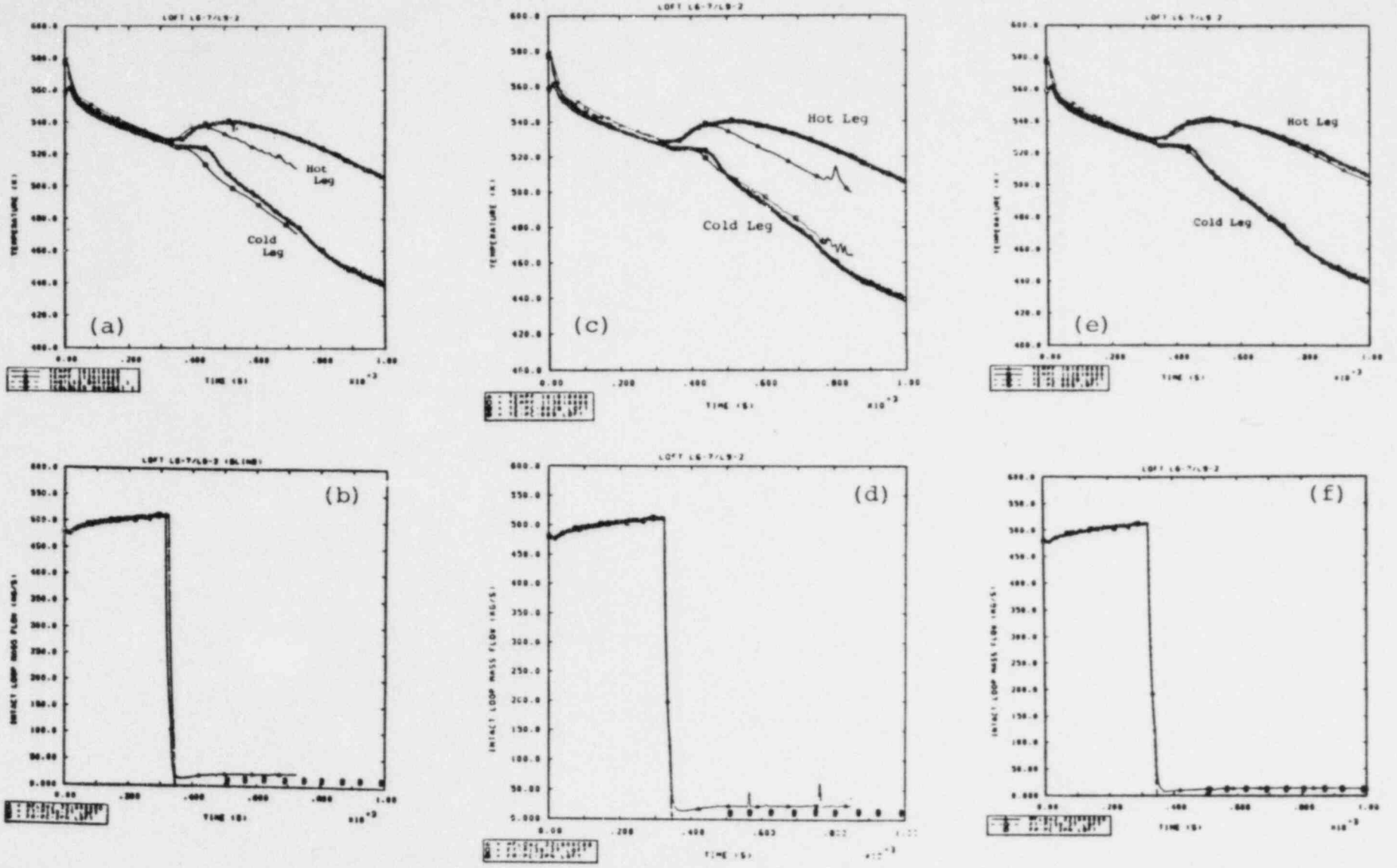

Figure 3.1.3.2 Intact Loop (a,c,e) Hot and Cold Leg Temperatures and (b,d,f) Mass Flow Rate for (a,b) Initial "Blind", (c,d) Preliminary Posttest and (e,f) Final Posttest Calculation for LOFT Turbine Trip Transient L6-7/L9-2

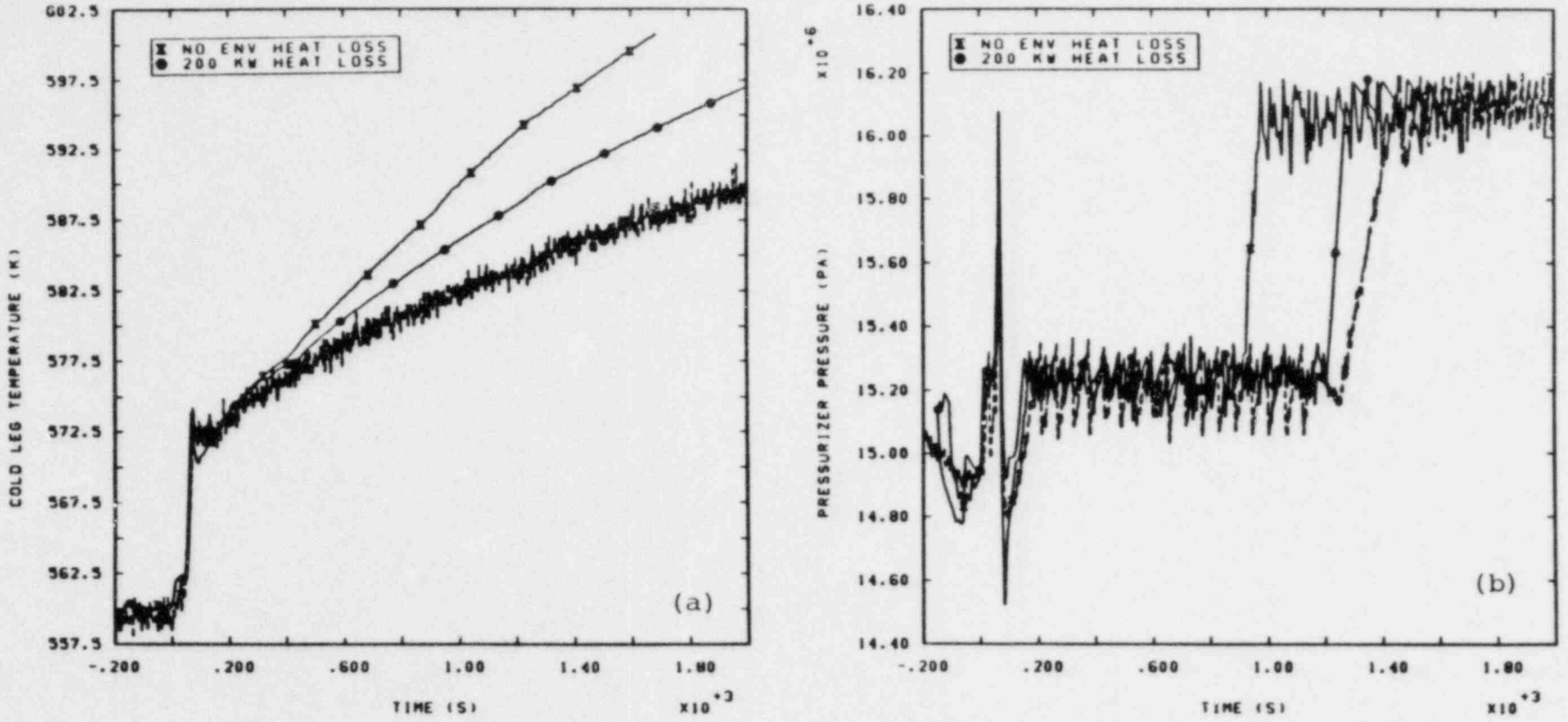

Figure 3.1.3.3 (a) Cold Leg Temperature and (b) Pressurizer Pressure with and without Environmental Heat Loss for LOFT Loss-of-Feedwater Transient L9-1

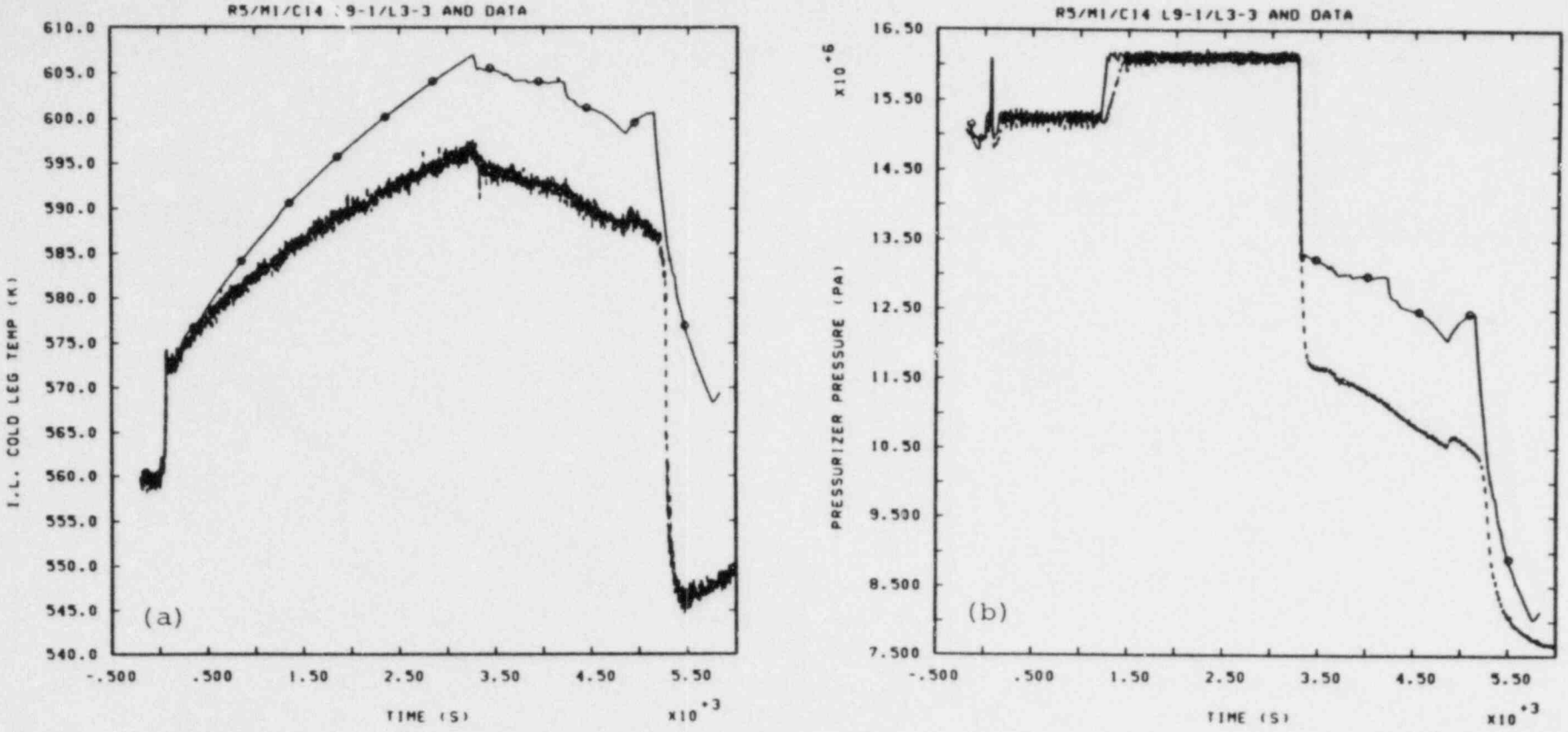

Figure 3.1.3.4 (a) Cold Leg Temperature and (b) Pressurizer Pressure for LOFT Loss-of-Feedwater with Recovery Transient L9-1/L3-3

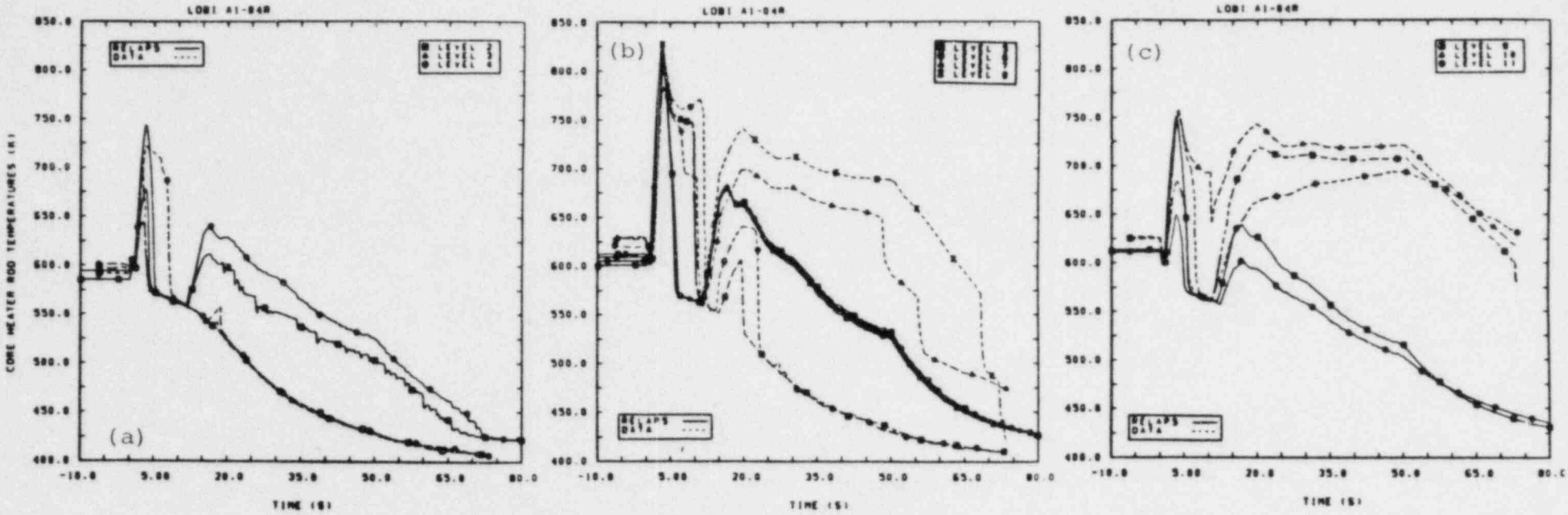

Figure 3.2.1.1 (a) Lower Core, (b) Mid-Core and (c) Upper Core Rod Temperatures for LOBI Large Break Transient A1-04R

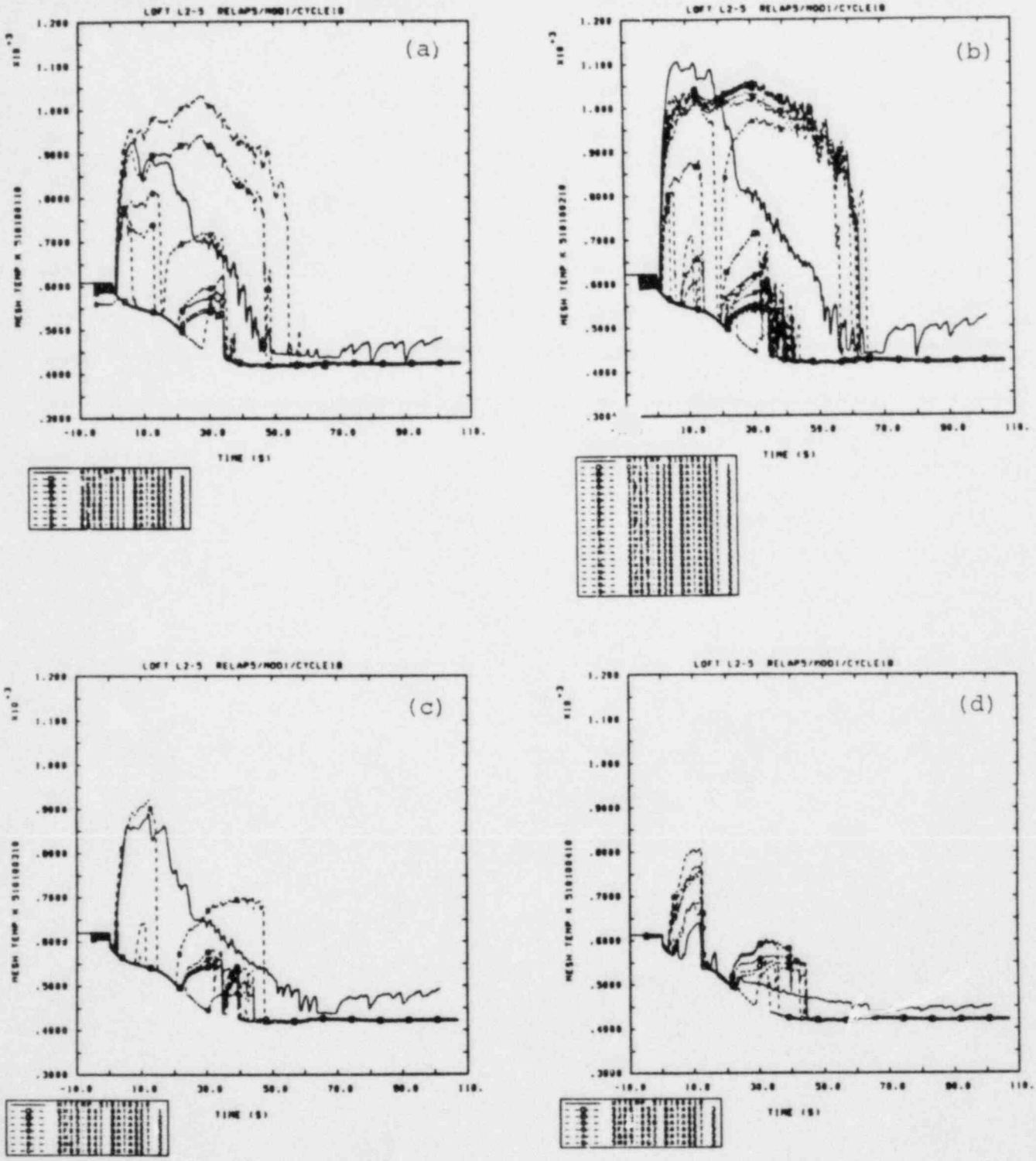

Figure 3.2.1.2 Clad Temperatures at (a) 0.21, (b) 0.64, (c) 1.06 and (d) 1.47 m Core Elevations for LOFT Large Break Transient L2-5

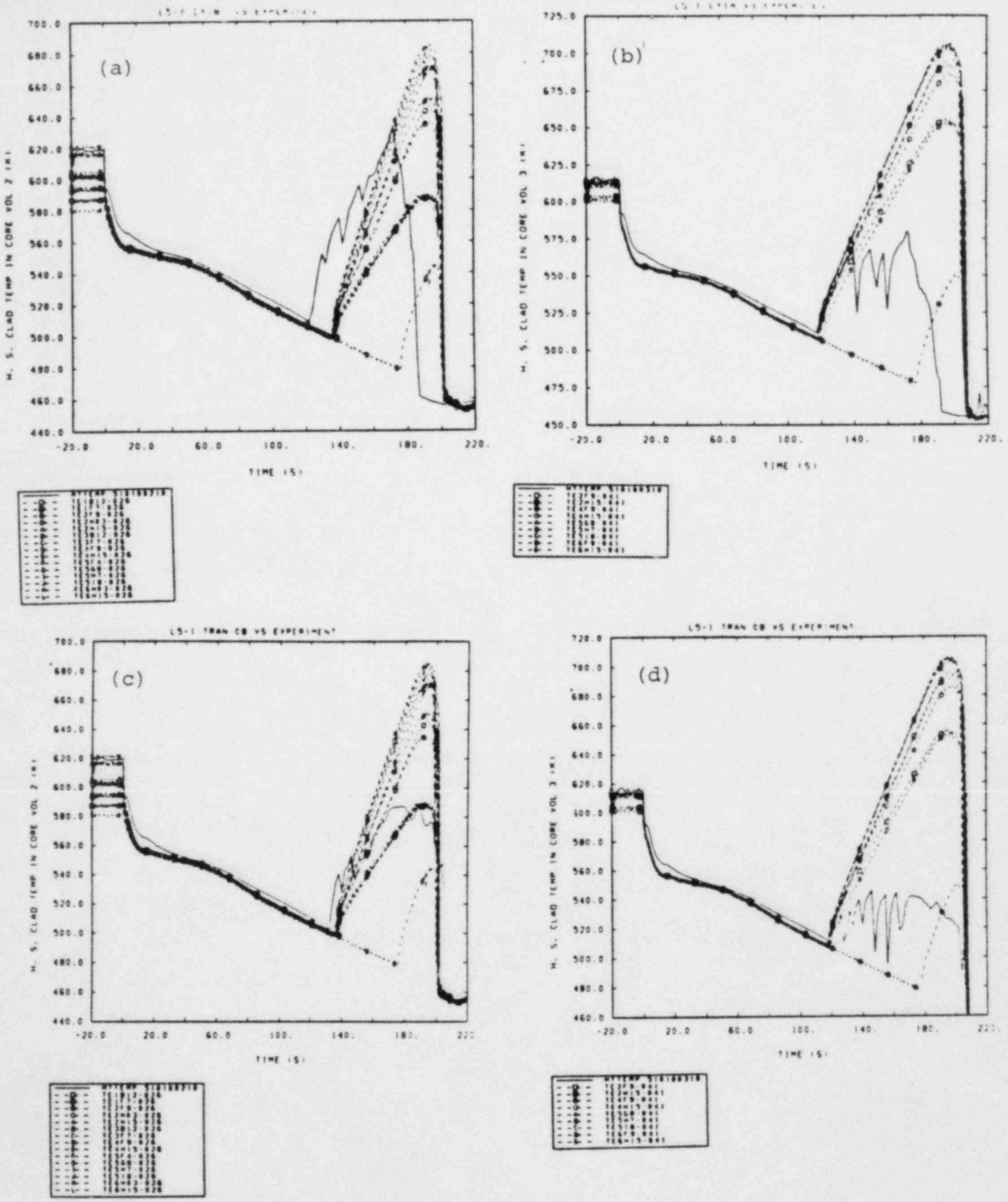

Figure 3.2.2.1 Clad Temperatures at (a,c) 0.64 and (b,d) 1.06 m Core Elevations Using (a,b) Cycle 18+ and (c,d) Cycle 14 for LOFT Intermediate Break Transient L5-1

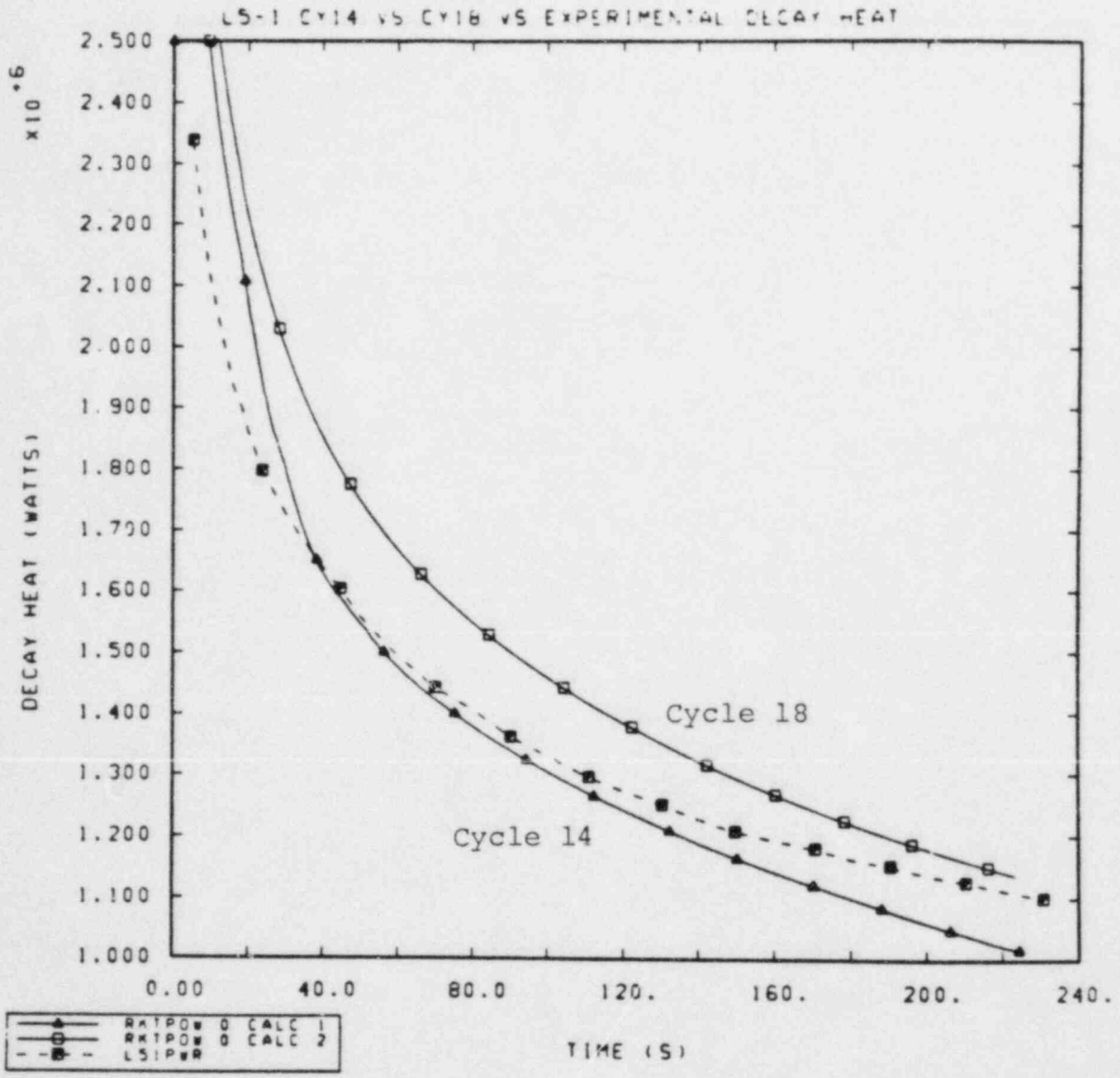

Figure 3.2.2.2 Core Decay Heats Using Cycle 14 and Cycle 18+ for LOFT Intermediate Break Transient L5-1

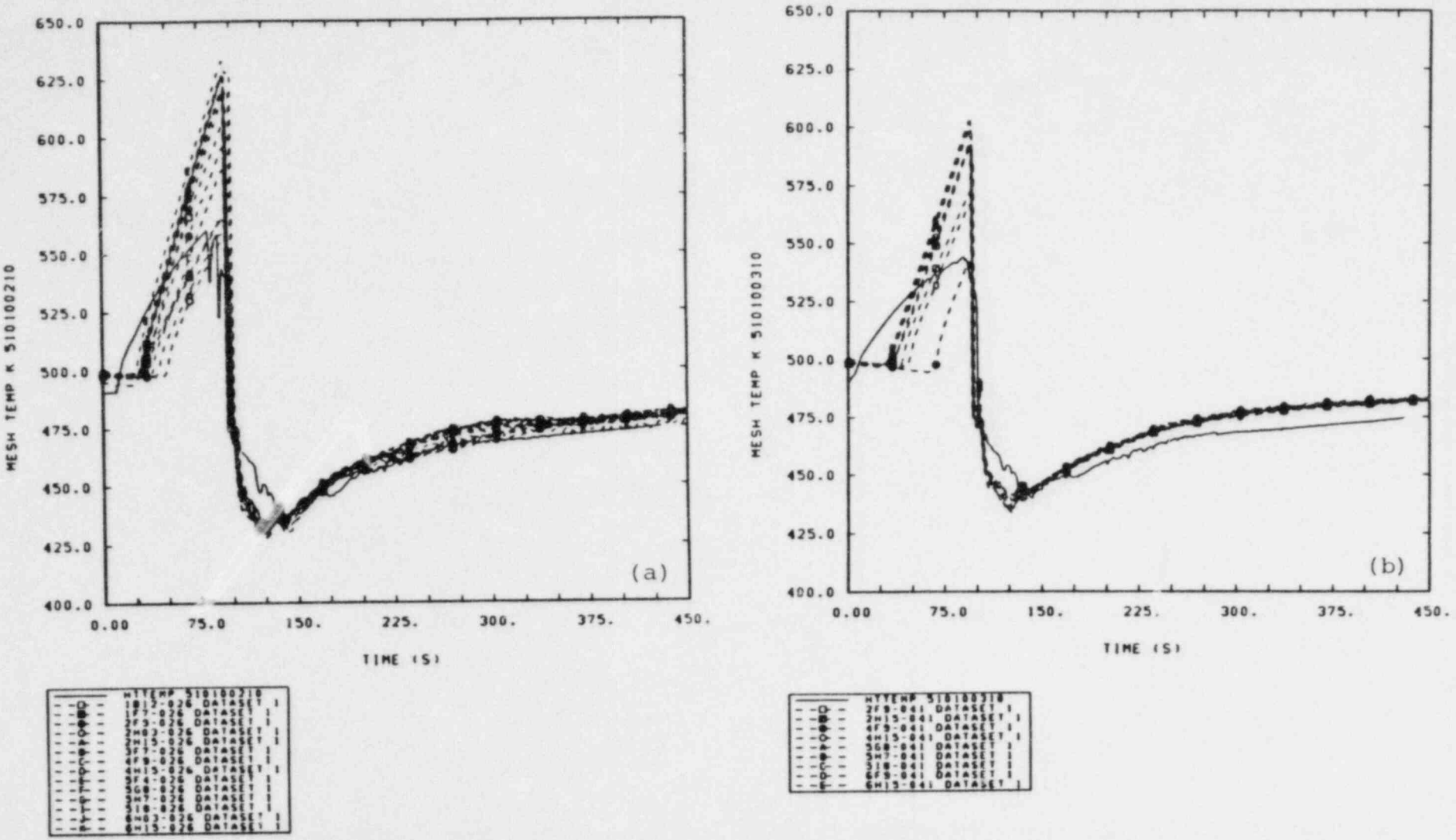

Figure 3.2.3.1 Clad Temperatures at (a) 0.64 and (b) 1.06 m Core Elevations for LOFT Small Break Transient L8-1

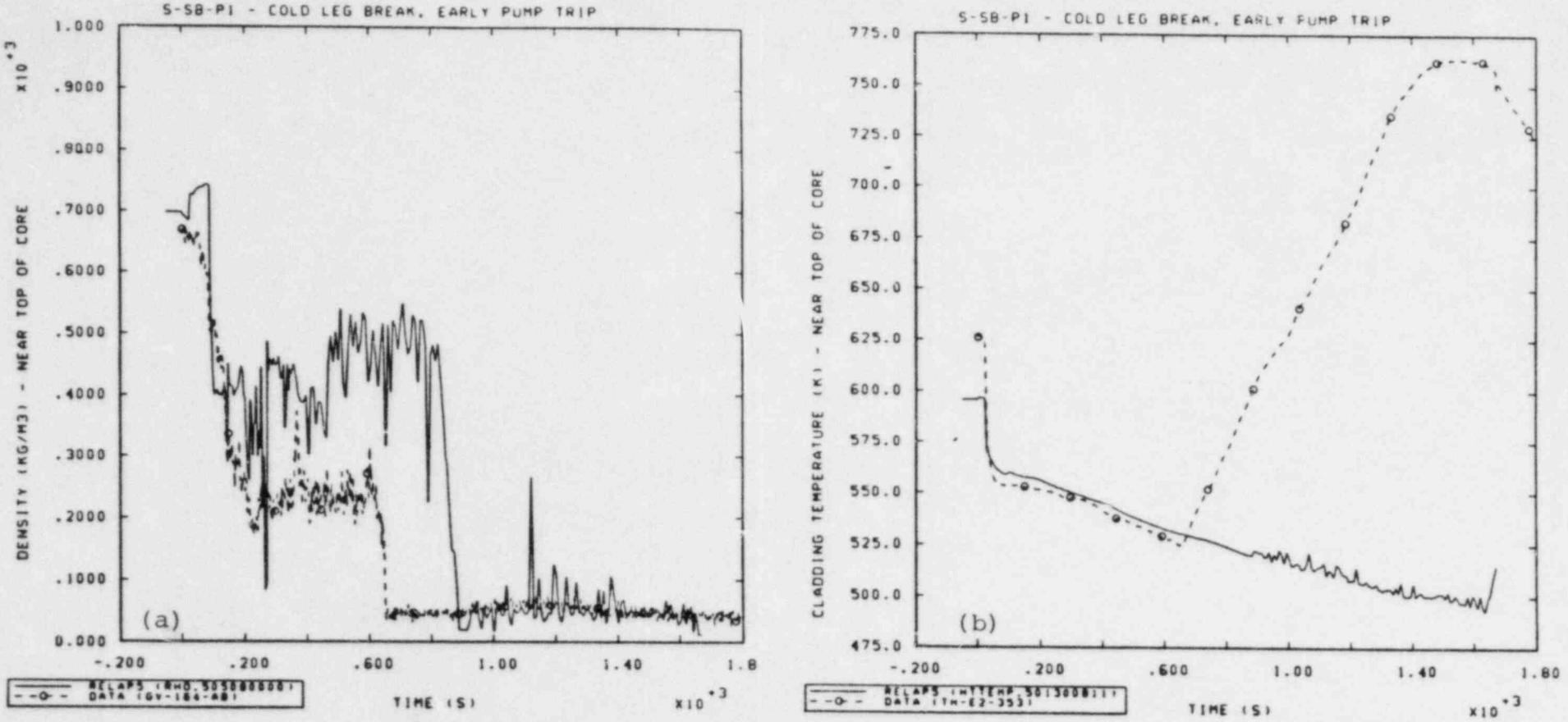

Figure 3.2.3.2 Upper Core (a) Density and (b) Clad Temperature for Semiscale Small Break Transient S-SB-P1

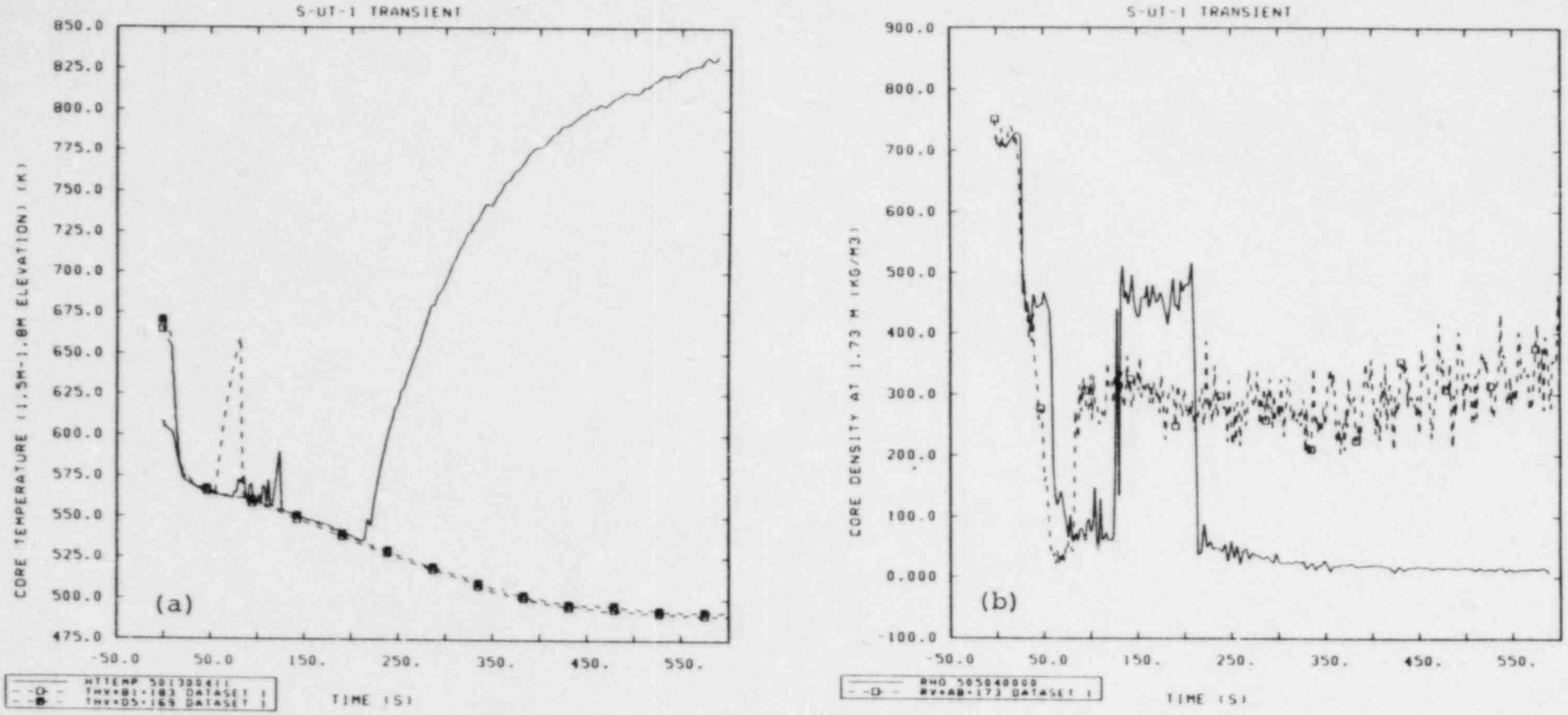

Figure 3.2.3.3 Upper Core (a) Clad Temperature and (b) Density for Semiscale Small Break Transient S-UT-1

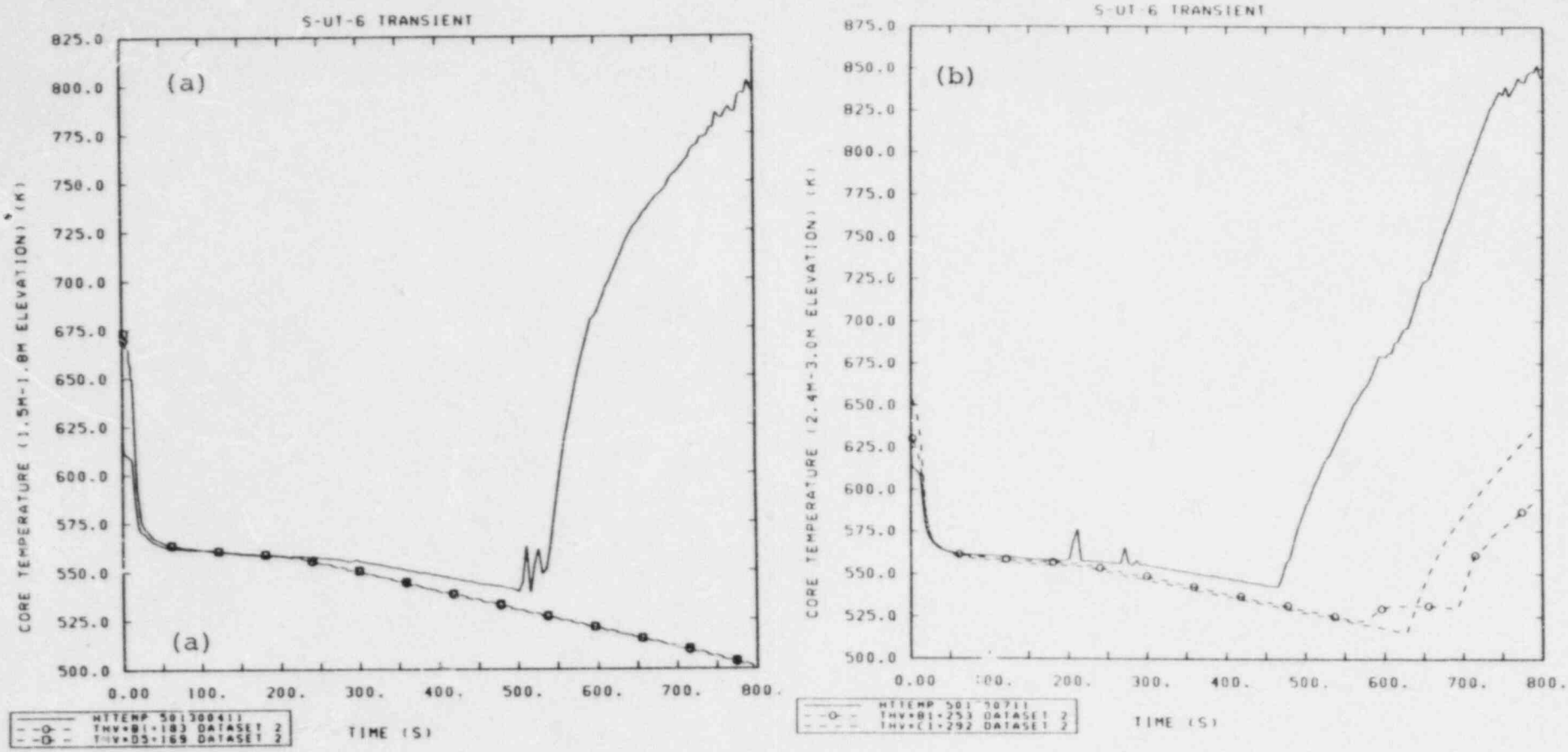

Figure 3.2.3.4 Core Clad Temperatures at (a) 1.5-1.8 m and (b) 2.4-3.0 m Core Height for Semiscale Small Break Transient S-UT-6

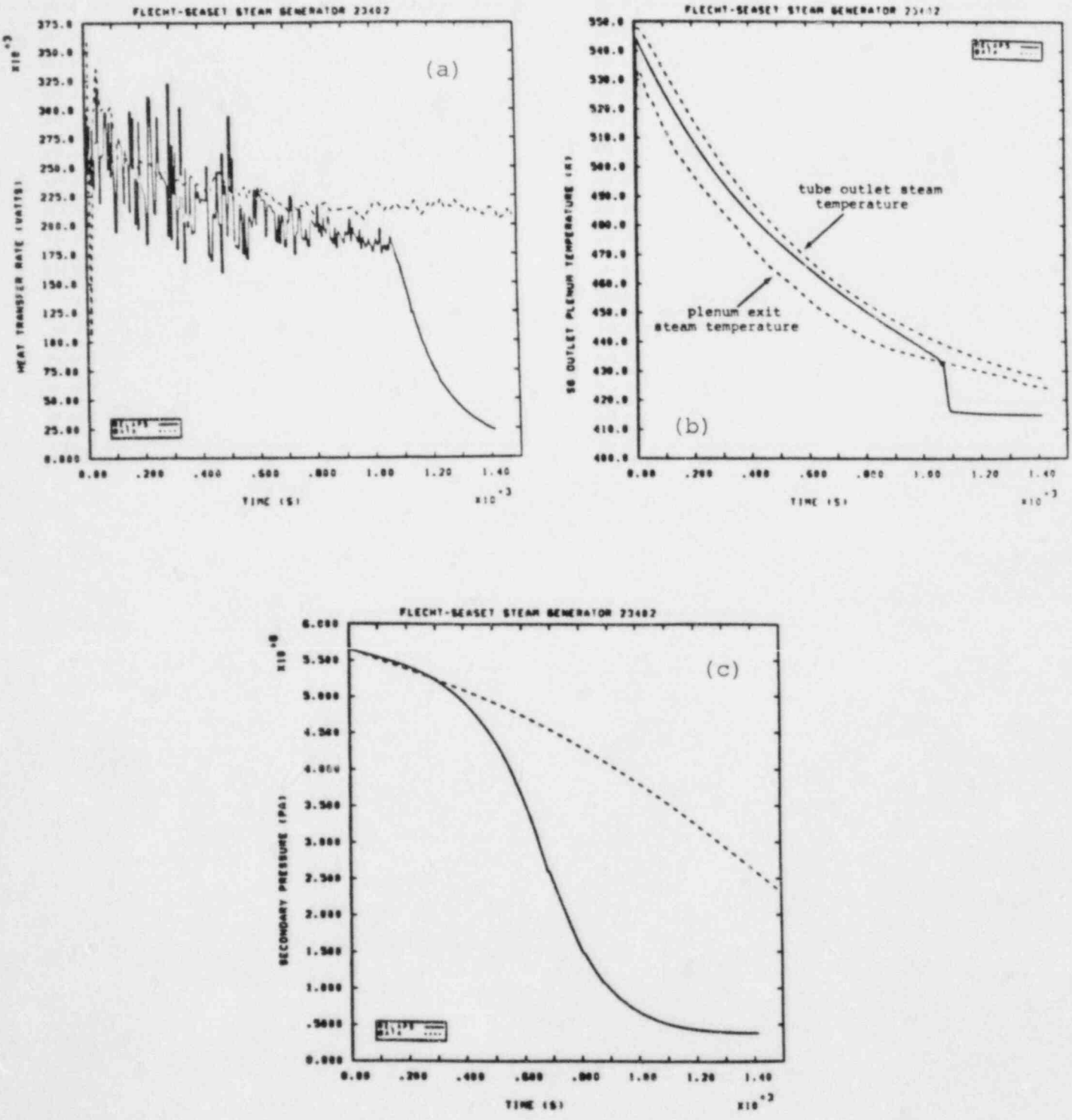

Figure 3.3.1.1 (a) Total Heat Transfer Rate, (b) Primary Outlet Plenum Steam Temperature and (c) Secondary Side Steam Dome Pressure for FLECHT SEASET Steam Generator Transient Test 23402

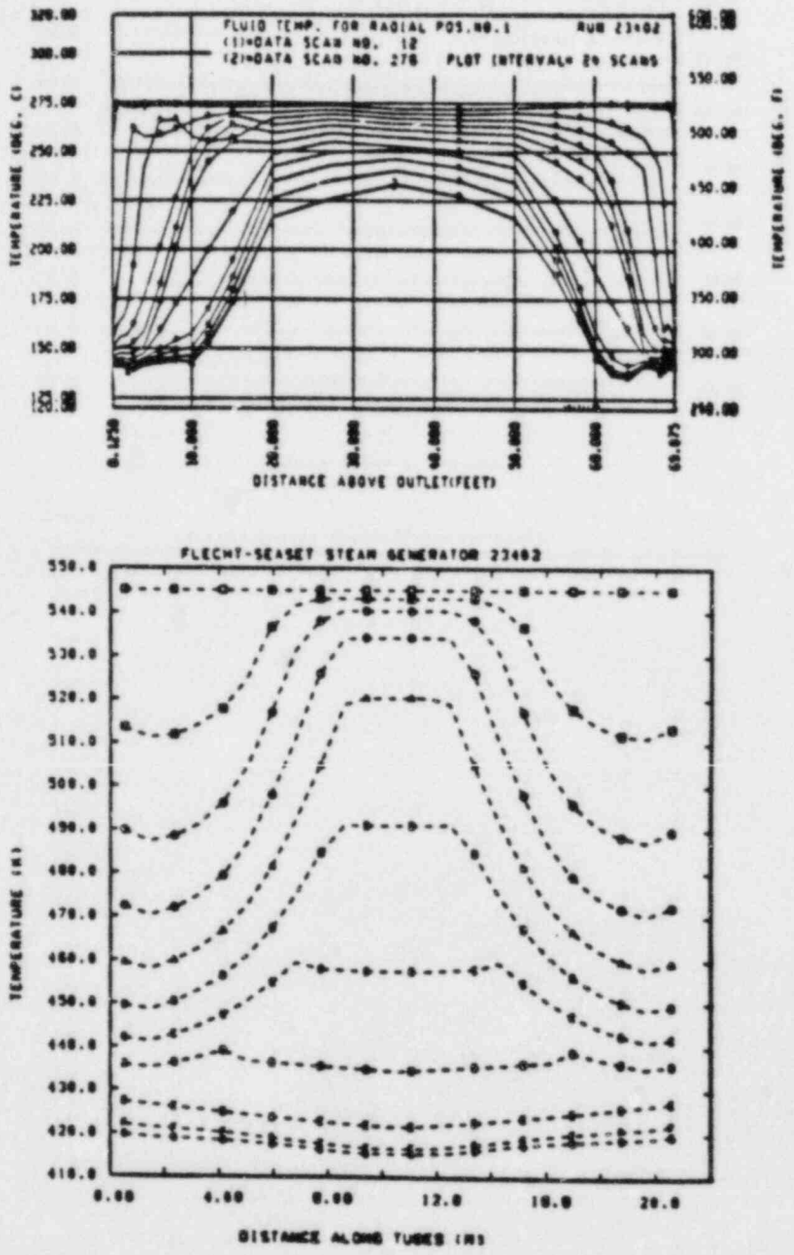

Figure 3.3.1.2 Secondary Side Temperature Profiles for FLECHT SEASET Steam Generator Transient Test 23402

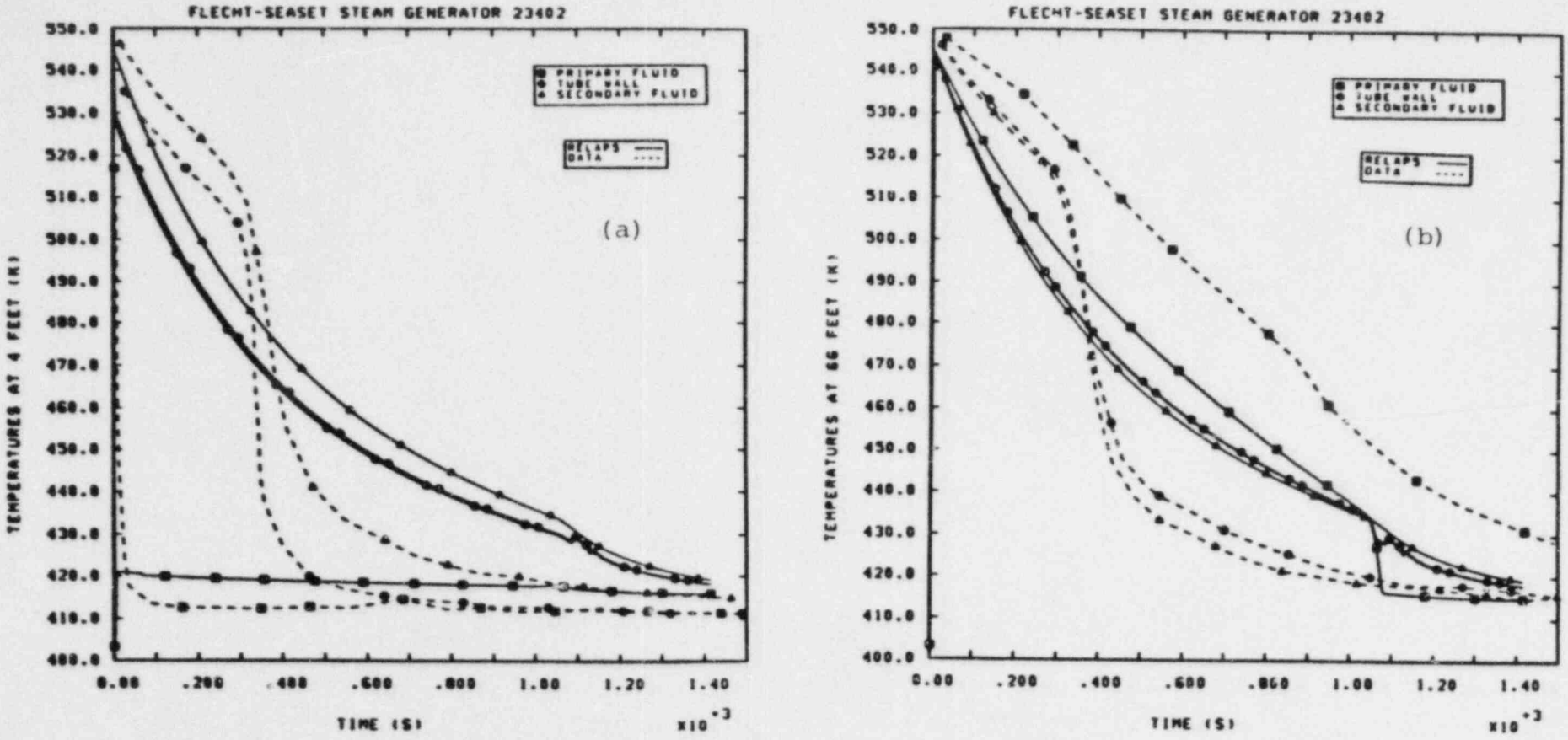

Figure 3.3.1.3 Primary Steam, Tube Wall and Secondary Fluid Temperatures at (a) 4 ft and (b) 66 ft Locations for FLECHT SEASET Steam Generator Transient Test 23402

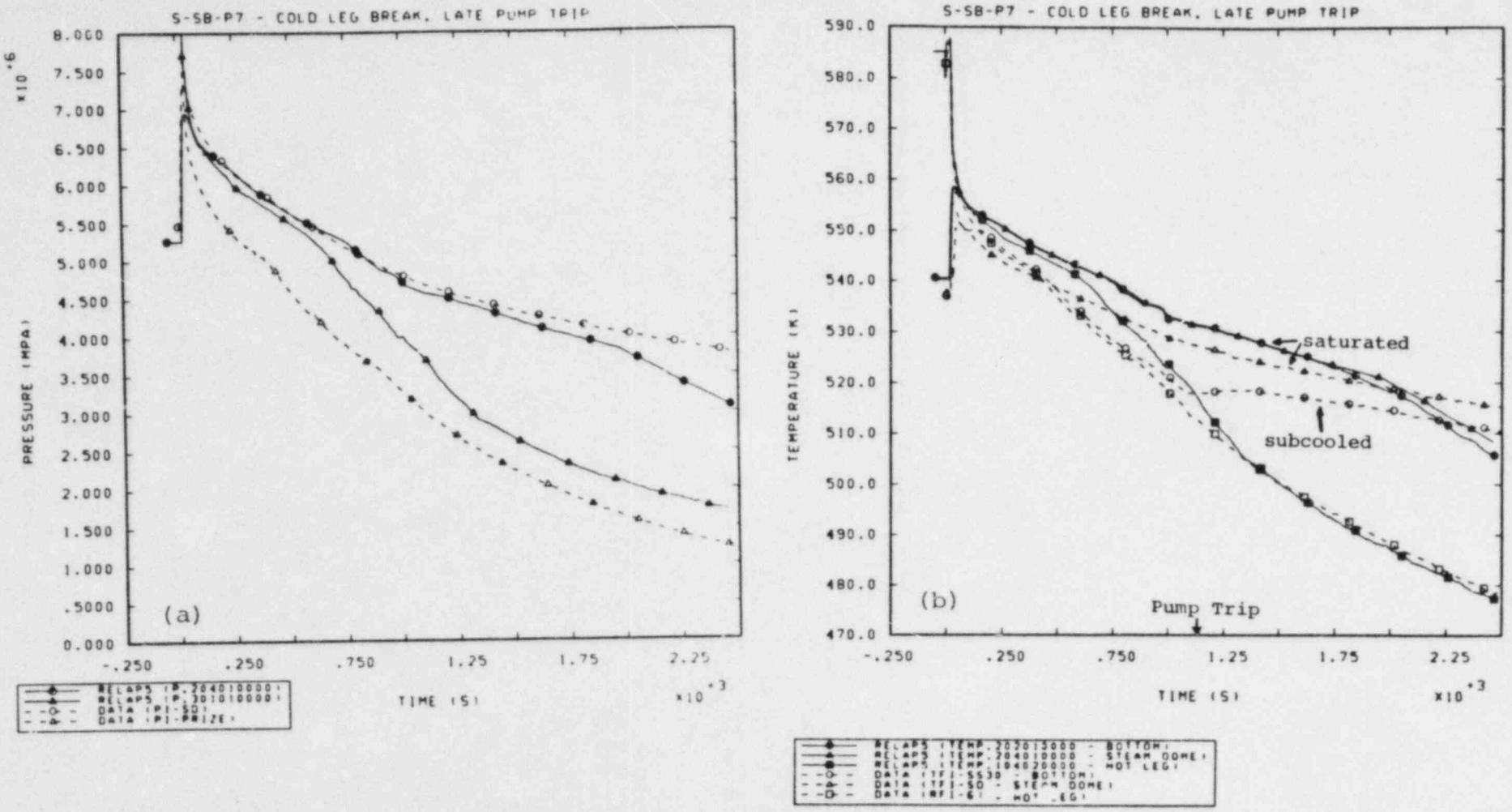

Figure 3.3.2.1 Primary and Intact Loop Secondary (a) Pressures and (b) Temperatures for Semiscale Small Break Transient S-SB-P7

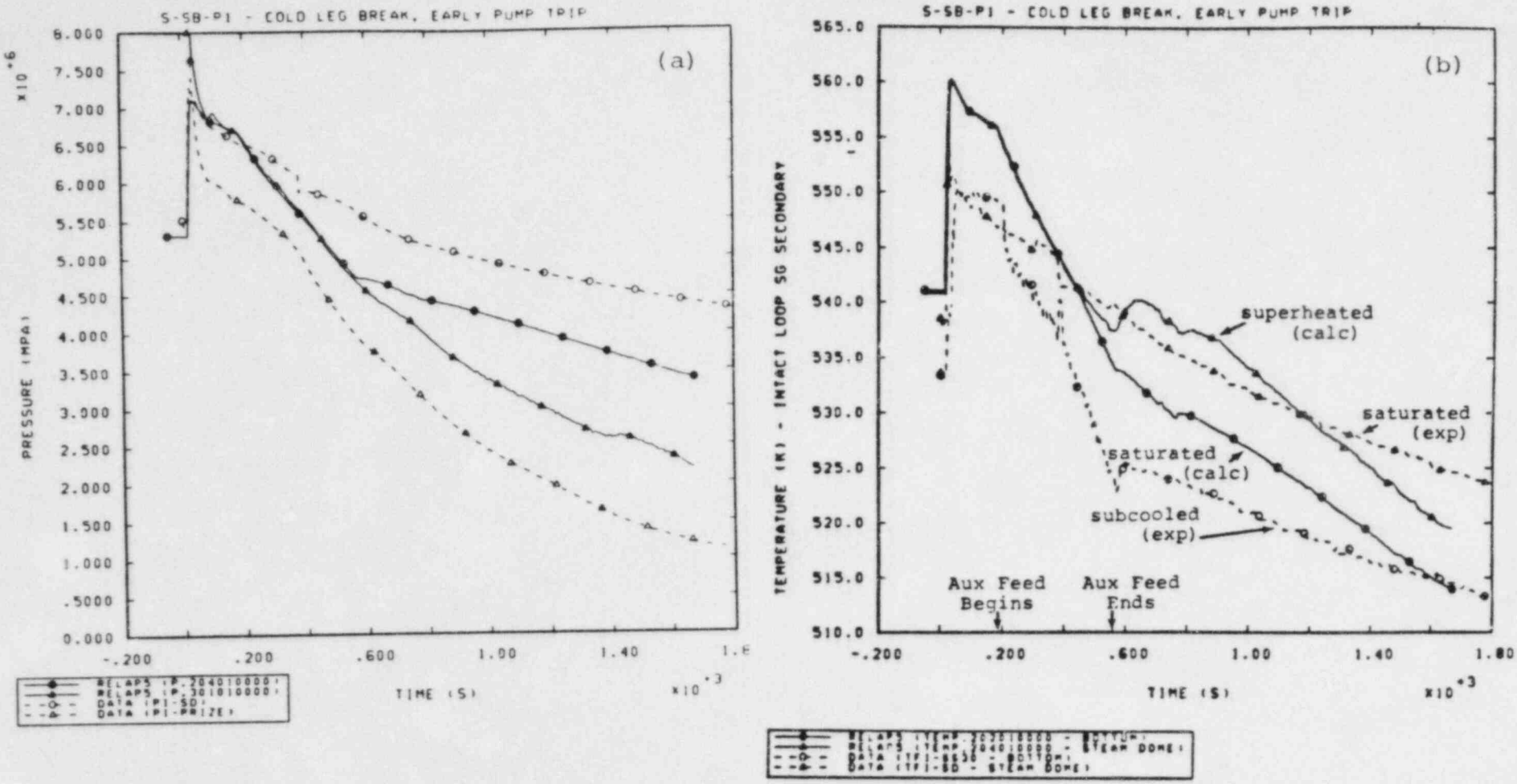

Figure 3.3.3.1 Primary and Intact Loop Secondary (a) Pressures and (b) Temperatures for Semiscale Small Break Transient S-SB-P1

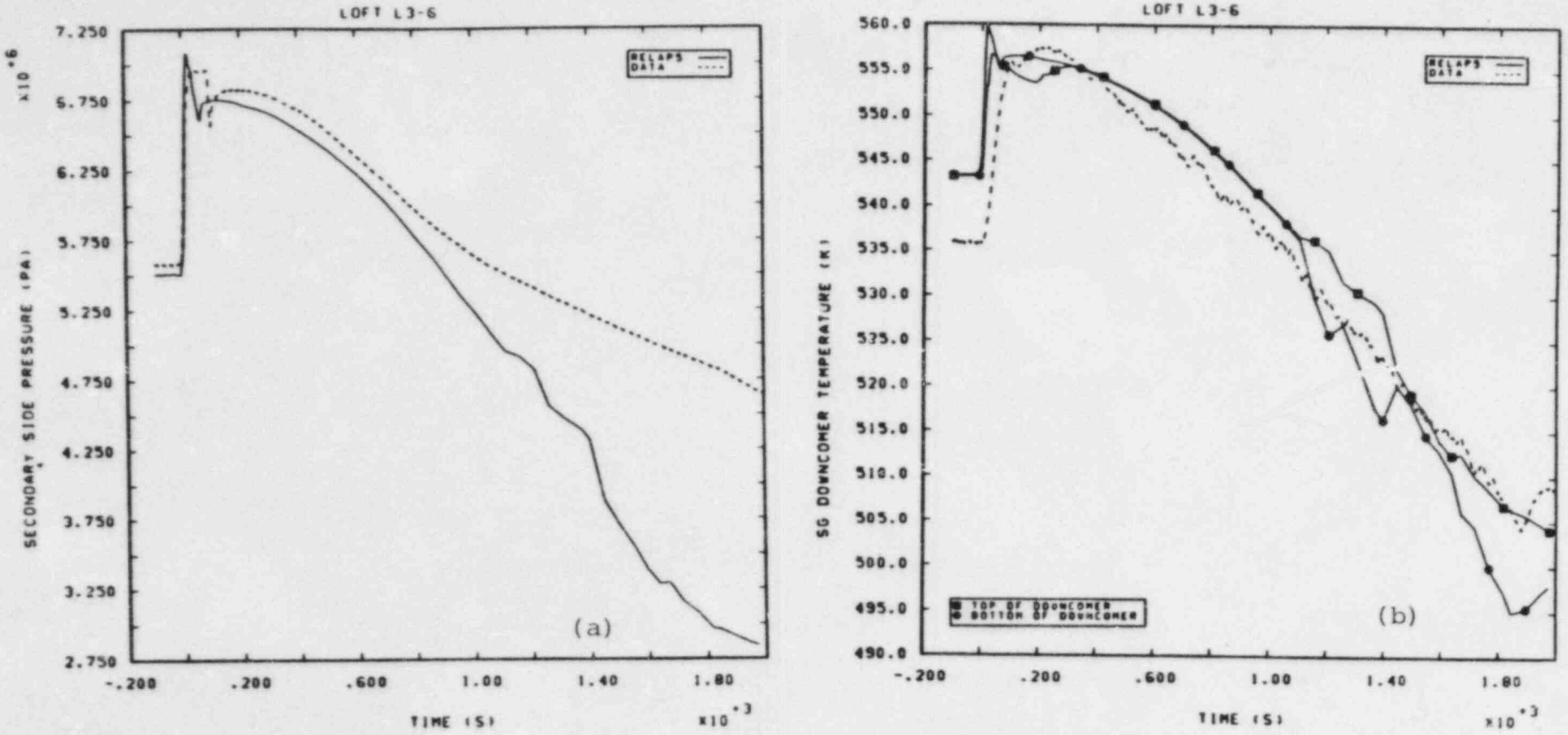

Figure 3.3.3.2 Steam Generator Secondary (a) Pressure and (b) Temperatures for LOFT Small Break Transient L3-6

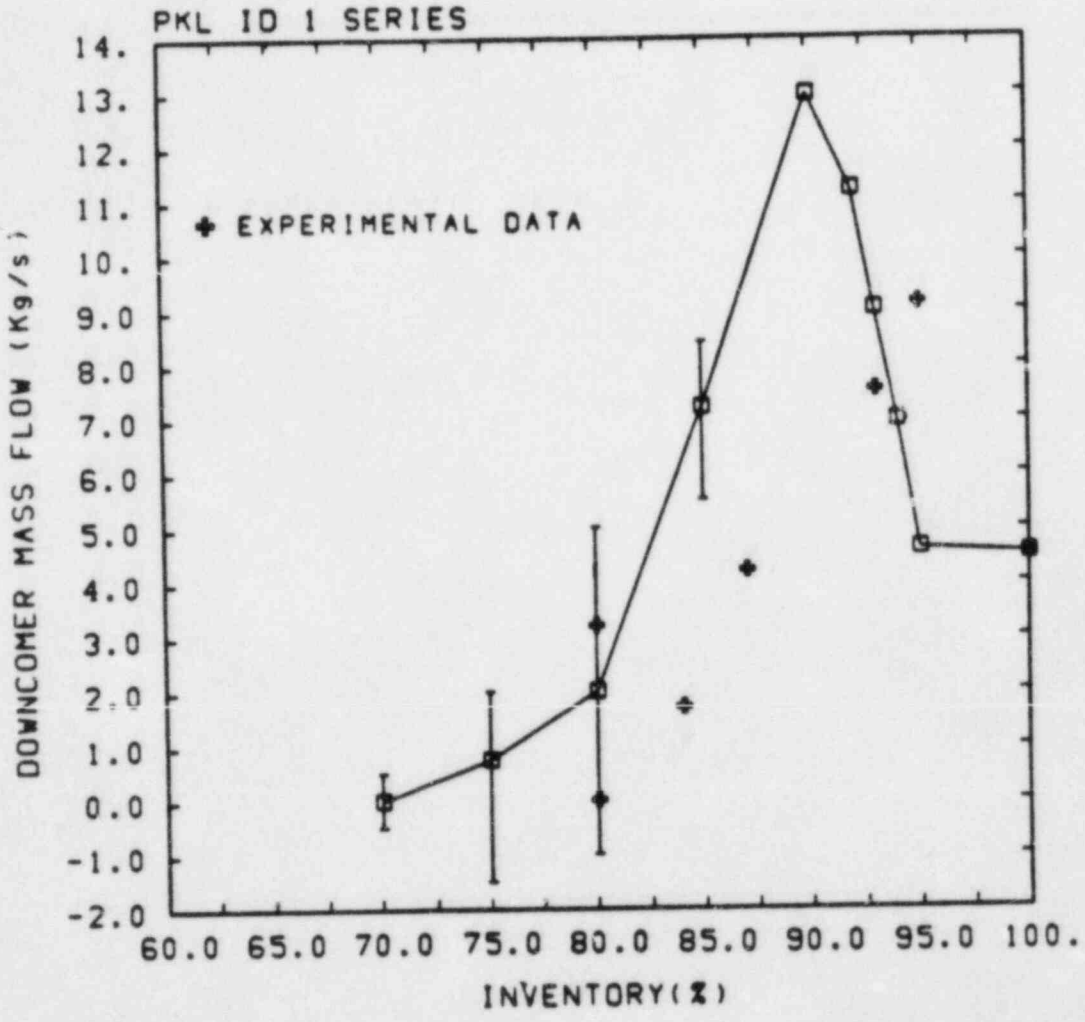

Figure 3.4.1 Downcomer Mass Flow for PKL ID1 Natural Circulation Tests

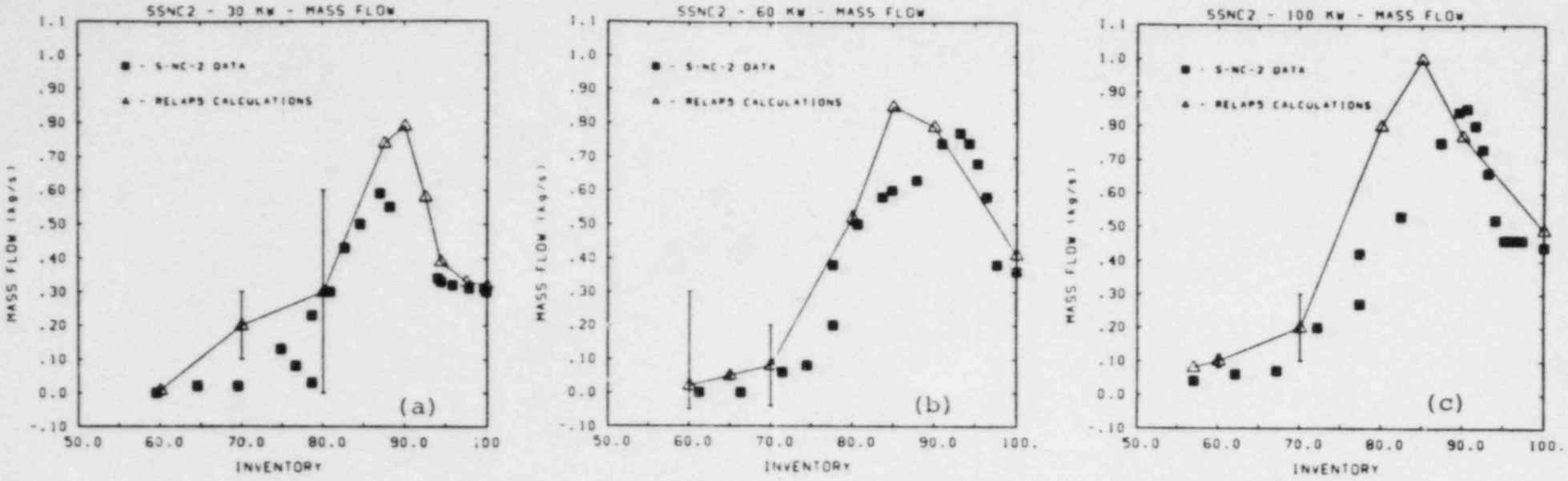

Figure 3.4.2 Mass Flows at (a) 30, (b) 60 and (c) 100 kW Core Powers for Semiscale Natural Circulation Test S-NC-2

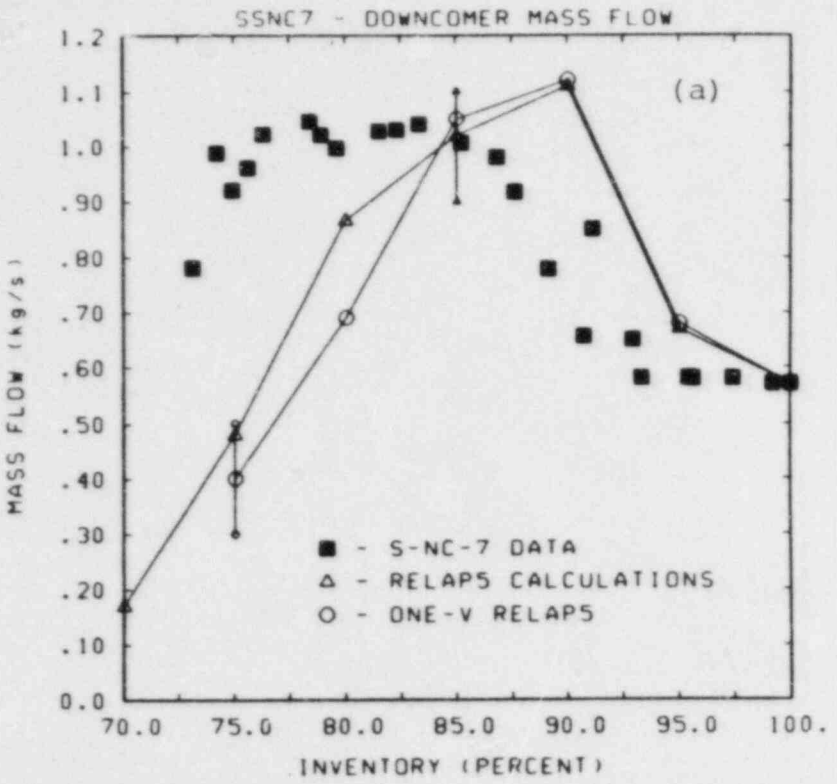

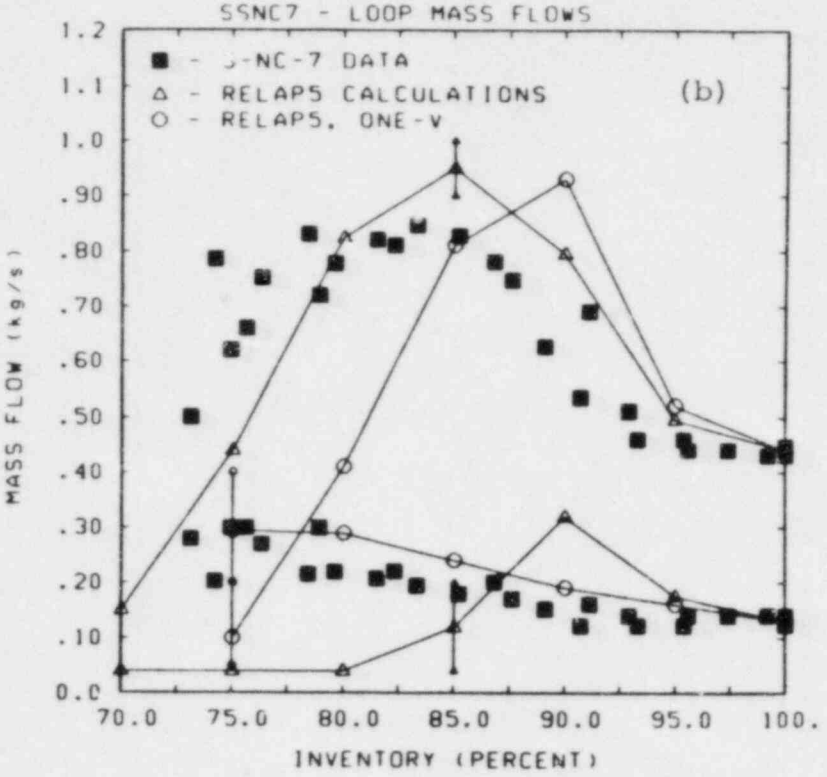

Figure 3.4.3 (a) Downcomer and (b) Intact and Broken Loop Mass Flows with and without One-Velocity Assumption for Semiscale Natural Circulation Test S-NC-7

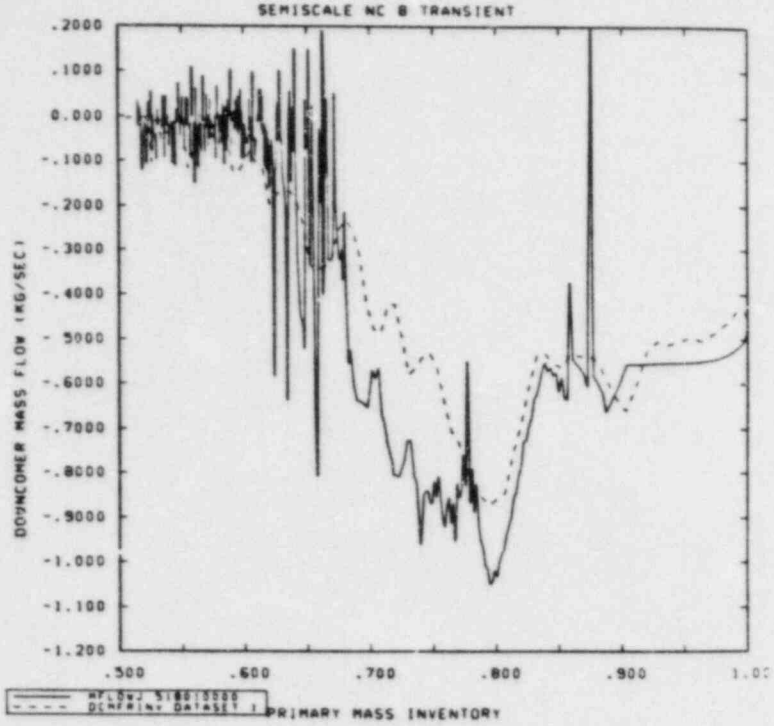

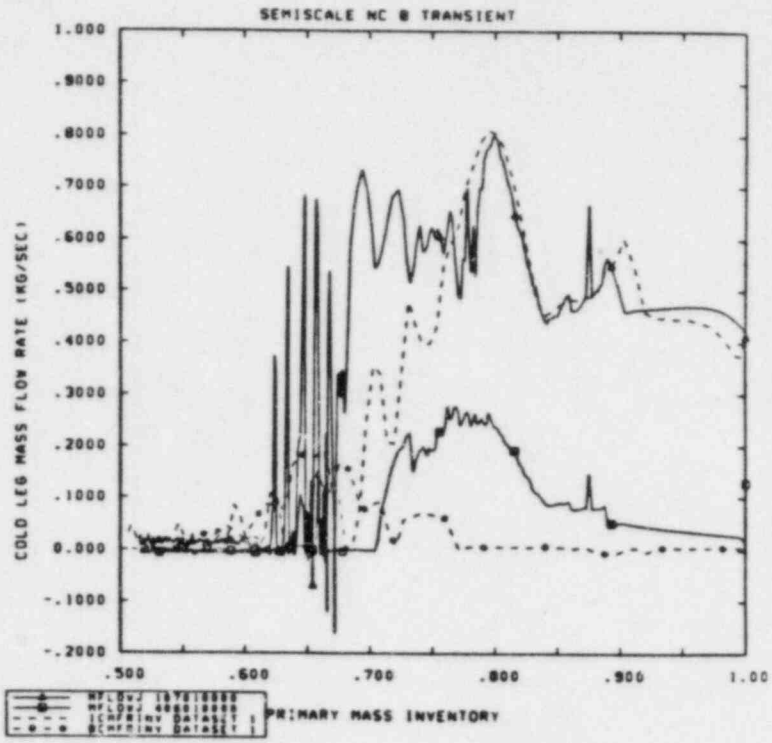

Figure 3.4.4 (a) Downcomer and (b) Intact and Broken Loop Mass Flows for Semiscale Transient Natural Circulation Test S-NC-8

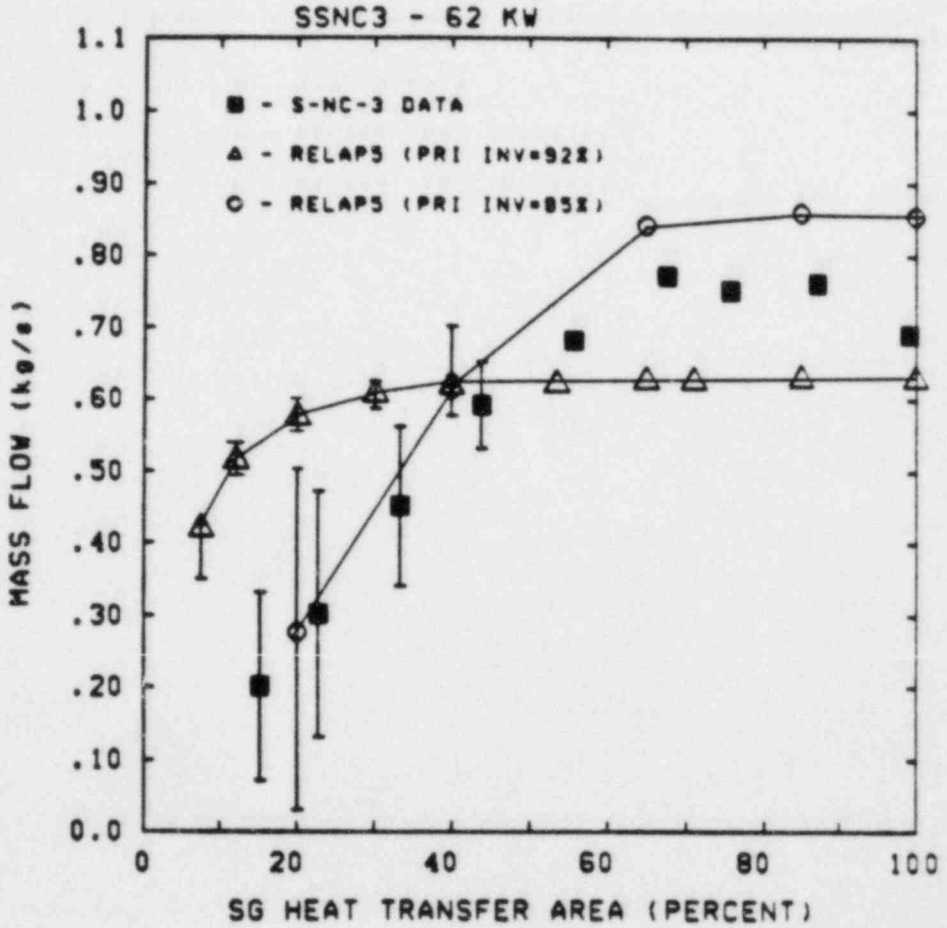

Figure 3.4.5 Mass Flows at Measured and Calculated Peak Two-Phase Flow Primary Inventories for Semiscale Natural Circulation Test S-NC-3

4.0 PROBLEM CALCULATIONS

A large number of our steady state, transient and separate effects test analyses exhibited unphysical behavior in the form of single excursions and/or repeated oscillations in pressure, temperature, mass flow, etc., which often were of sufficiently large amplitude to cause code failures. This unphysical behavior is apparently related to both the time step and the nodalization used; some oscillations seem more related to the time step, such as the temperature oscillations seen during steam generator heat transfer, while others are closely tied to nodalization, such as the cell heatup/cooldown resulting from inappropriate modelling of the bypass and leakage flow paths (although the behavior being calculated can be affected by changing the time step being used).

One of the major weaknesses we found in RELAP5/MOD1 was the time step control algorithm. The majority of the calculations performed in our assessment project required significant user time step manipulation, sometimes to reduce oscillations to a level where the average behavior could be discerned, but often merely to get the code to run at all. If the user was forced to reduce the time step to ensure "good" results, the calculations did not run efficiently since multiple reruns with reduced time steps based on user hindsight were usually required; however, there are no good criteria for determining how far to cut the time step to eliminate the observed difficulties, so it is usually cut down farther than might be strictly required. If the user was not forced to reduce the time step to ensure "good" results, the calculations running at code-selected time steps were generally inefficient in that they were not running at the maximum allowable time step, but at some significantly lower value accessible to the quantum time step controller.

4.1 Time Step-Dominated Oscillations

As discussed at the end of section 2.2.4, liquid level oscillations (induced by mass flow oscillations) were seen on the steam generator secondary side in several steady state calculations [22,26]; these could usually be eliminated by reducing the maximum allowed time step to force the code to run at a time step significantly below its desired value. During our various assessment calculations, we have seen numerous such oscillations, both in steady state and transient analyses, the majority of which could be controlled by manually reducing the time step.

We have found that some of the manifold oscillations observed can be grouped into three major categories:

-- temperature oscillations associated with steam generator heat transfer,

-- mass flow oscillations associated with two-phase natural circulation (including the steam generator liquid level oscillations mentioned above), and

-- pressure oscillations associated with ECC condensation.

The temperature oscillations calculated are definitely non-physical, the mass flow oscillations may or may not be physical, and the pressure oscillations are definitely physical. However, even with "real" oscillations, the code appears to exaggerate the behavior until calculations fail or give meaningless results.

4.1.1 Steam Generator Heat Transfer

Temperature oscillations have been seen in both LOBI steam generators during large break transient analyses [12] as well as in the FLECHT SEASET [14] and B&W [21] steam generator separate effects test analyses. These oscillations generally occur when a high-quality two-phase mixture passing inside the U-tubes is cooler than the adjacent secondary side fluid, i.e., during steam generator reverse heat transfer; however, they are also seen in steady state analyses of a once-through steam generator, where the high-quality fluid is on the outside of the tubes and the oscillations occur during normal heat transfer.

The basic problem is the high-quality fluid picking up enough energy in one time step to become hotter than the attached heat slab and heat source volume (since small changes in internal energy and enthalpy correspond to relatively large temperature changes for steam). During the next time step, the direction of heat transfer reverses and some energy is returned to the U-tube heat slab. However, the thermal inertia of the U-tubes is quite large compared to that of high-quality steam, and the U-tube temperature cannot adjust during one or a few time steps. The resulting nonmonotonic temperature gradient developing in the U-tube heat slab can drive further temperature oscillations, which can grow large enough to cause steam table failures.

Figures 4.1.1.1 and 4.1.1.2 show temperature oscillations occurring in the LOBI A1-04R large break transient analysis when the code-selected time step was used, and the absence of any such unphysical oscillations when the time step was substantially reduced. The plots show the steam generator primary side inlet and outlet temperatures (with the oscillations visible in the outlet fluid temperature), as well as the secondary side (heat source) temperatures. The original transient calculation used a code-selected time step of ~16 ms, with occasional dips to ~8 ms; studies with user-input time steps of 2.5 and 1 ms showed that, while some oscillations between the (secondary) heat source

and the primary side saturation temperature persisted, the gross unphysical oscillations of the primary side high-quality steam becoming hotter than its heat source were indeed eliminated, and the final calculation was run with a user-imposed time step limit of 2.5 ms throughout the latter part of the transient.

The FLECHT SEASET steam generator calculation wanted to run at an average time step of ~12.5 ms; the transient calculation was rerun with user-imposed maximum time steps of 10, 5 and 2.5 ms. The results showed that the temperature oscillations and other unphysical behavior (i.e., the startup temperature spike described below in section 4.3.2) started to damp out and finally disappear as progressively smaller time steps were used, with no other observable effect on the overall behavior calculated. Although small oscillations were still visible with a time step of 5 ms (they were not observed at all when the time step was further reduced to 2.5 ms), we decided this calculation was adequate for our purposes, since each cut in time step resulted in progressively longer run times, and hence higher costs.

Figure 4.1.1.3 shows the temperature oscillations observed during the B&W steam generator steady state calculation and their gradual disappearance with user-reduced time step. For the initial time step of 0.05 s, the secondary side steam outlet temperature oscillated across the primary inlet temperature value, a physical impossibility in an OTSG. When the time step was reduced to 0.002 s, small oscillations still occurred but the secondary outlet temperature remained slightly lower than the primary inlet temperature, as would be expected in reality.

All the temperature oscillations we have encountered to date could be eliminated by the user reducing the time step. (Similar temperature oscillations were also seen and reported by BNL [38] in their RELAP5 analyses of other FLECHT SEASET steam generator separate effects tests, and they were also able to eliminate these unphysical oscillations with a user-imposed smaller time step.)

4.1.2 Natural Circulation Mass Flow

A different class of oscillations, also primarily caused and influenced by the time step used, has been encountered mostly for two-phase flow conditions in PKL [13] and Semiscale Mod-2A [20,23] natural circulation test analyses; related oscillations are seen in steam generator secondary sides during steady state operation where the recirculation is being driven by the same natural circulation phenomena. (Examples of these oscillations in steam generator secondary steady state operation were given above in section 2.2.4; examples from the steady state natural circulation analyses will be given in this section.)

The time step calculated by RELAP5 was too large at low primary side inventories in all the natural circulation test analyses done, but was generally adequate at higher primary system inventories. The dividing value of ~90% inventory corresponds to the onset of two-phase natural circulation; i.e., the code-selected time step gave good results during single-phase natural circulation. Below this inventory value it was necessary to impose a smaller (by about a factor of four) time step to eliminate spurious oscillations, as shown in Figure 4.1.2.1 for the Semiscale two-loop baseline test S-NC-7. Without the time step reductions, the actual average loop flows are impossible to discern. Although the code time step was generally acceptable at higher primary system inventories, this was strictly true only for the baseline tests (i.e., the PKL test series and Semiscale tests S-NC-2 and S-NC-7). Other natural circulation tests analyzed (S-NC-3 and S-NC-4) which studied the effects of degraded steam generator heat removal capability required time step reductions at lower secondary side inventories as well as at lower primary inventories.

Some of the oscillations observed in these natural circulation calculations, however, were apparently real and were not affected by changes in time step. Loop-to-loop oscillations with a long time constant (as long as hundreds of seconds) were seen in the PKL analyses; with three separate loops in the facility and in our model, no frequency determination for these oscillations was possible. Reducing the time step changed, but did not damp or eliminate, these oscillations. Steady state long-period oscillations were also calculated at certain inventories for each power level in the Semiscale single-loop baseline test S-NC-2 and in the degraded heat transfer tests S-NC-3 and S-NC-4; they appeared to be physical because their period was much longer than the time step used and because user-forced variations in time step did not influence them. Although it was not fine enough to prove that these oscillations were real, the experimental data did suggest the presence of oscillations at approximately the same inventories as calculated for each power level.

4.1.3 ECC Injection

ECC injection oscillations do occur in reality, as shown in Figure 4.1.3.1a for Semiscale small break transient S-UT-1. [37] When the accumulator begins injecting, the condensation effect of the cold water causes the primary pressure to drop, in turn increasing the injection rate. But the effect of injecting mass into the system and dropping the pressure is to increase the overall vapor generation rate and cause the primary pressure to plateau or, in some instances, even to rise. This in turn causes

the pressure-driven accumulator flow to slow down or stop and the total vapor generation rate and system pressure to decrease, starting a new cycle. The problem seen with various calculations during this RELAP5 assessment is that the code allows time steps big enough that the ECC injection oscillations, driven by the same mechanism as just described, become large enough to at best cause intermittent and unsteady accumulator injection not seen experimentally, or at worst to cause steam table failures and code aborts.

Figure 4.1.3.1b shows that qualitatively similar ECC injection oscillations were calculated in our S-UT-1 analyses [24], although there is less calculated total injection than measured and the calculated injection oscillations are not as well-behaved as those in the experiment.

While the S-UT-1 analysis is a clear example of the code giving ECC injection oscillations that are present in the data, our S-UT-7 analysis is a good counterexample of the code predicting ECC "oscillations" (actually large flow surges) that are apparently completely fictitious. Figure 4.1.3.2 shows the measured and calculated UHI accumulator pressure (already discussed above in Section 3.1.2) and the calculated UHI flow rate in Semiscale small break test S-UT-7 [24]. A number of very large flow outsurges are indicated by the dramatic drops in pressure shown by Figure 4.1.3.2a; the pressure drops caused the accumulator built-in check valve to close and the flow surge to cut off, until the vessel upper head depressurized sufficiently to cause the cycle to repeat. Some of these flow surges cannot even be seen in Figure 4.1.3.2b because they are so rapid that our plot frequency (every two seconds) could not catch them.

Similar accumulator flow surges were calculated with both cycle 14 and cycle 18 during the LOFT L5-1 intermediate break transient analysis [19]. The calculated (cycle 14) accumulator flow, shown in Figure 4.1.3.3a, began a few seconds early but, shortly after, the flow shut off because the pressure in the surge line rose above the accumulator pressure, shown in Figure 4.1.3.3b. These pressure plots also explain the late-time lack of any accumulator injection; the large outflow during the second flow spike dropped the accumulator pressure (and, briefly, the surge line and cold leg pressures) below the later-reestablished nominal cold leg pressure, causing the built-in accumulator check valve to remain closed.

Calculations with reduced time steps, different surge line loss coefficients and different surge line nodalizations all showed no significant improvement in calculated behavior. Because a number of changes had been made in the accumulator model since cycle 14, we reran this transient using cycle 18 to see what

accumulator injection behavior that version predicted. The results were better than those with cycle 14, but still not satisfactory, as shown by the accumulator injection in Figure 4.1.3.3c and the associated accumulator, surge line and cold leg pressures in Figure 4.1.3.3d. A pressure spike still occurs in the surge line, but smaller than the one seen in the cycle 14 calculation. (The cycle 18 accumulator updates do correctly fix a coding error in the accumulator component subroutine, which we bypassed in our cycle 14 calculations, as discussed below in Sections AI.1.1 and AI.1.3.)

We also encountered problems attempting to calculate accumulator injection in the LOBI A1-03 large break analyses. [12] In that transient, unlike the other large break tests we analyzed, ECC water is injected into both the intact loop hot and cold legs (from one accumulator with a branching surge line) as well as into the broken loop hot leg (from a second accumulator); since the existing accumulator component logic in RELAP5 does not allow for branching surge lines, the downstream regions of such surge lines must be modelled using piping components.

Here also, we tried varying nodalization, time step, surge line losses, choking flags and initial conditions. Although the exact failure mode might vary, all (cycle 14) calculations inevitably aborted soon after accumulator injection began, in some cell inside or adjacent to the branching surge line piping. Figure 4.1.3.4 summarizes the pressure behavior seen in a typical calculation. The accumulator itself is quite well-behaved, as shown in Figure 4.1.3.4a. The branch below it experiences some small preliminary oscillations before the final failure, as shown in Figure 4.1.3.4b, mirrored in the piping going to the hot and cold leg injection points (Figures 4.1.3.4c and 4.1.3.4d, respectively). The pressures immediately downstream of the hot and cold leg injection points remain well-behaved throughout, as seen in Figures 4.1.3.4e and 4.1.3.4f, respectively.

When this was reported to the code developers at INEL, they thought that the source of the problem was the branch component rather than the accumulator itself, and that an update to the branch logic used then at INEL (but not formally released) might help. We therefore reran the transient with cycle 18 and a few other recommended, but not then released, INEL updates. These code updates did ameliorate the problem seen with cycle 14, but did not eliminate it completely (just as for LOFT L5-1), since this calculation also failed in the branching surge line, albeit much later in time. Even running the transient out that far required many time step cuts to coax the calculation past trouble spots, some of which can easily be seen in Figure 4.1.3.5. (We did not attempt restarting and reducing the time step again at ~64 s to see if the calculation could be continued further.)

Perhaps the best example of code-exaggerated ECC-driven oscillations is found in our BCL 2/15-scale vessel separate effects test analyses [25]. In the two transient experiments considered in our assessment matrix, the vessel is initially filled with steam flowing from the core region through the lower plenum and downcomer out a broken cold leg. Several seconds after time zero, ECC injection is begun in the other three (intact) cold legs. In all our calculations, the code would run during the initial steam-only period using a time step of 0.05 s and then abort when the ECC injection began; however, if the user manually specified a time step of 0.05 or 0.025 ms at the time the ECC was to begin the calculation would run much farther before aborting. The code time step control algorithm apparently could not back up and reduce the time step either early enough or sufficiently far to avoid the premature code abort.

4.2 Nodalization Dominated Oscillations

RELAP5/MOD1 can have large mass and/or energy conservation errors. There appears to be a problem in the basic finite-difference formulation, possibly related to velocity reversal. In some of our calculations, problems were eliminated by changing the leakage path modelling. However, the exact source of the conservation errors was not located; it was merely bypassed. The logic errors which allow the mass and energy errors are still present in the code (as of cycle 18+). Stagnant sections of piping in a two-phase state are a particular trouble spot for mass errors, but these same sections of piping can also show energy errors during single-phase conditions; we have seen large fractions of the fluid mass in a pipe vanish although there was almost no flow out of the ends.

4.2.1 Bypass and Leakage Flow Modelling

There were a number of posttest calculations performed for LOFT L6-7/L9-2 [16], in which we eliminated the reflood assist bypass valve (RABV) flow path to improve the late-time agreement with data. This seeming minor nodalization change led to the discovery of several problems with energy and mass conservation. The difference is that the broken loop is now stagnant during much of the transient; errors from the numerical methods thus remain at a single location and can add together and grow. The small flow in the previous calculation had masked the difficulty. When the RABV flow is eliminated, very little should happen in the broken loop until it flashes. There should be a slow depressurization and cooling from the environmental heat losses, but this was not the case. Instead, a rapid heating of one of the stagnant cells was calculated, as shown in Figure 4.2.1.1a.

Within 40 seconds the cell had heated to saturation. Greatly decreasing the time step led to some improvement but would not eliminate the problem.

We traced the cause of this cell heatup to small but cyclic velocity oscillations throughout the broken loop, and then traced the source of these oscillations to the use of the abrupt area change model for the leakage paths in the vessel model, with the help of the code developers at INEL. The nodalization in the vessel was changed to eliminate the use of the "abrupt area change" junction model in the description of vessel leakage paths; the flow paths were modelled with the "smooth area change" junction model and very large form loss coefficients, adjusted to yield the correct steady-state leakage flows. This change was successful in eliminating the cell heatup problem, as shown in Figure 4.2.1.1b.

A similar difficulty was observed in the virtually stagnant broken loop in our LOFT L9-1/L3-3 steady state calculations. [17] Figure 4.2.1.2 shows the temperature of the cell in question and of all cells connected to it. In this particular case, the cell would insist on cooling -- to the freezing point if the calculation were run long enough.

Errors in the code's numerical methods can also cause mass to magically disappear from the primary coolant system. In our early LOFT L9-1 transient calculations, mass was being lost from the closed primary system rapidly enough to prevent the PORV setpoint from being reached in ~1700 s of transient; when we isolated portions of the broken loop, most of the variations in system mass were eliminated, and we were able to proceed. Figure 4.2.1.3 presents comparisons of primary masses and pressures with and without the full broken loop active in the primary system. There is an early period of ~200 s during which both calculations adjust to slightly inconsistent initial conditions; however, once spray cycling starts, the pressures are virtually the same, until the better mass conservation in the second calculation allows the pressurizer to fill with liquid and its pressure to reach the PORV setpoint.

We believe that the use of the abrupt area change model for the various LOFT bypass and leakage flow paths (in conjunction with the presence of a number of quasi-stagnant volumes) was responsible for both the "cool-down" and the global mass errors we observed in our L9-1 analyses, as it was for the cell heatup in our L6-7/L9-2 calculations, and that if we had rerun this L9-1 calculation with the bypass and leakage junctions modelled as smooth area changes and large user-input loss coefficients the mass loss would not recur. (The large cost of the long L9-1 transient calculation prevented us from rerunning it with the "fixed" bypass and leakage flow path modelling.)

4.2.2 Quasi-Stagnant Cells

We have seen other problems originating in quasi-stagnant regions which do not appear to be caused by the use of the abrupt area change model for bypass and leakage flow paths. The major symptom of such problems is a series of temperature "jogs" as an almost-isolated volume attempts to come to equilibrium with its neighbor cells. Such almost-isolated cells tend to remain nearer the initial temperatures than the rest of the system for a significant period of time, and then suddenly attempt to compensate, sometimes catastrophically. The behavior can be somewhat smoothed or entirely eliminated by reducing the time step used; however, the ultimate source of the difficulty appears to lie in the modelling limitations and assumptions inherent in the code's one-dimensional formulation, rather than in the time step control per se.

After the bypass and leakage flow junctions were redefined with smooth area changes and large user-input loss coefficients to eliminate mass and energy conservation errors, we still calculated some unphysical behavior in our LOFT L6-7/L9-2 analyses, which could be eliminated by using the nonstandard equilibrium option in the stagnant sections of the broken loop. [16] There should be a slow flow out of these cells as the system depressurizes, assuming pure one-dimensional flow as RELAP5 does (in the actual situation, we would expect phase separation in the vertical direction of such a horizontal component). In our analyses, to the contrary, the calculated behavior was far from equilibrium and led to the wrong depressurization rate.

Figure 4.2.2.1a shows the fluid history for one broken loop cell using the standard nonequilibrium option; also shown are the saturation line and two nearby isentropes for water. The path that the cell should follow is roughly parallel to the isentropes with a slow downward drift from environmental heat losses, from right to left on the plot as time increases. The correct behavior is seen while the fluid is in a single-phase state to the right of the saturation line; however, the calculated behavior in the two-phase region is clearly wrong. The errors are very likely related to the mass and energy errors discussed above. Figure 4.2.2.1b shows the same cell history using the nonstandard equilibrium option. This model yields physically correct behavior and the correct system depressurization rate.

The last half of our LOFT L6-7/L9-2 transient analysis also showed numerous "condensation events", numerical in nature, which were the result of two factors: an inadequate pipe tee model and the lack of a good treatment of the interface between hot vapor and cool liquid with gravity separation. The problem can be reduced by cutting the time step; however, this is expensive in terms of computation time.

After the pump trip initiating L9-2 at ~325 s, the primary system is in single-phase natural circulation. There are several points in the system where vapor collection is calculated after ~530 s, some artificially generated by one-dimensional modelling. In addition to the pressurizer itself, void also forms in the spray cooling line, the upper vessel and all broken loop cells; in effect, there are a number of pressurizers in the system. Numerical noise and the lack of a good liquid/vapor interface separation model cause a very rapid reverse flow into one of these cells, resulting in a rapid cooling of the vapor and a step decrease in the pressure as shown in Figure 4.2.2.2a. The plotted results past 900 s are from a restart in which we attempted to increase the time step; reducing the time step again produces the results shown in Figure 4.2.2.2b. (Both calculations used time steps considerably smaller than the code-calculated value.)

These "condensation events" are a serious problem resulting from the numerical methods employed, and have nothing to do with real physical events. To illustrate, consider the temperature history of the cell representing the downcomer above the cold leg nozzle. With the junctions used in our nodalization, this cell is not directly included in the main cold leg/downcomer flow path. It thus tends to remain near the initial temperature and then flash as the pressure decreases. (In this calculation, flashing occurred at ~530 s, when the cell was about 50-60 K hotter than the rest of the downcomer.) A series of such small condensation events produces the temperature history shown in Figure 4.2.2.3.

The real root of this problem is a shortcoming of the component models available in RELAP5. The question is how to model a pipe "tee" when one of the tee ends is closed off. The two possible options with RELAP5 are shown in Figure 4.2.2.4 and can lead to quite different results. We have used both forms in different places in our nodalizations. For different conditions, either form can lead to incorrect behavior. In this particular case, option B yields fewer numerical problems, while option A tends to isolate a cell from the rest of the problem. (Different behavior calculated with these two modelling options has been recognized, but not formally documented, by INEL analysts, who identify option A with "no mixing" and option B with "perfect mixing"; such details in nodalization can therefore determine what physics is to be calculated.)

Problems were encountered in the same "pseudo-pressurizer" cells in our LOFT L9-1/L3-3 analyses. [17] The first L3-3 calculation ran smoothly from 3270 s to 5116 s, when we noticed an input error affecting the steam generator secondary at 4850 s. We restarted a corrected calculation from the last appropriate time; this calculation aborted due to problems in a small cell at

the top of the vessel at 5033 s. We then specified a smaller maximum time step and restarted at 4870 s; in this case, the calculation aborted, for the same reason, at 4873 s.

There are two points of interest in this behavior. First, a change in the model caused very different results in a part of the problem which was not connected with the region where the change was made. Second, a reduction in the allowed time step is not necessarily the cure for all computational problems with RELAP5. Some experimentation may be necessary in order to discover a set of values for which the time step control and time step change algorithms will allow results to be obtained.

By an arduous and time-consuming sequence of water property failures, time step experimentation and restarts, the L3-3 calculation was forced to proceed to a time well past the beginning of steam generator refill. At ~5484 s, we became aware of another input error, and decided to redo the calculation.

This repeat calculation was also made difficult by water property failures in the same cell. The slightly different system conditions caused the problems to occur at different times, so the time step sets from the first calculation could not be used. The failures were characterized by a period during which the cell's temperature would increase in an oscillatory manner, while temperatures in adjacent volumes would be relatively constant. The calculation would abort when the pressure in that cell suddenly jumped to an extremely high value. Such failures could be averted by specifying a reduced maximum time step for a short period before the code abort occurred. The last fatal temperature increase would then not take place and the calculation proceeded until the next instance of an aborted calculation. Temperatures calculated in the upper vessel cells are shown in Figure 4.2.2.5 for all of L3-3; the bypass cell temperature displays traces of some, but not all, of the difficulties we encountered.

We also encountered problems traced to a stagnant cell in our BCL ECC bypass/delivery separate effects test analyses. [25] The first calculations done failed consistently when the ECC water injection was started. These aborts were caused by excessively high pressures in the dead-end intact loop piping cell (modelling the closed-off piping upstream of the injection point), when all the injected ECC water backed up into that cell rather than flowing into the other intact loop volumes and then into the vessel. The problem could not be eliminated by reducing the time step or by changing the rate of ECC injection startup. The only solution found was to remove that cell from the nodalization, although the portion of pipe it represented is physically present in the facility; removing the cell, however, introduces an error in the time that ECC water reaches the vessel by decreasing the intact loop cold leg piping volume where the injected water can accumulate.

4.2.3 Other Mass and Energy Conservation Errors

Proper modelling of bypass and leakage flows will eliminate some of the mass and energy conservation errors that we have encountered, as discussed above in Section 4.2.1; however, the basic problems remain, and only one potential trigger has been removed. Similar mass and energy errors have been seen in other analyses, where the particular problem of the abrupt area change model causing oscillations at secondary flow paths whose effect accumulates in stagnant cells is not likely to be the reason.

Mass conservation problems (with mass in this case appearing in a closed system, in contrast to the mass loss seen in the LOFT L9-1 analysis discussed above in Section 4.2.1) were seen in our PKL steady state natural circulation analyses. [13] We first noticed the problem because the valve controller set up to drain the mass inventory to the desired value would intermittently activate at two "fixed" primary inventories (90% and 92%). At all other inventories the total primary mass remained constant to a small fraction of a percent over several thousand seconds of problem time; at these two inventories, on the other hand, there were mass increases of 0.5% (which automatically tripped the drain controller) in ~500 seconds, as shown in Figure 4.2.3.1 for 90% inventory. At these two inventories, the liquid level in the vessel has dropped sufficiently that the hot leg is starting to uncover; we feel that the two-phase mixture level crossing the vessel and hot leg cell boundaries at this elevation is the ultimate source of this mass conservation error, although the exact mechanism is not known.

In one of our LOBI large break transient analyses, we got code failures late in the transient, due to the temperature in a pressurizer surge line cell rising to 1500 K; the observed behavior is similar to the cell heatup discussed in Section 4.2.1, except that the heatup is not occurring in a stagnant region and there are few bypass or leakage flow paths modelled. The pressurizer is mostly void late in the transient and still discharging as the system pressure continues to drop; the other cells in the surge line remain well-behaved throughout. We could slow down this heatup by reducing the time step, but we felt a more economical solution was to simply disconnect the pressurizer, since it should not greatly influence the late-time transient behavior. A possible culprit causing this heatup (as it did the similar problem in our early L6-7 analyses, discussed above in Section 4.2.1) is the abrupt area change model, used at the surge line inlet and outlet junctions, although the junction areas are not that much smaller than the adjacent volume flow areas and, as mentioned, the heatup does not occur in a stagnant cell but in a cell with visible through-flow.

This same heatup problem was also encountered in our LOFT large break analysis, in one of the broken loop hot leg cells. Just as in the LOBI calculation, the unphysical behavior could be eliminated by cutting the time step back far enough.

4.3 Quantum Time Steps

Another problem with the time step control algorithm is the fact that the time step can only be changed by factors of 2 (i.e., the time step used can only be halved or doubled), starting from the user-specified maximum time step. This is a very inconvenient and inefficient feature of RELAP5, since most calculations do not run at the largest possible time step, but at the next lowest value of the quantum set of time steps determined by the user-set maximum time step. Also, rather than beginning a calculation with the minimum allowed time step (apparently hardwired in RELAP5 to be 10**-06 whatever the value input by the user) and then progressively increasing it as is done in TRAC startup, RELAP5 begins with the maximum allowed time step; results indicate that the code can calculate some quite peculiar behavior without the code time step control algorithm noticing and repeating the iteration with a reduced time step. Other problems have been encountered which can be traced back to assumptions made about trip and time-dependent volume and junction initial values during the zero step processing.

4.3.1 Inefficient Run Times

As an example, suppose a calculation is run with a user-input maximum time step of 0.5 s; the allowed code time steps are then 0.5, 0.25, 0.125, 0.0625, 0.03125 s, etc. Now suppose the Courant limit time step would be ~0.03 s; since this is less than the allowed value of 0.03125 s, the code is forced to run at the next lowest allowed value, or 0.015625 s, a time step only ~52% of that which would still permit stable solution, almost doubling the required run time for an otherwise identical problem. (If the calculation were run with an unusual maximum time step of 0.47 s, the allowed time steps would include the much more efficient value of 0.029375 s, but this requires detailed foreknowledge of the limiting time step history, and is normally impossible.)

Early in our assessment project [18], during the steady state calculation and early parts of the transient calculation for our LOFT L3-6 analysis (which are mostly Courant-limit dominated), we tried to improve the run time by renodalizing the pump inlets and outlets (the major source of the Courant limits). If the limiting region was renoded by combining smaller cells into somewhat larger cells, a larger Courant limit usually ensued. However, a

10% or 20% increase in the Courant time step limit did not usually result in an equivalent decrease in run time, since the code could only halve or double the time step. In order to double the Courant limit at any given time, very extensive renodalization would have been necessary, but such renodalizations cannot be effectively undertaken during the course of a long transient since most cells in our input models have associated heat slabs, and heat slab input cannot be changed on restart in MOD1.

While our LOFT calculations showed that massive renodalizations might be required before the time step could be increased (and hence run time decreased), the FLECHT SEASET steam generator calculations [14] pointed out the reverse side of the coin; limited changes in input, by causing small decreases in Courant limits or other time step limits, can result in large increases in run time since the time step used must be halved.

The final FLECHT SEASET steam generator calculation was run using cycle 18+ on the CRAY-1 computer, with a CPU:problem time ratio of 12.5. The transient had earlier been run on the CYBER-76 using cycle 14, with a CPU:problem time ratio of 14.1 for the same nodalization and maximum time step. At first glance, this was very surprising since CRAY runs should be about twice as fast as CYBER runs. The only differences between the two calculations were some small changes in initial conditions and the addition of several control functions in the CRAY calculation, but the differences were great enough to allow the CYBER-76 calculation to run at a larger average time step throughout the transient. To determine if the differences were due to the CRAY/CYBER dichotomy or the cycle 14/cycle 18+ dichotomy, the first part of the CRAY calculation was rerun on the CYBER using cycle 18+. The time steps used were identical to the CRAY values, indicating that either the small differences in input or differences in the code time step control algorithm were sufficient to cause a halving of the time step. Further calculations with cycle 14 indicated that the small differences in the input, not differences in time step control, were responsible for the factor of ~2 change in average time step.

4.3.2 Startup (Zero Step) Problems

User-imposed smaller maximum time steps also allow calculations to start in a smoother well-behaved manner. Results indicate that the code can calculate some quite peculiar behavior without the time step control algorithm cutting the time step and trying again.

The initial use of the maximum allowed time step led to problems in starting up the FLECHT SEASET steam generator separate effects test transient [14], with a spurious temperature peak (~565 K, substantially hotter than the secondary side heat source of ~540 K) occurring at very early times. When the startup maximum allowed time step was reduced as discussed earlier in section 4.1.1, this early time temperature spike disappeared.

Before beginning the actual calculation of the LOFT L9-1 transient, we performed a number of analyses involving only the secondary feedwater train, starting with steady conditions. We wished to determine whether, when the pump was tripped, it would be necessary to model the pump response in detail. (We wanted to avoid the possibility of oscillations arising from coupling of the pump and the rather "touchy" secondary side.) We observed that, whether or not the pump was present, the initial flow increased by a factor of 20. This was due in large part to the fact that RELAP5 begins a calculation with the maximum time step; in addition, zero values for code-calculated junction flow resistances are evidently used during the first calculated time step. By reducing the time step by 2 orders of magnitude, the flow excursion could be limited to ~25% over the correct value, and would disappear rapidly. [17]

Besides the maximum allowed time step being used for the zero step, several other startup problems have been found. As just mentioned above, zero values for code-calculated abrupt area change form losses are used in the junction flow resistance calculation during the first calculated time step, and zero values are always printed for these code-calculated form loss coefficients during the first ("zero time") major edit.

Also, during the first time step, the code apparently does not correctly look up the "zero time" values in time-dependent volume and junction input, but uses the first table entry in the input. This is correct if the table either starts at t=0 or if the table is based on a trip which is false at t=0, but incorrect for many other cases (such as flow as a function of pressure or an arbitrary control function). A major source of this problem seems to be that the code does not process all the required data (e.g., initial values of control functions or logical states of trips) before beginning the first time step advancement.

Problems traceable to zero step assumptions have been encountered when using latched trips, which can only change logical states once during a calculation. The user would tend to define a trip expected to be true for the first part of a calculation and false for the second part as a latched trip, to save constant testing during the latter portion of the

calculation. However, the code assumes all trips false for the first time step. A latched trip which is supposed to be really (physically) true at t=0 (but is false according to the code) will change state to true at the end of the first time step, using up the one allowed change, and then be held true for the rest of the calculation, even though the user criterion later requires the trip to become false. In this case, the less efficient "no-latch" trip input option must be used. (The code also assumes all trips introduced or redefined on restart as false for one time step, leading to similar problems.)

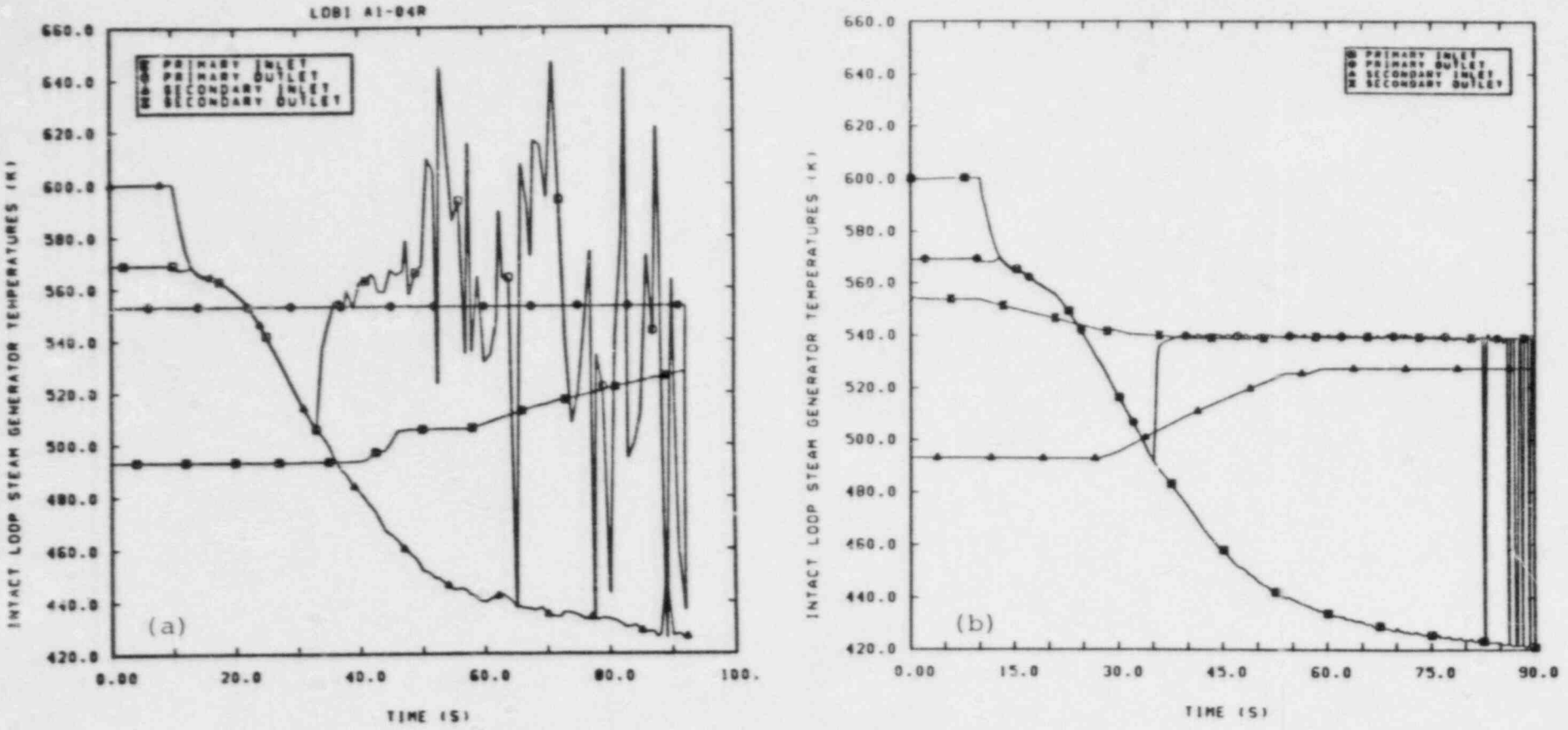

Figure 4.1.1.1 Intact Loop Steam Generator Temperatures Calculated for LOBI Large Break Transient A1-04R Using (a) Code and (b) Reduced Time Steps

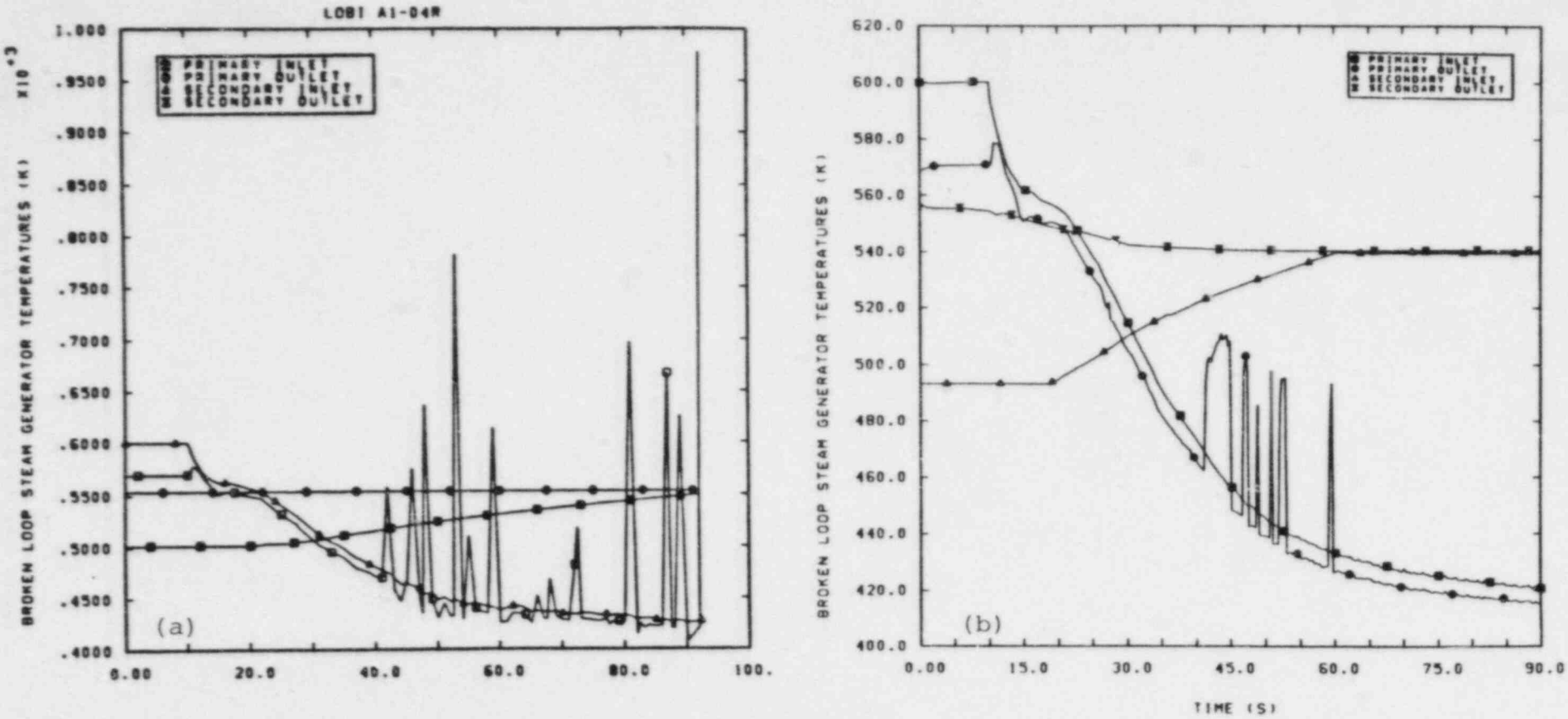

Figure 4.1.1.2 Broken Loop Steam Generator Temperatures Calculated for LOBI Large Break Transient A1-C4R Using (a) Code and (b) Reduced Time Steps

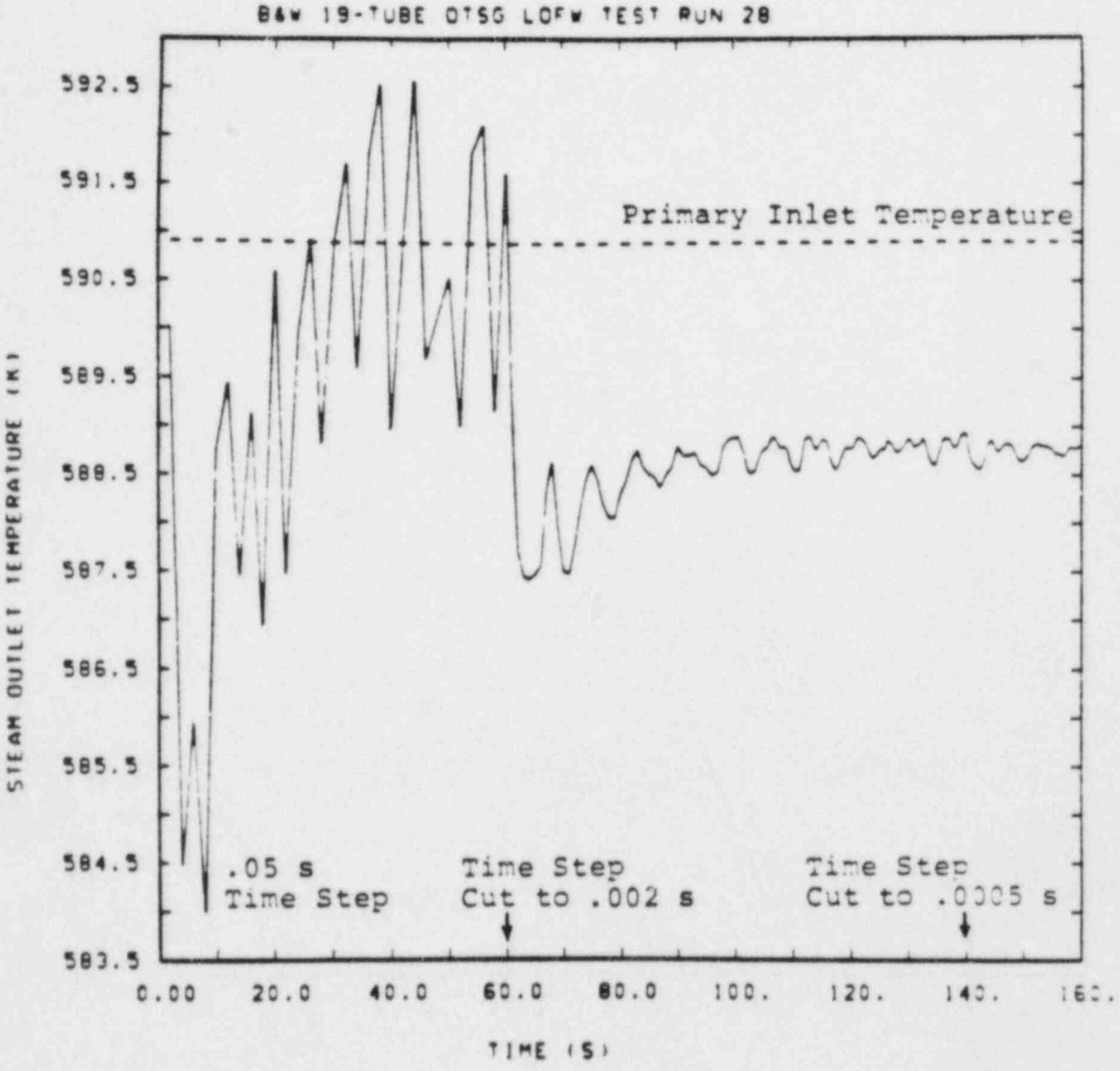

Figure 4.1.1.3 Primary and Secondary Steam Outlet Temperatures for B&W Steam Generator Steady State Test 28 Using Code and Reduced Time Steps

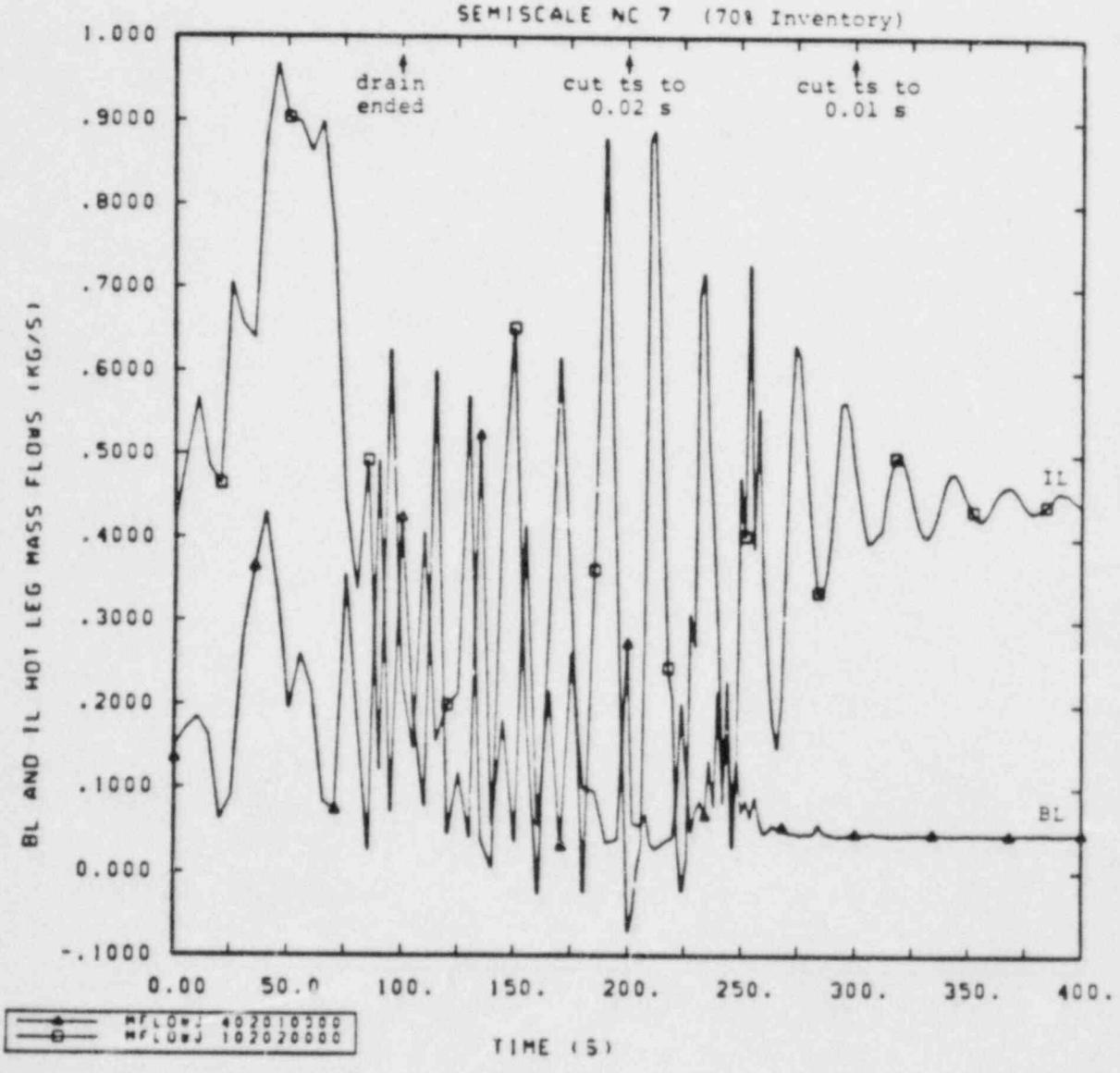

Figure 4.1.2.1 Intact and Broken Loop Mass Flows for Semiscale Natural Circulation Test S-NC-7 (70%) Inventory) Using Code and Reduced Time Steps

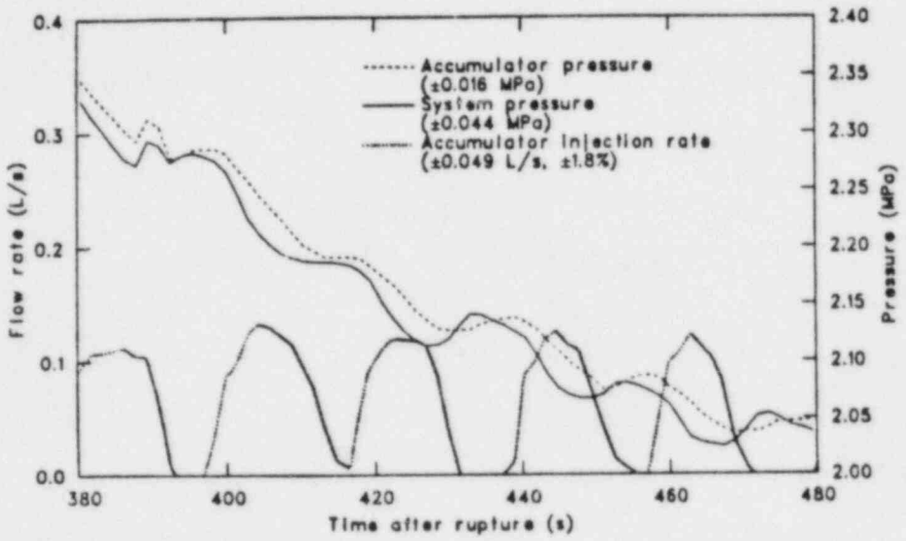

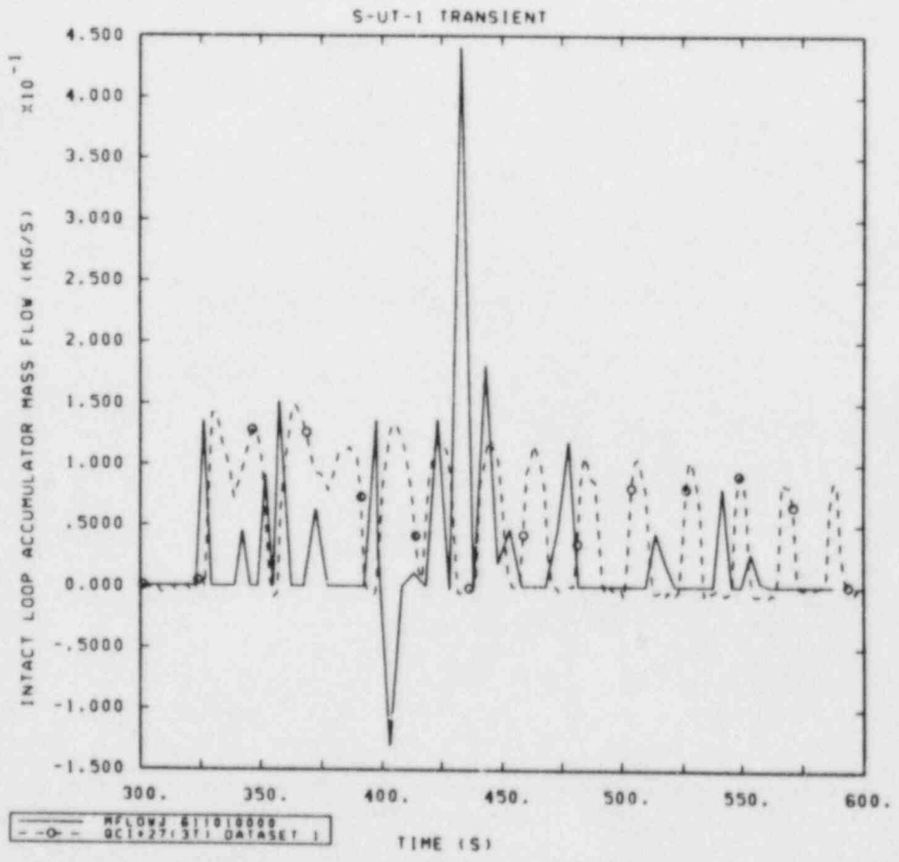

Figure 4.1.3.1 Loop Accumulator Injection Oscillations Driven by Differential Pressure Behavior in Semiscale Small Break Transient S-UT-1

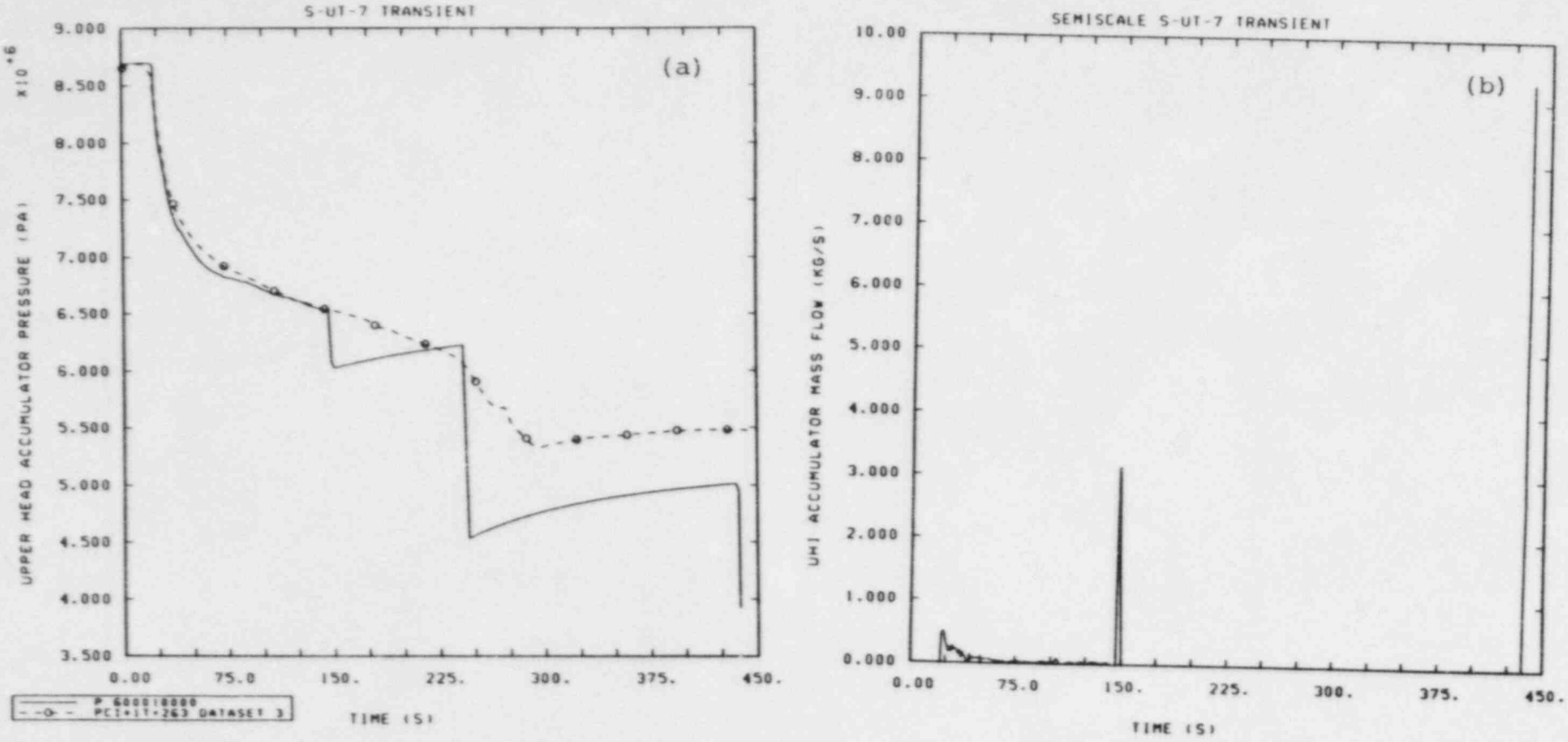

Figure 4.1.3.2 UHI Accumulator (a) Pressure and (b) Flow Rate for Semiscale Small Break Transient S-UT-7

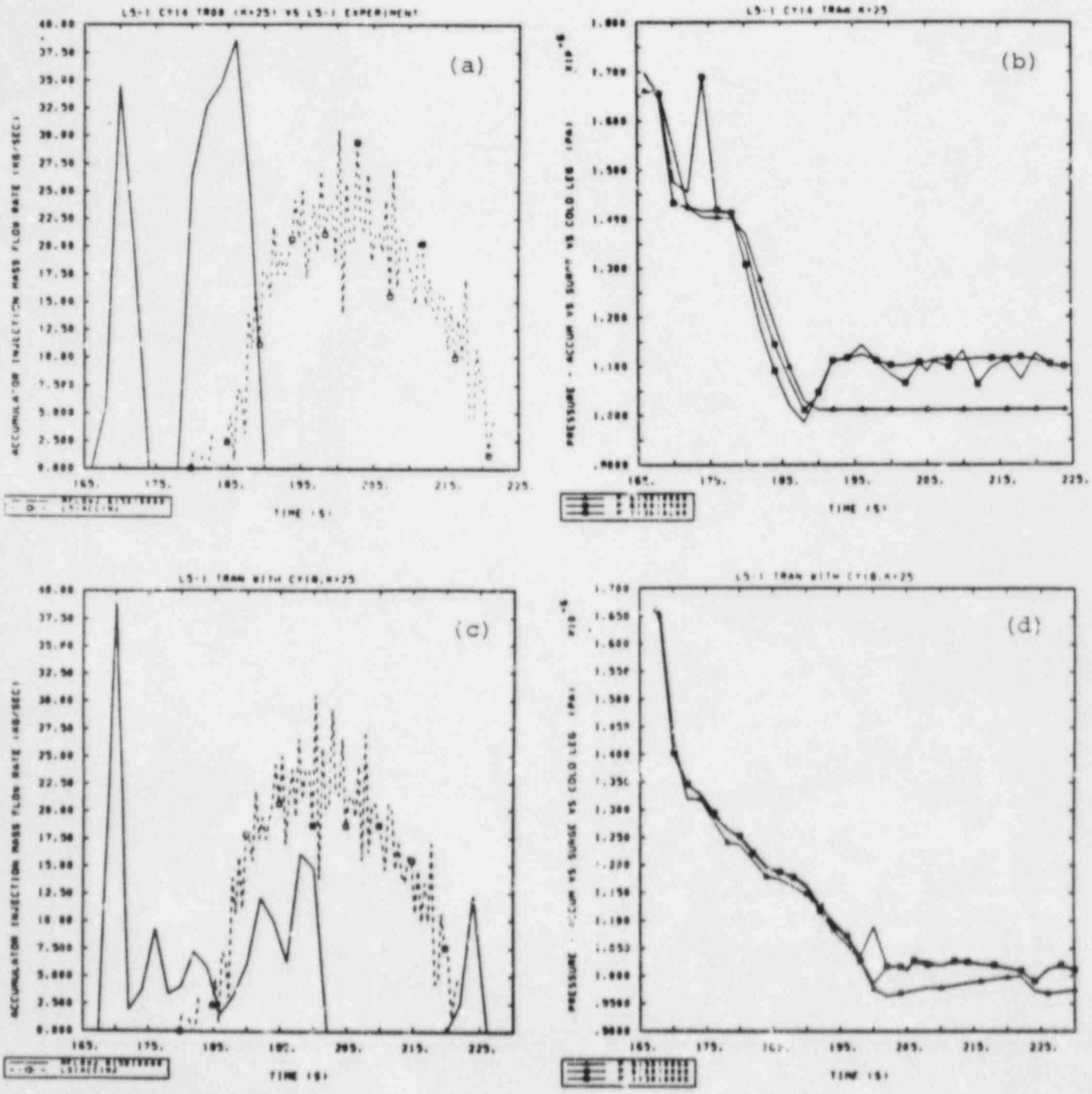

Figure 4.1.3.3 (a,c) Accumulator Injection and (b,d) Accumulator, Surge Line and Cold Leg Pressures Calculated by (a,b) Cycle 14 and (c,d) Cycle 18+ for LOFT Intermediate Break Transient L5-1

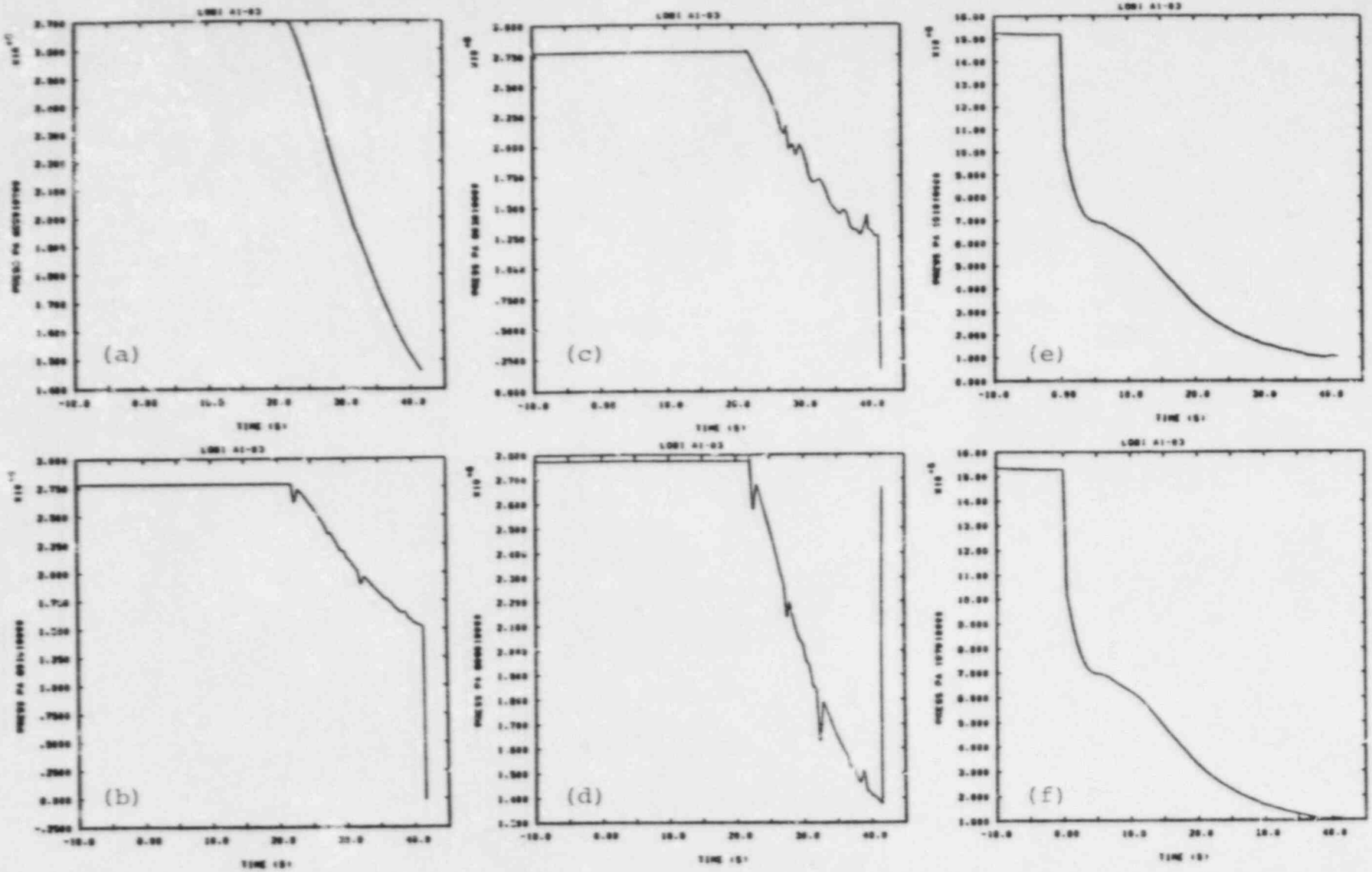

Figure 4.1.3.4 (a) Accumulator, (b) Outlet Branch and (c,d) Surge Line Pressures and (e,f) Pressures Downstream of Injection Points Calculated by Cycle 14 for LOBI Large Break Transient A1-03

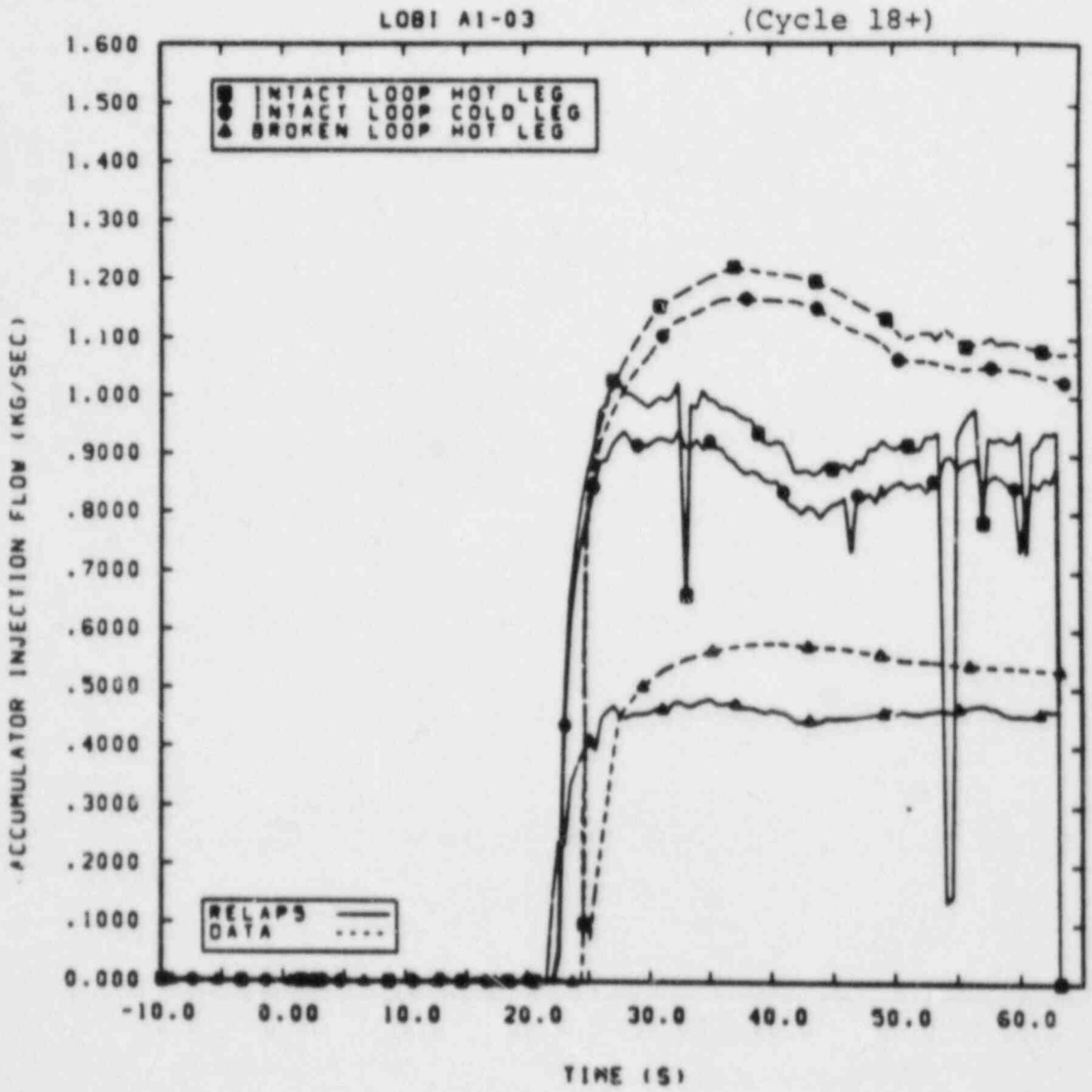

Figure 4.1.3.5 Accumulator Injection Rates Calculated by Cycle 18+ for LOBI Large Break Transient A1-03

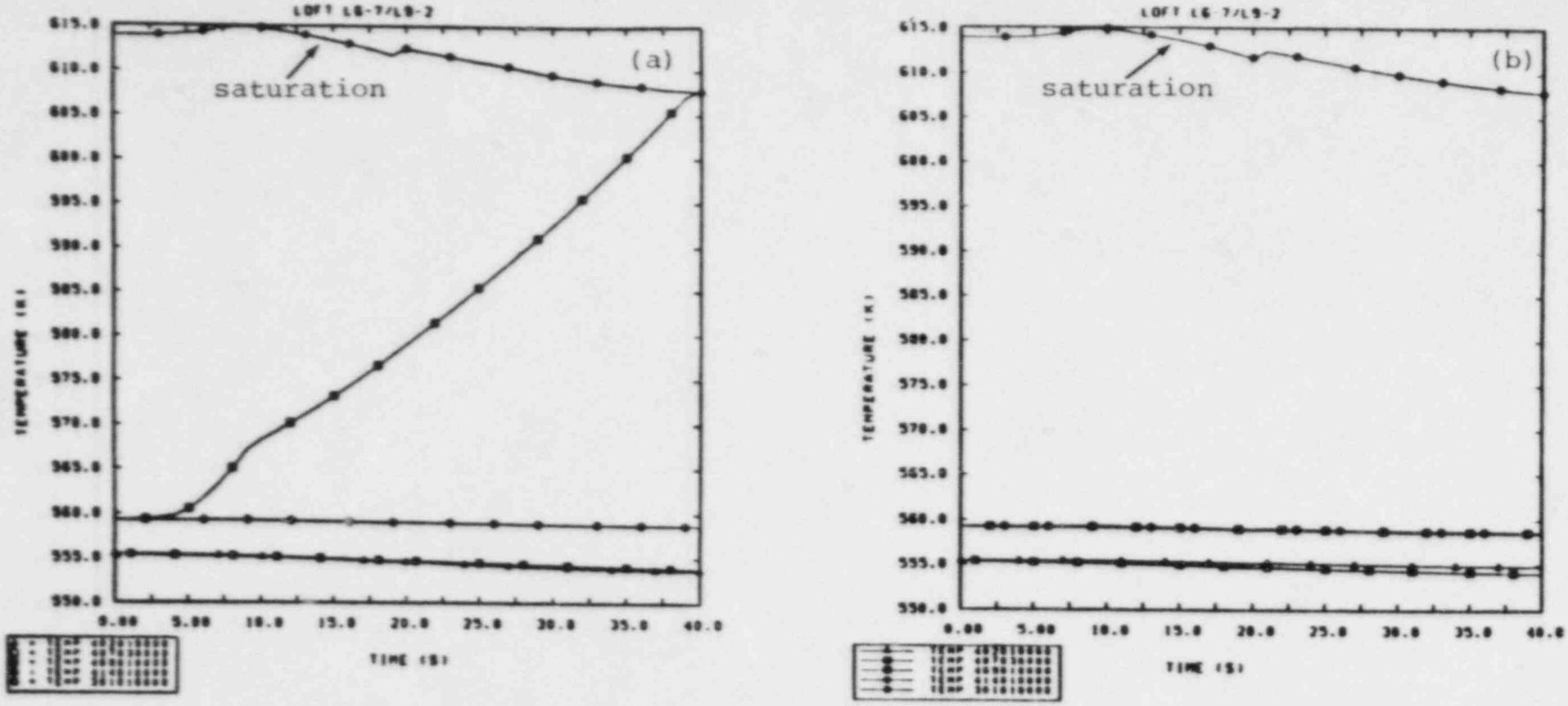

Figure 4.2.1.1 Broken Loop Volume and Saturation Temperatures with (a) Cell Heatup and Flashing and (b) No Cell Heatup after Bypass and Leakage Flow Modelling Changed in LOFT Turbine Trip Transient L6-7/L9-2

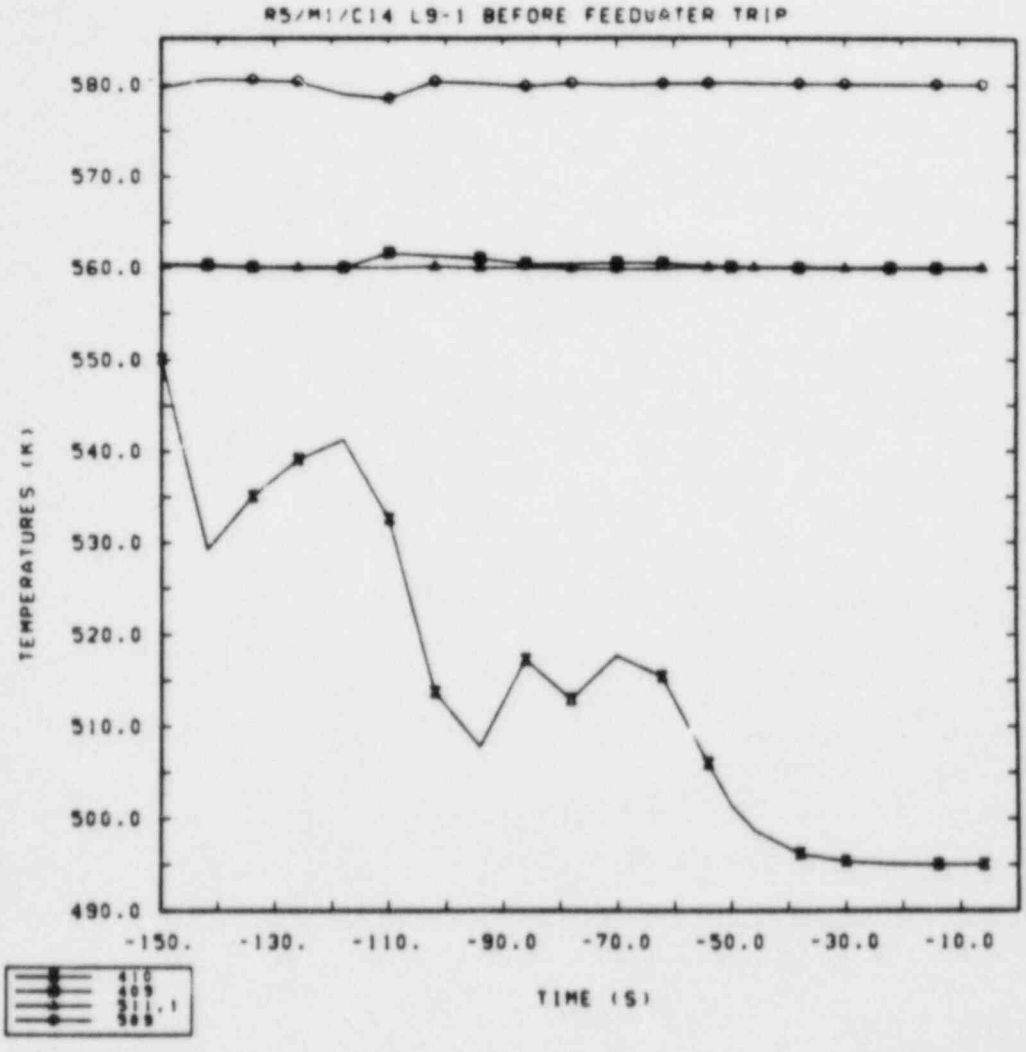

Figure 4.2.1.2 Broken Loop Temperatures with a Cell Cooling Down for LOFT Loss-of-Feedwater Test L9-1

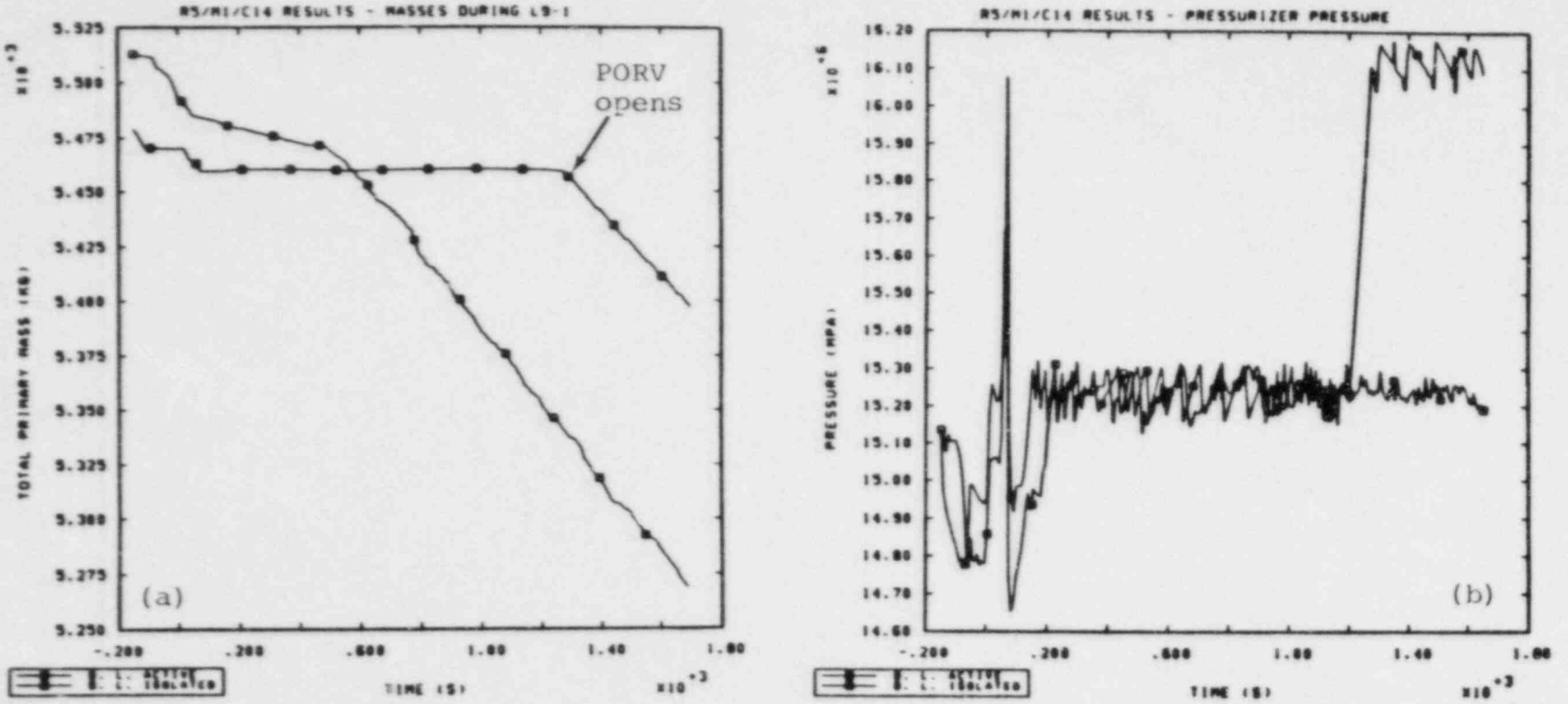

Figure 4.2.1.3 (a) Primary System Mass and (b) Pressurizer Pressure with and without Broken Loop Active in System for LOFT Loss-of-Feedwater Transient L9-1

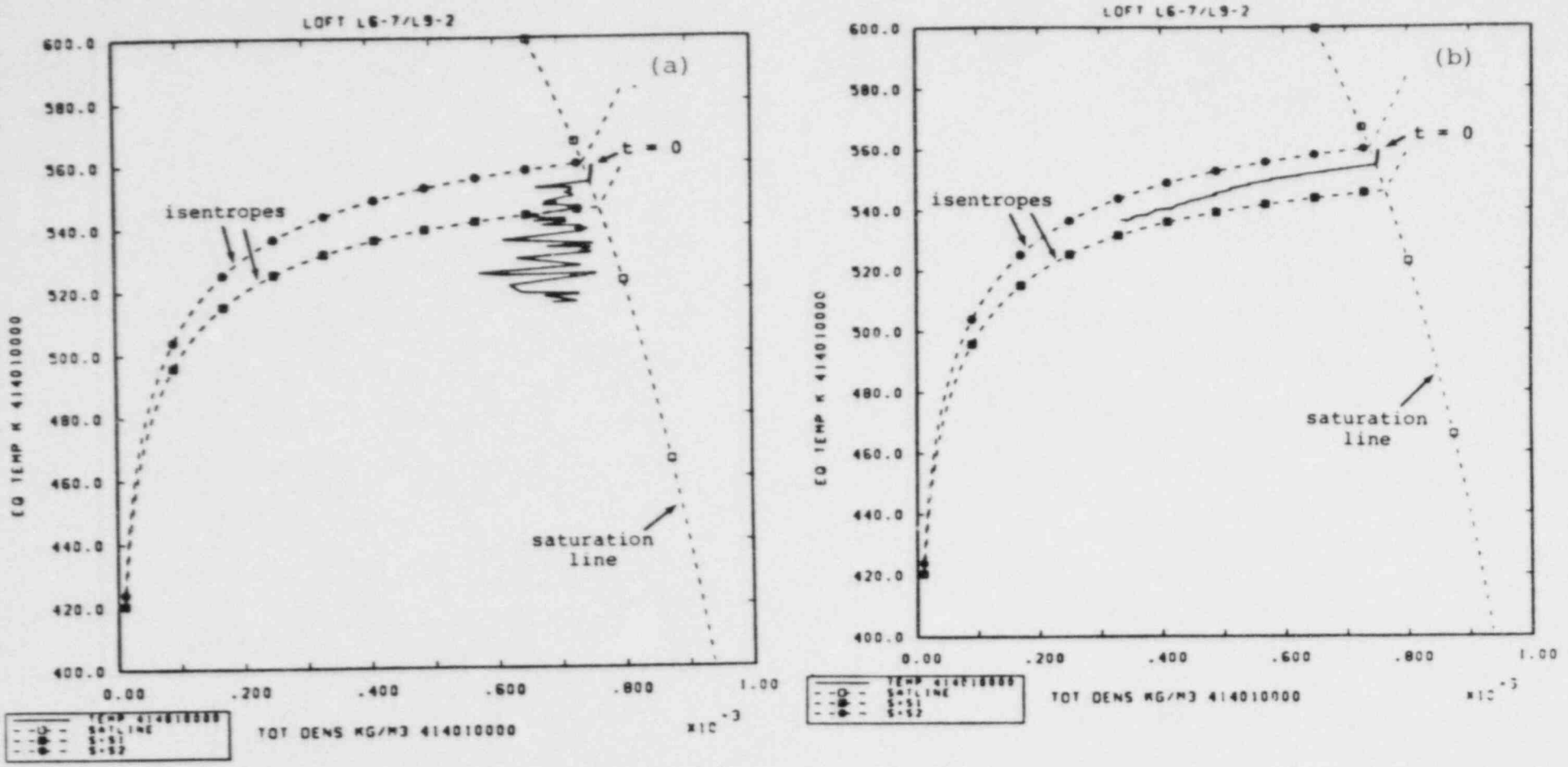

Figure 4.2.2.1 Temperature vs Density History of a Broken Loop Volume Using (a) Standard Nonequilibrium and (b) Nonstandard Equilibrium Options for LOFT Turbine Trip Transient L6-7/L9-2

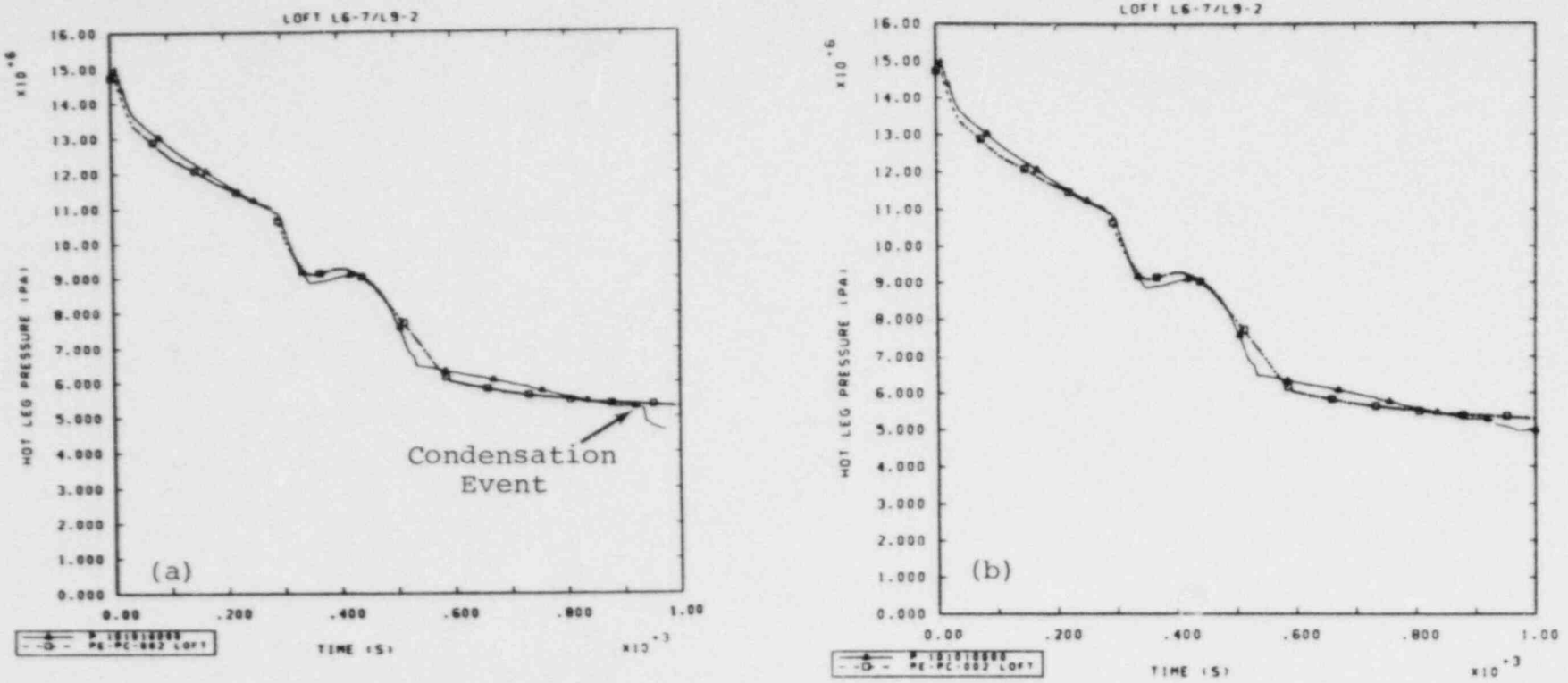

Figure 4.2.2.2 Hot Leg Pressure Showing (a) Presence and (b) Absence of "Condensation Event" for LOFT Turbine Trip Transient L6-7/L9-2

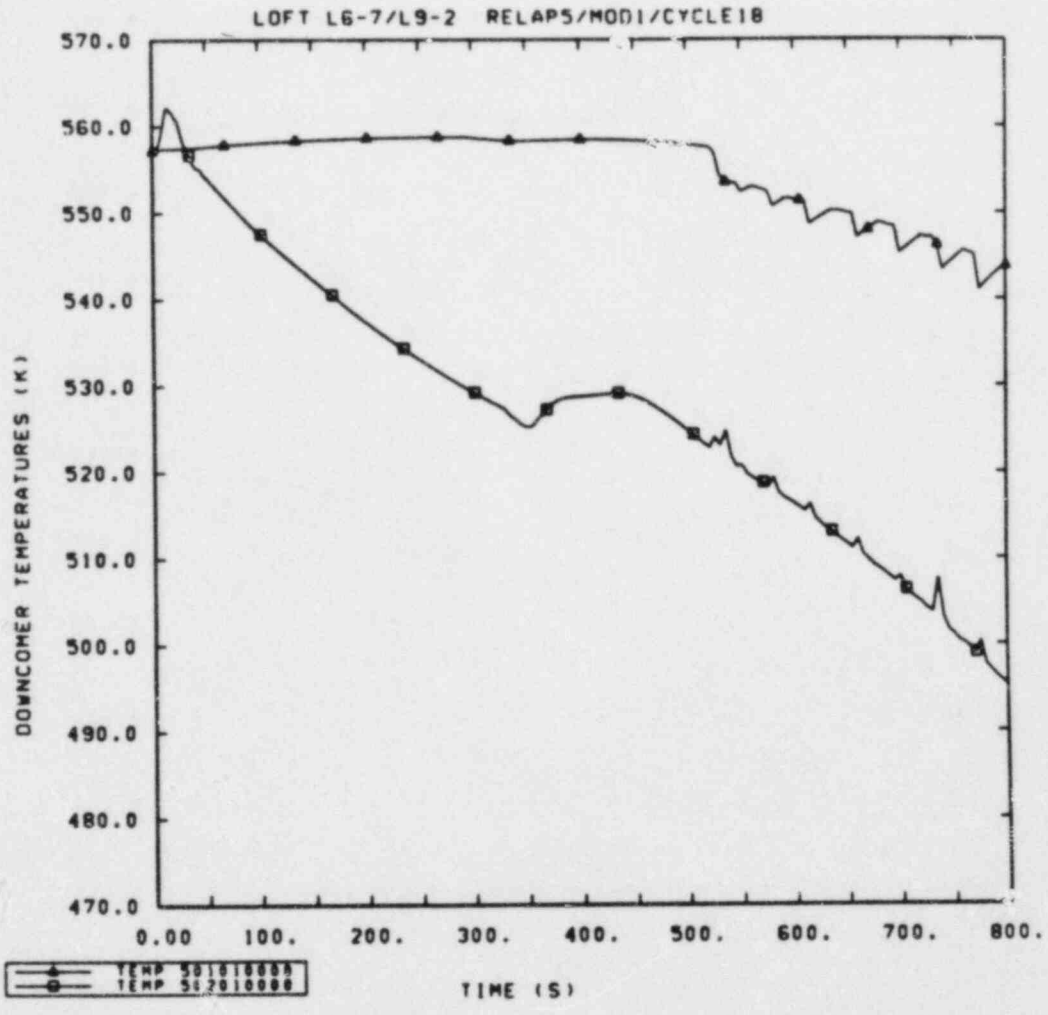

Figure 4.2.2.3 Temperatures in Vessel "Pseudo-Pressurizer" and Adjacent Cells for LOFT Turbine Trip Transient L6-7/L9-2

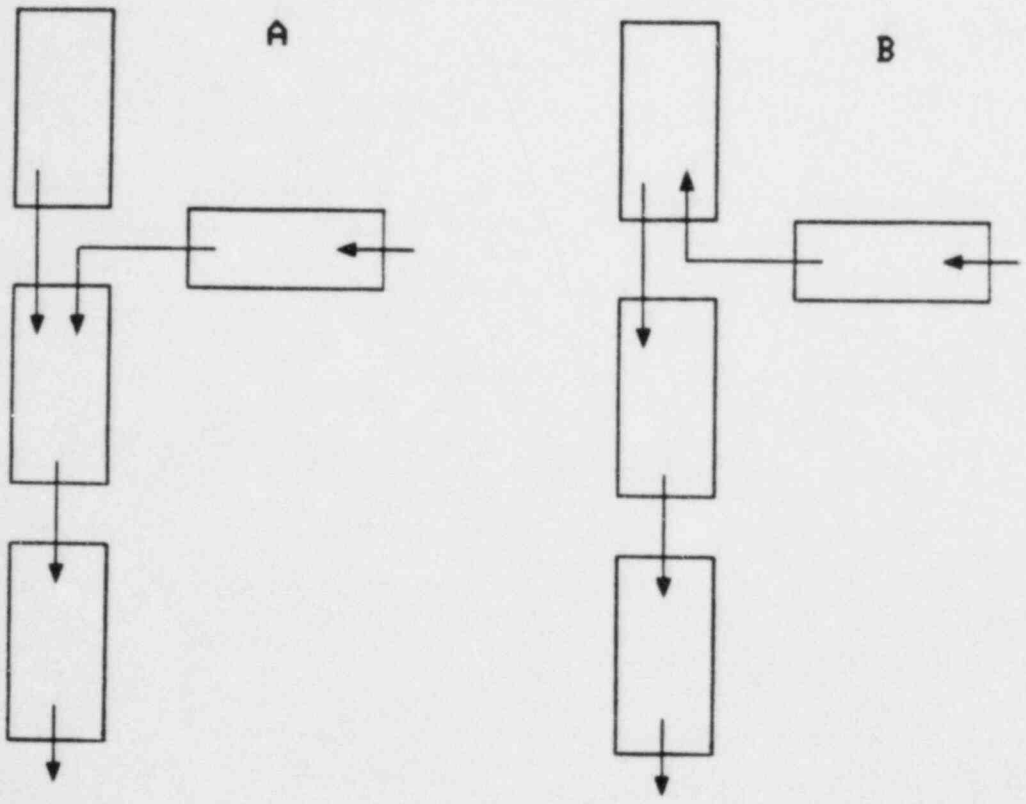

Figure 4.2.2.4 "Tee" Connection Modelling Options
Using Branch Component

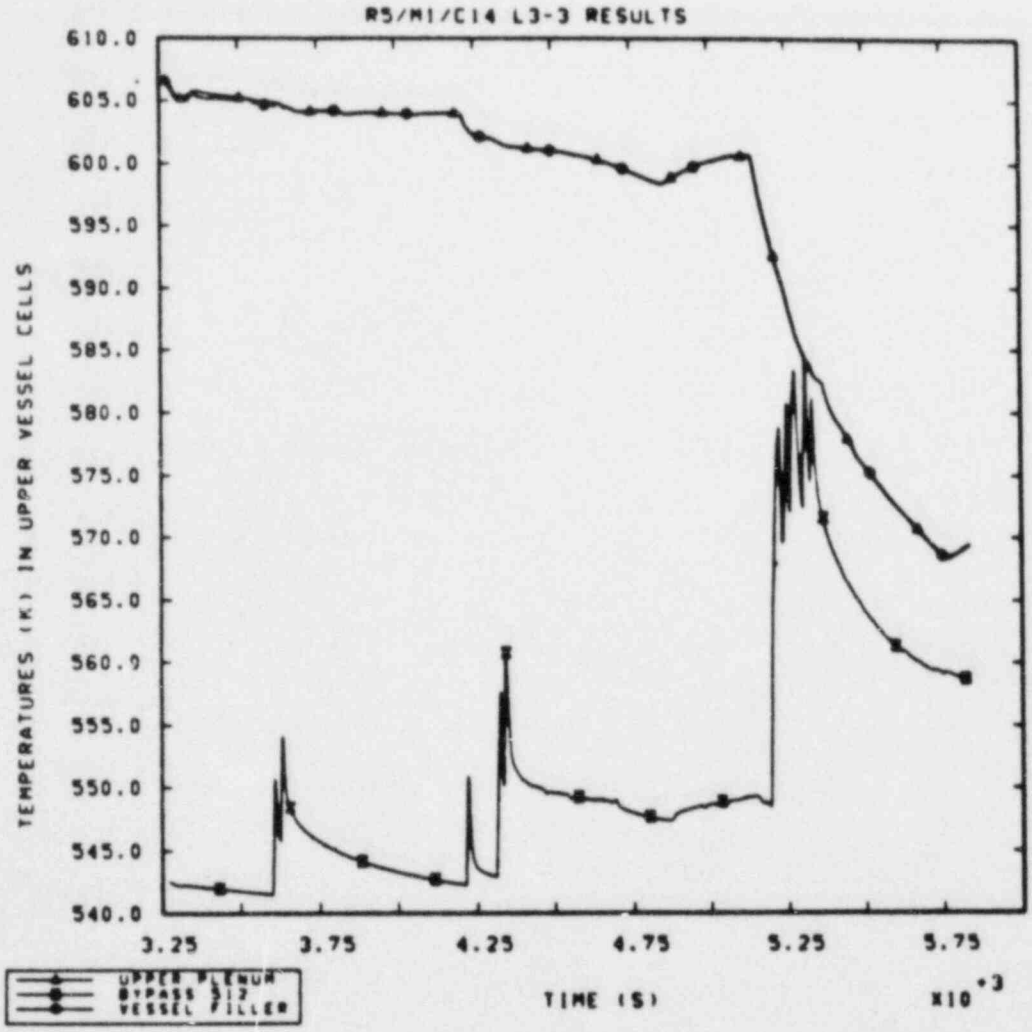

Figure 4.2.2.5 Temperature in Vessel "Pseudo-Pressurizer" and Adjacent Cells for LOFT Loss-of-Feedwater with Recovery Transient L9-1/L3-3

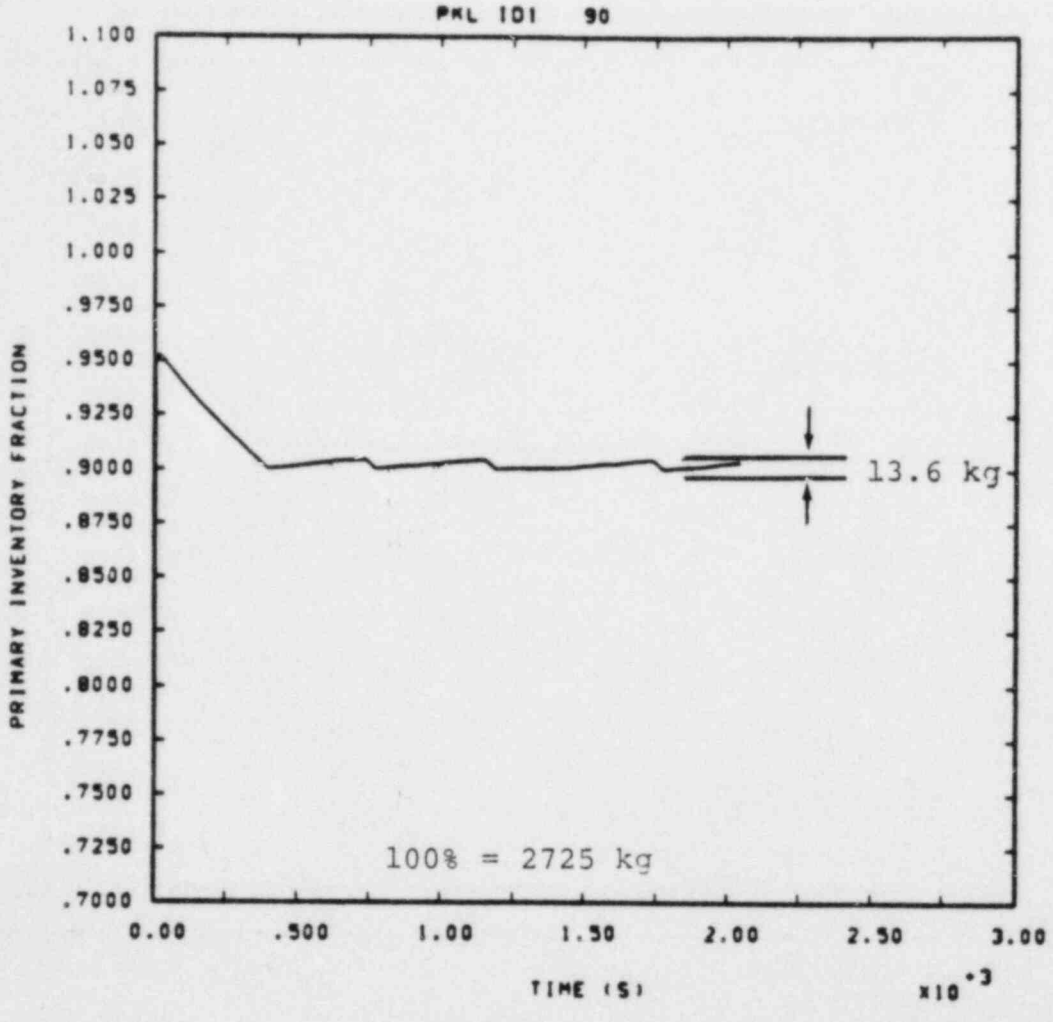

Figure 4.2.3.1 Primary Mass (at 90% Inventory) for PKL IDl Natural Circulation Test

5.0 CONCLUSIONS

The conclusions we have drawn about the RELAP5/MOD1 code are scattered throughout this report; they are summarized here for convenient reference, organized according to the major divisions used in the main body of this report. We hope this will allow ready location of supporting evidence and qualifying discussion. (We also include some conclusions on documentation and code portability, discussed in detail in Appendices I and II.)

Steady state analyses:

1. With some user guidelines and after some user experience, good primary side steady states (i.e., in good agreement with measured experimental initial or plant operating conditions) are relatively easy to obtain.

2. The temperature difference across the steam generator U-tubes must always be adjusted in order to match primary and secondary temperature data simultaneously; our recommended adjustment is to use the minimum tube-to-tube spacing for the secondary side heated equivalent diameter.

3. Unlike the primary side, good secondary side steady states matching desired data cannot always be obtained.

Once-through steam generators:

4. The MOD1 code cannot calculate the correct steady state operation of once-through steam generators; in particular, secondary side outlet superheated steam is not calculated because the low-flow CHF correlation used underpredicts CHF at high qualities.

5. Steady state calculations with our modified version of MOD1 and with the MOD1.5 code are in good agreement with data.

6. Both the MOD1 and MOD1.5 codes calculate the correct loss-of-feedwater transient behavior once the initial conditions calculated using the released (unmodified) version of MOD1 are somehow corrected, either by modifying MOD1 or by using MOD1.5.

Primary side transient response:

7. Code results for primary side pressure and break flow(s) are in good-to-excellent agreement with data for large and intermediate breaks; the only significant discrepancies seen are due to problems calculating other features such as accumulator injection and ECC bypass/delivery.

8. While calculated pressure and break flow for small break analyses are usually in good qualitative agreement with data, known code errors and/or model deficiencies can cause significant quantitative discrepancies, as can difficulties with poorly quantified initial and/or boundary conditions.

9. Both qualitative and quantitative disagreements in primary system behavior are seen in the few operational transients analyzed, although it is sometimes possible to force much better agreement using esoteric input model changes.

Core thermal response:

10. Calculated peak clad temperatures are generally in good agreement with data (within 50 K) for large break blowdowns and for intermediate breaks, but the location in terms of core elevation is often inaccurate, with the calculated PCT generally seen at a lower core elevation than occurred; calculated clad temperatures progressively lower than data in the upper core are most likely caused by MOD1's inability to maintain entrained droplets in superheated vapor.

11. A code error correction to the reactor kinetics introduced in cycle 18 increases the calculated decay heat by 10-20%, and thus increases the calculated PCTs (by ~60 K in our analyses, compared to cycle 14 results).

12. Unphysical heatup interruptions are calculated in a number of intermediate and small break analyses which have been traced to density and void fraction oscillations around MOD1's simplistic dryout/rewet criterion of α=0.96.

Secondary side thermal/hydraulic response:

13. The secondary side is calculated to depressurize more rapidly than observed in data, in separate effects and integral tests with U-tube steam generators.

14. The major reason for the more rapid predicted depressurization is the apparent inability of the MOD1 code to allow a layer of subcooled water to exist in the bottom of the secondary.

15. Despite major disagreements in calculated and measured secondary side responses, the code does apparently calculate the correct overall heat transfer between secondary and primary for long periods of time.

Natural circulation:

16. All modes of natural circulation (subcooled and saturated single-phase, two-phase and reflux cooling) are calculated to occur, although manual time step reductions are required before some two-phase circulation and any reflux cooling can be observed.

17. The two-phase natural circulation flow rates are consistently ~10-40% higher than data, although the single-phase natural circulation flow rate is always in excellent agreement with measurement.

18. The peak two-phase flow rate and the natural circulation mode transitions are calculated to occur at different inventories than in the data, although the shift is not consistently in the same direction for a given facility or test series.

Time step control:

19. Three classes of oscillations (temperature, mass flow and pressure), which can usually be affected or eliminated by the analyst reducing the time step used, have been identified.

20. The restriction that the time step can only be halved or doubled leads to inefficient run times and unnecessary increases in costs.

21. A number of minor but annoying misassumptions are made by the code during the first ("zero") time step iteration, partly due to incomplete processing of input before beginning the iteration.

Bypass and leakage flow modelling:

22. Small secondary flow paths (bypass and leakage flows) should be modelled as default flow areas with the smooth area change option and large user-input loss coefficients.

23. If the abrupt area change model is used for such secondary flow paths with the true (small) geometric areas, large mass and energy conservation errors can occur, usually observed in stagnant regions.

24. The same mass and energy errors can be triggered in other ways, most of which are not known.

Documentation:

25. We have found some code manual errors and deficiencies, and have suggested some additional output variables we believe would be useful.

26. Problems with faulty, out-of-date and/or incomplete facility and test documentation can be a major source of uncertainty in assessment calculations.

27. Evaluating the code results by comparison with calculations performed by other users is almost impossible because few such analyses are adequately documented.

Code portability:

28. RELAP5 is a very computer-dependent code, written for INEL's CDC CYBER-176 and requiring extensive changes to run on any other computer. Most other laboratories have CDC 7600's, CYBER-76's, and CRAY-1's. In a few years, as obsolete hardware is phased out, only more modern systems such as the CRAY-1 and CYBER-205 will be available.

29. The most serious difficulty we had with putting RELAP5 on our CDC machines was the availability of sufficient small core memory (SCM). Since no problems of significant size could run, a major effort was required to change the code so that less SCM would be needed.

30. Most of the CRAY updates result from the fact that RELAP5 is highly dependent on the CDC computer word containing 60 bits, while the CRAY has 64 bits in its words; about 2000 lines of code had to be changed for the program to run correctly on the CRAY.

6.0 REFERENCES

1. V. H. Ransom et al, RELAP5/MOD1 Code Manual Volume 1: System Model and Numerical Methods; Volume 2: User Guide and Input Requirements, NUREG/CR-1826, EGG-2070, Idaho National Engineering Laboratory, March 1982.

2. V. H. Ransom et al, RELAP5/MOD0 Code Description Volume 1: RELAP5 Code Development; Volume 2: RELAP5 Code Development Update and Sample Problems; Volume 3: RELAP5 Users Manual, CDAP-TR-057, Idaho National Engineering Laboratory, May 1979.

3. V. H. Ransom et al, RELAP5/MOD1.5: Models, Developmental Assessment, and User Information, EGG-NSMD-6035, Idaho National Engineering Laboratory, October 1982.

4. S. L. Thompson et al., Thermal/Hydraulic Analysis Research Program Quarterly Report, October-December 1981, NUREG/CR-2690, SAND82-0953, Sandia National Laboratories, June 1982.

5. S. L. Thompson et al., Thermal/Hydraulic Analysis Research Program Quarterly Report, January-March 1982, NUREG/CR-2843, SAND82-1788, Vol. 1 of 4, Sandia National Laboratories, October 1982.

6. S. L. Thompson et al., Thermal/Hydraulic Analysis Research Program Quarterly Report, April-June 1982, NUREG/CR-2843, SAND82-1788, Vol. 2 of 4, Sandia National Laboratories, November 1982.

7. S. L. Thompson et al., Thermal/Hydraulic Analysis Research Program Quarterly Report, July-September 1982, NUREG/CR-2843, SAND82-1788, Vol. 3 of 4, Sandia National Laboratories, March 1983.

8. S. L. Thompson et al., Thermal/Hydraulic Analysis Research Program Quarterly Report, October-December 1982, NUREG/CR-2843, SAND82-1788, Vol. 4 of 4, Sandia National Laboratories, April 1983.

9. S. L. Thompson et al., Thermal/Hydraulic Analysis Research Program Quarterly Report, January-March 1983, NUREG/CR-3329, SAND83-1171, Vol. 1 of 4, Sandia National Laboratories, June 1983.

10. S. L. Thompson et al., Thermal/Hydraulic Analysis Research Program Quarterly Report, April-June 1983, NUREG/CR-3329, SAND83-1171, Vol. 2 of 4, Sandia National Laboratories, September 1983.

11. S. L. Thompson et al., Thermal/Hydraulic Analysis Research Program Quarterly Report, July-September 1983, NUREG/CR-3329, SAND83-1171, Vol. 3 of 4, Sandia National Laboratories, December 1983.

12. L. N. Kmetyk, RELAP5 Assessment: LOBI Large Break Transients, NUREG/CR-3075, SAND82-2525, Sandia National Laboratories, March 1983.

13. S. L. Thompson and L. N. Kmetyk, RELAP5 Assessment: PKL Natural Circulation Tests, NUREG/CR-3100, SAND82-2902, Sandia National Laboratories, January 1983.

14. L. N. Kmetyk, RELAP5 Assessment: FLECHT SEASET Steam Generator Test 23402, NUREG/CR-2887, SAND82-2894, Sandia National Laboratories, January 1983.

15. R. M. Summers, RELAP5 Assessment: Semiscale Mod-3 Small Break Tests, Sandia National Laboratories, NUREG/CR-3277, SAND83-1038, Sandia National Laboratories, July 1983.

16. S. L. Thompson and L. N. Kmetyk, RELAP5 Assessment: LOFT Turbine Trip L6-7/L9-2, NUREG/CR-3257, SAND83-0832, Sandia National Laboratories, July 1983.

17. R. K. Byers and L. N. Kmetyk, RELAP5 Assessment: LOFT L9-1/L3-3 Anticipated Transient with Multiple Failures, NUREG/CR-3337, SAND83-1245, Sandia National Laboratories, August 1983.

18. L. N. Kmetyk, RELAP5 Assessment: LOFT Small Break L3-6/L8-1, NUREG/CR-3163, SAND83-0245, Sandia National Laboratories, March 1983.

19. J. L. Orman and L. N. Kmetyk, RELAP5 Assessment: LOFT Intermediate Break L5-1/L8-2, NUREG/CR-3406, SAND83-1575, Sandia National Laboratories, August 1983.

20. J. M. McGlaun and L. N. Kmetyk, RELAP5 Assessment: Semiscale Natural Circulation Tests S-NC-2 and S-NC-7, NUREG/CR-3258, SAND83-0833, Sandia National Laboratories, May 1983.

21. R. M. Summers, RELAP5 Assessment: B&W 19-Tube Once-Through Steam Generator (OTSG) Loss-of-Feedwater Test, NUREG/CR-3302P, SAND83-2169, Sandia National Laboratory, December 1983.

22. S. L. Thompson and L. N. Kmetyk, RELAP5 Assessment: LOFT Large Break L2-5, NUREG/CR-3608, SAND83-2549, Sandia National Laboratories, January 1984.

23. C. C. Wong and L. N. Kmetyk, RELAP5 Assessment: Semiscale Natural Circulation Tests S-NC-3, S-NC-4 and S-NC-8, NUREG/CR-3690, SAND84-0402, Sandia National Laboratories, May 1984.

24. A. C. Peterson, RELAP5 Assessment: Semiscale Mod-2A Small Break Tests, NUREG/CR-3777, SAND84-0884, Sandia National Laboratories, June 1984.

25. L. N. Kmetyk, RELAP5 Assessment: BCL ECC Bypass/Delivery Transient Analyses, to be published.

26. to be published

27. Flow of Fluids Through Valves, Fiitings, and Pipes, Technical Paper No. 410, Engineering Division, Crane Co., New York NY, 1981.

28. T. K. Knight, U-Tube Steam Generator Modelling, TRAC Newsletter No. 7, Los Alamos Scientific Laboratory, May 1982.

29. Dr. H. Staedke of J.R.C.-Ispra, private communication, January 20, 1983.

30. J. C. Lee et al., Transient Modelling of Steam Generator Units in Nuclear Power Plants: Computer Code TRANSG-01, EPRI-NP-1368, Electric Power Research Institute, March 1980.

31. Code Assessment Review Meeting, Bethesda MD, May 3-5 1983.

32. L. N. Kmetyk, L. D. Buxton and R. K. Cole, Analyses of 1/15 Scale Creare Bypass Transient Experiments, NUREG/CR-2606, SAND81-1932, Sandia National Laboratories, September 1982.

33. P. N. Demmie, T. H. Chen and S. R. Behling, Best Estimate Prediction for LOFT Nuclear Experiment L2-5, EGG-LOFT-5869, Idaho National Engineering Laboratory, May 1982.

34. R. J. Wagner, RELAP5/MOD1 Update Synopsis and Listing of Updates to Create Cycle 19, RELAP5 News No. 2, Idaho National Engineering Laboratory, November 1982.

35. K. G. Condie, RELAP5 Reference Calculation for LOFT Experiment L6-7/L9-2, EGG-LOFT-6014, Idaho National Engineering Laboratory, January 1983.

36. R. J. Beelman, RELAP5 Reference Calculation and Posttest Analysis of Anticipated Transient with Multiple Failures Experiment L9-1/L3-3, EGG-LOFT-5895, Idaho National Engineering Laboratory, September 1982.

37. D. J. Shimeck, Analysis of Semiscale Mod-2A System UHI/SBLOCA Experiments, NUREG/CR-3195, EGG-2246, Idaho National Engineering Laboratory, April 1983.

38. G. Slovik, FLECHT-SEASET Steam Generator Tests in BNL Quarterly Progress Report for April-June 1982 and July-September 1982, NUREG/CR-2331, BNL-NUREG-51454, Vol. 2, Nos. 2 and 3.

APPENDIX I DOCUMENTATION

A complaint was once made during a summary presentation of our assessment results that our project was assessing the documentation and the user as much as the code. Not only do we not deny this, we claim that proper code assessment must include both these features. The physics in the code and the programming itself could be perfect, but if the documentation and the guidelines do not allow the user to set up a correct model, the wrong answers may, and usually do, result. The danger of relying on "inside knowledge" or "previous experience" without adequate written documentation is, of course, that the possessors thereof may leave for greener pastures without passing that knowledge on to their successors.

AI.1 Code Documentation

The documentation and guidelines for the RELAP5/MOD1 code, as for all codes, are inadequate and, in some cases, incorrect. As examples of errors and/or oversights in the code manual, the pump "look-back" input problem (mentioned earlier in Section 2.1.2) and the absence of any formal definition of "energy loss coefficients" come to mind. The input description also contains many irritating instances where required information is in another section of the document. Some input restrictions can only be discovered by violating the restrictions.

Further, RELAP5/MOD1 has a very short list of variables available for editing, plotting and for use in control functions, which can result in significant difficulties in interpreting results obtained. One obvious example is the lack of the saturation temperature as an edit or plot variable. Moreover, a number of variables which are available in the output are either not obviously and/or consistently useful, possibly due to an inadequate writeup on how to interpret them; for example, the enthalpy might be a more useful edit quantity than the internal energy.

A few coding errors have been found during the course of this assessment project; some of these we could bypass through input changes, while others we fixed after consulting the code developers, and some (such as the use of the first entry in a time-dependent volume or junction table lookup during the first time advancement, rather than the correct "looked-up" value) we left alone. Generally, the only programming errors we found were those that caused code aborts (e.g., the attempted square root of a negative number found during the L3-6 analysis) or very obvious wrong behavior (e.g., the excessive superheat in the B&W OTSG steady state calculation).

AI.1.1 Input Manual

We are not attempting to present a complete list of all errors and shortcomings in the code manual(s); after all, Murphy's law says there's always one more. We are merely trying to point out both some of the more blatant and some of the more subtle problems we have encountered to date. Errors or difficulties we found in the RELAP5/MOD1 manual include:

1) Time Step Control -- The MOD1 code appears to have a hardwired minimum time step of 1.0**-06, rather than use whatever the user inputs for this lower limit.

2) Minor Edit Variables -- In the volume variable list, "VAPGEN" is incorrectly listed as having units of mass/time; the units of what is printed are mass/volume/time. In the component variable list, valve stem position, VLVSTEM, is omitted. In the heat structure list, "HTHTC" is really what amounts to a heat transfer coefficient.

3) Volumes -- The annular flow regime map can only be specified for use in a pipe component, although physically one would also want to have this option for single volume and branch components. The statement "except for connections to a branch component, only one junction may be connected to the inlet and only one junction may be connected to the outlet" (referring to single volumes, pipes and annuli) is false.

4) Branches -- The code permits, and computes with, the specification of a branch junction which is not connected to the branch. (Such a junction specification is more usually due to a typo than to being intentional, and should probably be forced to cause an input error.)

5) Separators -- The instructions (given in Volume 2 of the manual) state that "the volume coordinate direction should be vertical and directed upwards" [1]. Although this is correct for MOD1.5, whenever we have tried to adhere to this guideline with MOD1, unstable flows have resulted; when the separator is directed vertically downwards, the behavior is greatly improved. [16]

6) Pumps -- Pump frictional torque is described as a cubic in pump speed; it's really a cubic in the absolute value of the normalized (to rated) speed. In the pump index and option card, if the instruction to enter -3 for word 3 if word 2 is -1 is followed, an input error results; if word 3 is set to -1 when word 2 is, it "works". Homologous curve data must be entered in order of increasing independent variable. Simultaneous homologous curve "look-back" and pump speed table specification do not work together, resulting in a constant pump speed (as already discussed in Section 2.1.2).

7) Junctions -- Forward and reverse flow energy loss coefficients do not appear to be defined anywhere in the manual(s).

8) Valves -- The statement in the instructions for the valve junction geometry card that "either the TO or the FROM connection code must refer to this component" is incorrect, and attempts to adhere to it result in an input error. If a motor valve has the abrupt area change selected, and default input area is selected, an input error results; there may be other cases of this type.

9) Accumulators -- The input instructions state that the mass of water in the surge line is included in the liquid volume; this is apparently not correct. The accumulator component causes a code abort (in both MOD1 and MOD1.5) when it empties and should start injecting nitrogen, although all documentation indicates that the accumulator can inject nitrogen when required. (Earlier versions of MOD1, before cycle 18, have a coding error (a misplaced parenthesis) in the accumulator subroutine that in effect divides the user-input surge line loss coefficient by the surge line area; this can be "corrected" through input by multiplying these two variables to redefine the loss coefficient before it is input.)

10) Heat Slabs -- If the "look-back" feature is used with heat slabs, the number input for the left boundary coordinate is overwritten by that of the referenced heat slab; this should be made clearer in the instructions. Many, if not all, of the heat transfer correlations use the hydraulic diameter input for the heat slab (rather than the heated equivalent diameter input); the distinction, if any, between these two input numbers, and when each is used, should be made clearer. (These two equivalent diameters are distinct from the hydraulic diameter input for volumes, as discussed above in Section 2.1.4, although they can be defaulted to the volume value.)

11) Control Functions -- The list of available control functions given in the manual is incomplete; MIN and MAX are left out. The control functions need several additional options, especially a decision function ("IF" statement). At first, it appears that this could be treated by the trip logic already present; however, the control function and trip evaluations can not be logically mixed because of evaluation order.

AI.1.2 Output Variables

RELAP5/MOD1 has a very short list of quantities that are available for editing, plotting, and for use in control functions. (The code developers evidently agree since MOD1.5 has a significantly expanded list of minor edit and plot variables, and MOD2 has an improved and expanded set of major edit variables.) This was probably intentional, in an effort to hold down the size of the code output, but many of the variables omitted (e.g., fluid enthalpy or saturation temperature) might have been more useful than some of the variables included in the output (e.g., the various junction void fractions). Of course, control functions can be used to generate desired variables, but doing things in this way can result in an input deck that is more complicated and longer than should be required. Furthermore, the user may be required either to foresee all quantities that may be of interest in a particular analysis, or be prepared to rerun a calculation in order to investigate a particular question. As an example, if one wishes to observe the saturation temperature during the course of a calculation, it is a simple matter - by means of a "time-dependent" volume and a control function - to do so. However, doing this for more than a few cells in a large nodalization (e.g., LOFT) would result in memory allocation difficulties; these could be overcome by reducing the accuracy of the model, thereby sacrificing the quality of the result in favor of the ability to examine it.

Interpretation of the results we obtained in this assessment project was thus hampered by some lacks in the standard RELAP5 output variables available. In order to simplify the calculation of primary mass inventory, a variable called the component mass was added to our version of the code. Otherwise one would have to compute and then sum the average density times the geometric volume for every cell in the primary side nodalization. The analysis of the steam generator secondary side response would have been greatly simplified, in this and in other calculations, if the saturation temperature were available as an edit and plot variable; this has been recently implemented in our version of MOD1 (and MOD1.5).

Another output feature that might prove very useful would be the ability to turn on the "debug print", normally given for the last time step at a code failure, for a single time step through user input. We have often found that trying to trace down the source of some discrepant results involves guessing what subroutine, correlation and/or regime the code is in at a particular time for a particular volume, junction or heat slab, usually requiring knowledge of variables not available through major or minor edits. The failure diagnostic printout already contains most, if not all, of the information of interest; rather

than the user introducing local "debug prints" (which often require either much iteration or much output), the built-in code time step printout should be made easily accessible to in-depth code users.

AI.1.3 Coding Errors

In several instances during the LOFT L3-6 small break analysis [18], we had the calculation aborted by the code sending a negative argument to the square root function. The error would usually occur after an hour or more of CPU time; when we backed up and reran the job in order to obtain a restart record and finer frequency output just before the code abort, the error would disappear, eventually reappearing when we were not prepared for it. (This is a common problem in trying to exactly diagnose a code problem; introducing more restarts and edits can change the time step structure enough that the problem moves, so that trapping the problem for examination is a major effort in itself.)

We eventually traced the negative square root to a code sequence treating horizontally stratified flow at a junction; the junction causing the abort was prescribed in the input to have a smooth area change and a flow area larger than the adjacent volume areas (by accident due to roundoff error). However, this treatment was intended for abrupt area changes only (which by definition must be less than or equal to the adjacent volume flow areas), and should have been bypassed for smooth area change junctions. This code error resulting in the negative argument to the square root function is in subroutine JPROP, which computes the hydrodynamic properties of liquid and vapor in junctions. INEL personnel suggested a code modification to bypass the calculation for junction areas larger than 90% of the minimum adjacent volume area, and for smooth area changes. No significant differences were later observed in the results, other than the obvious one of being able to continue computing.

As mentioned above in Section AI.1.1, a coding error was found in the accumulator subroutine (which has since been fixed in cycle 18). Because of a misplaced parenthesis in the momentum equation calculation, the user-input surge line loss coefficient was incorrectly divided by the surge line area before being used in the equation. In our early cycle 14 calculations, we bypassed this coding error by redefining the loss coefficient input; so of course, when we first ran a calculation with cycle 18, we forgot to correct the loss coefficient back to its normal value and again got incorrect accumulator injection.

Another code error was discovered during steady state calculations for the UHI plant model. In preliminary analyses, the secondary side would not balance at or near the feedwater flowrate estimated from a simple enthalpy balance argument. Although the discrepancy was later traced to the unintentional injection of aux feedwater during the steady state period, the search for the problem led us to carefully study the energy balance around the system. We found that the fraction of the reactor power we had specified to go into direct moderator heating was not appearing in the energy balance. Discussions with the code developers revealed that there was a known (but undocumented) problem with trying to specify direct moderator heating, complicated enough that no "fix" had yet been developed, and that the problem (related to normalization) could result in either far too little or far too much moderator heating, depending on the details of the model involved. The easiest fix is not to attempt to use the direct moderator heating option at the present time. (This would only affect plant calculations and, possibly, LOFT analyses; modelling experimental facilities with electrically heated rods does not exercise this portion of the code.)

Two other code errors were discovered in the course of the B&W OTSG analyses [22], where the initial poor results forced us to look at the code heat transfer logic in detail. (Remember, we do not consider inadequate, incorrect or inapplicable code models as code errors in the sense of this section.) After modifications to the CHF correlation permitted good predictions of the locations of dryout and initial steam superheat, we found the steam temperature rising much too high in the superheat region, reaching the primary inlet temperature at the boiler outlet and oscillating about this temperature due to inadequate time step control (as already discussed in Section 2.3).

We then discovered that the MOD1 code always uses a film boiling correlation in the wall-to-(single phase)vapor heat transfer regime, which uses the saturation temperature as the vapor fluid temperature in calculating the heat transfer rate. This can lead to significant overprediction of the heat transfer rate as the primary-secondary ΔT becomes small relative to the degree of steam superheat. We modified the code to call the DITTUS subroutine, which calculates the heat transfer coefficient from the Dittus-Boelter correlation and uses the actual fluid temperature in calculating the heat transfer rate, whenever the quality is greater than 0.9999. This change resulted in quite good agreement with the steady state primary and secondary temperature data throughout the steam generator. We did not use these modifications in other analyses, but did report the results to the code developers.

While studying the B&W OTSG analysis results, we also discovered another code "bug" which could result in large errors in the calculated heat transfer coefficient under some circumstances. In the POOLNB subroutine, which calculates the boiling heat transfer coefficient for low flow conditions, a simple approximation to the Chen suppression factor is calculated to force the use of the Chen convective boiling correlation at larger flows. The problem we found is that, for large hydraulic diameters, the approximation overestimates the suppression factor and forces the use of an incorrectly high heat transfer coefficient, higher by 50-100% than would be calculated using the actual suppression factor; we therefore changed the POOLNB routine to calculate the actual suppression factor with subroutine SUPFAC rather than use the approximation.

AI.2 Test Documentation

Accurate code assessment depends not only on the code documentation available, but also, and sometimes much more strongly, on the test documentation. If the facility geometry must be guessed at, if the boundary conditions are ill-defined, or if the instrumentation is inadequate, then the assumptions made in the input can dominate the results obtained. The code should not be used as a tool to back out missing experimental information by seeing how results using different assumptions match with data, and then assessed against this same (or closely related) data, like the worm Ouroboros biting its own tail.

AI.2.1 Facility Description

The vast majority of the information needed to model the experimental test facilities was taken from readily available published sources, data such as one might expect to have available for plant analyses. In the cases of LOFT and Semiscale Mod-3, the primary sources of information on the facility geometries were the system descriptions and the presentations and associated handouts at the LOFT/Semiscale modelling workshop. Although the LOFT documentation was reasonably complete, the more sketchy Semiscale Mod-3 system description and handouts had to be supplemented by numerous blueprints (obtained earlier during a project requiring a TRAC Semiscale nodalization). For PKL and LOBI, both foreign facilities, we received copies of all available reports on both system geometries and test results from people modelling these experiments with the TRAC program at Los Alamos, thus saving us much time and effort. The documentation on Semiscale Mod-2A in any given configuration has proved almost nonexistent, and we had to rely almost solely on the INEL Semiscale Mod-2A RELAP5 input model writeup.

In every case, we found it necessary to use engineering judgement about some system details in the nodalizations since all required information was not available. While the basic primary geometries are usually well-documented, descriptions of pump curves, valve sizes, set points and characteristics, steam generator secondary sides and ECC trains are often incomplete or totally lacking. We also found that many facility description documents are inaccurate due to equipment changes over the life of the facility or inadequate due to shifts in experimental emphasis. Thus, relief valves and secondary sides might be negligible in large break LOCAs but can dominate small break accident scenarios.

The integral test facility descriptions were often incomplete and inadequate as a source of primary information for nodalization development; the separate effects test facilities are usually relatively simple in the important geometry, and the documentation is more adequate. We cannot in this report itemize all the individual problems encountered (because of the sheer bulk of such detailed difficulties); we will simply present some generic, and a few specific, comments on the uncertainties introduced in code assessment through inadequate and incomplete knowledge of a given experimental test facility.

In general, the two European integral facilities modelled (PKL and LOBI) seem better documented than the two US integral facilities (LOFT and Semiscale). The facility descriptions for PKL and LOBI are more complete because the test results are routinely used by analysts throughout the European community, who must rely on formal documentation (rather than on conversations in hallways and drawings on blackboards); these foreign facility descriptions probably also appear better documented because of the simpler nature of the tests we analyzed (large break transients and steady state natural circulation tests), which do not demand detailed knowledge of valve controllers, for example.

Of the two US integral test facilities modelled for assessment calculations, the LOFT facility is better documented than Semiscale, mainly (in our opinion) because it is a (sealed) nuclear facility preventing numerous trivial piping modifications from being made in between tests (as is apparently the custom in Semiscale). The constant facility modifications in Semiscale (both major ones, such as the differences between Mod-3 and Mod-2A, and minor ones, such as the substitution of a venturi nozzle for an orifice plate in the broken loop pump discharge after the pump had been partially characterized) are very poorly documented, especially the less recent changes, and it is usually impossible to determine the exact facility configuration for a given test.

Besides the more simple piping changes made between tests in Semiscale (e.g., replacing 3" spool pieces by 2-1/2" spool pieces in the intact loop), new features are sometimes added for particular tests or test series but not formally documented. As examples, the EOS for the S-UT test series does not contain any drawing or detailed formal description of the required upper head accumulator and its surge line piping; the EOS for the S-NC test series does not contain a drawing or description of the intact loop pump replacement spool piece and orifice plate, or a detailed write-up of the upper plenum/upper head modifications in the various tests. (The missing information is also not given in the Quick-Look or Experimental Data Reports for these tests.) Without this information, adequate model development is impossible.

The test facility descriptions have a number of generic problems in common, besides the more test-specific items just discussed. Most if not all of the facility write-ups were done before TMI, so that they are slanted toward large break LOCAs. Thus the primary side geometry is often well documented, but the secondary side (not important in large break scenarios but quite important for small breaks and operational transients) is not. Besides detailed geometric description of the secondary side, more information is needed on the valve responses (e.g., how long it takes a valve to respond to a trip signal and how long it takes the valve to open or close once it starts moving). Sometimes there is not enough information to allow modelling all structural material (an important heat source/sink in long transients).

Ideally, one would like a complete set of facility drawings (i.e., blueprints) when developing a new nodalization, and such information should be available to the analyst if requested. However, the LOFT, PKL and LOBI facility descriptions (particularly the appendices in the LOFT write-up) are detailed enough (for the primary side piping, at least) to allow modelling without the actual drawings. Similar information should be available for the secondary side geometry; also, valves and pumps should be characterized by clearly defining valve behavior and pump homologous curves. The facility should then be left alone. ("If it ain't broke, don't fix it.") If this is not possible, documentation upgrades should be made readily available as soon as necessary equipment upgrades are made.

AI.2.2 Operational Procedures

Just as there can be a number of problems in identifying the experimental facility configuration for a given test, the analyst will probably run into difficulty attempting to determine the

exact way in which the given test was actually conducted. It is a general truism that experiments are rarely conducted as specified in the EOS, rendering pretest or blind calculations particularly difficult and often worthless. However, posttest documentation such as Quick-Look or Experimental Data Reports generally do not provide enough detail on test conduct either. The documentation on operator actions, interventions or overrides during any particular test is particularly bad.

Our first assessment calculation was to be a "blind" analysis of the LOFT L6-7/L9-2 test, followed up by a normal posttest analysis with all experimental data available for initialization and comparison. We soon found that the EOS did not give the secondary side steam flow rate to be used as an experimental boundary condition during L6-7 (since the test was to be a scaled counterpart to an ANO-2 plant turbine trip), and, after taking a steam flow rate table from an INEL RELAP5 deck, we found that attempting to match the operator-controlled specified secondary side cooldown rate during L9-2 caused the secondary pressure to drop below the (constant) condenser pressure.

The secondary side steam outflow during L6-7 was plotted in some subsequent data reports but the data was never provided in a user-oriented form; these data reports also revealed (in data plots, not in any written documentation) that during L9-2 the operators did not achieve anything like the cooldown rate specified, and that they adjusted the condenser conditions at late times to maintain pressures lower than the secondary pressure throughout the test.

Another example of inadequate or incorrect test procedure documentation (mentioned above briefly in Sections 3.3.2 and 3.3.3) is auxiliary feedwater injection during the Semiscale Mod-3 S-SB-P tests. Auxiliary feedwater was supposed to occur in all four of the tests analyzed; however, examination of the experimental data indicates that there was no aux feed to the broken loop steam generator in two of the tests (S-SB-P1 and S-SB-P3) and no aux feed injection to either the intact or broken loop steam generator in a third test (S-SB-P7). This was not clearly defined in the posttest documentation, but was implied by differential pressure measurements; that data also seemed to indicate that the magnitude and timing of the aux feed injection, if present, was often not what was specified.

Just as more valve data is needed as part of better facility documentation (as discussed in the previous section), more valve data is needed as part of better test operation documentation, also. This is especially important in calculating steam generator secondary side isolation; small delays in valve signals or actions can have an enormous effect on secondary response, such

as early-time pressurization and whether or not relief valve pressure setpoints are reached (as we saw in our LOFT L3-6 small break analyses, where a 2-second delay in valve motion changed the qualitative and quantitative secondary side behavior for the first ~100 seconds of transient). Automatic valve delays should be given as part of the required facility description and any deviations or manual operator actions should be given as part of the test operation description.

The Semiscale Mod-3 and Mod-2A tests analyzed tended to have the most uncertain test operation, because valve and pump operation, operator actions, etc., are particularly important in small breaks. However, such uncertainties can be found in any test. The documentation for the PKL ID1 natural circulation test series (part of which was in German) did not make clear whether the pump resistance orifice was installed in all three loops or only in the "single broken" loop, and did not explain the operation of the secondary side during these tests in any detail. The report containing the BCL 2/15-scale ECC bypass/delivery test data contained very little information on how the tests were performed.

AI.2.3 Experimental Results

Many analyses were hampered by odd gaps in the experimental test description and data provided. The primary mass inventory, a key parameter in small break transients, was shown in Quick-Look Reports but not mentioned in Experimental Data Reports and not given on the data tapes; the decay heat for LOFT was shown in Experimental Data Reports but was not available on the data tape. Both these variables were used by INEL in comparison plots, but in order to produce similar plots we had to digitize the experimental data from small published plots, with some loss of accuracy and substantial extra effort. The primary mass inventory was often described as being obtained "from differential pressure measurements" (most or all of which are available on the data tapes), but the algorithm used to convert the data to mass inventory is not given; if we derived our own algorithm, there is no guarantee that the same results would be obtained.

In the PKL natural circulation tests analyzed, the experimental reports never defined what value for 100% mass was used to normalize their reported primary system inventory fractions, resulting in large quantitative uncertainties in attempting to evaluate the RELAP5 results. Further, there are two sets of published flow-vs-inventory data for these PKL tests; the different mass flow numbers are currently explained by instrument recalibration, but the reason for the different inventory numbers is still not clear.

The accumulator injection rate, an important boundary condition for L8-1, L5-1 and L2-5, was not given anywhere (although the appropriate instrumentation is listed as available), and the lack of any documentation on downcomer ECC injection piping geometry (used in L8-1) precluded any attempt to calculate the accumulator injection rate based on the RELAP5 accumulator model. (The use of "unscaled" ECCS flow in L8-1 further complicated the issue.) We estimated the required accumulator flow rate data by differentiating the accumulator liquid level data which was given, multiplying by an area estimated from the volume vs level plots given in the facility description, and then multiplying by the appropriate subcooled water density. This injection flow rate was applied to the accumulator injection line as a user-specified boundary condition; the injection was begun at the time at which the calculation predicted the accumulator setpoint pressure had been reached.

One major variable for L3-6/L8-1 that could not be located in any of the experimental reports or on the data tape was the intact loop mass flow, although the required instrumentation certainly exists. In the Experimental Data Report, the three intact loop flow rate instrumentation are listed as "qualified, initial conditions only". The mass flow at the break for L3-6 is not given during the first ~50 seconds, the entire period of subcooled break flow.

The steam generator response could be better analyzed if more instrumentation were available on the secondary side, particularly more thermocouples in more locations and some method of determining flow rates through the downcomer and boiler regions. A data measurement of steady state secondary side recirculation ratio is particularly needed, to provide a convenient way of verifying and/or adjusting input models before transient calculations, especially in small break analyses where the secondary side response can be very important.

AI.3 Analysis Documentation

One of the more interesting and enlightening code assessment activities (theoretically) is comparing results of analyses done by different users with different nodalizations, assumptions and (perhaps) different codes. This was, in fact, included in our original program brief for this assessment project. For such comparisons to be meaningful, however, the calculations must be carefully documented in order to prevent unknown differences from prejudicing the conclusions drawn; this has generally not been the case. Many calculations have probably never been documented at all, and thus cannot even enter into consideration (mostly because we may be unaware of their existence). Others may have

been done so long ago, or be so inadequately documented, that they are almost immediately eliminated. A number of calculations, however, fall into a third class, in which the results at first indicate that valuable comparisons can be made; but closer examination reveals a number of unanswered (and usually unanswerable) questions about the details of the analysis, which preclude firm conclusions being drawn, although permitting interesting suggestions. (There should be a fourth class, that of fully and correctly documented calculations, but we have not encountered a single specimen to date, probably including our own.)

At the risk of being nasty, we would like to take this opportunity to formally point out that documented calculations which are either in informal reports with no outside distribution or are in draft form with indefinitely delayed publication and distribution are of no benefit to anyone but the "insiders". A number of potentially interesting and useful analyses, including both some developmental and independent assessment ones and some applications calculations, unfortunately seem to belong to these two categories. Results are presented at various meetings, but no subsequent formal detailed documentation is available.

AI.3.1 Input Model

Any report on a code calculation should, without question or argument, contain an input listing; the input listing should correspond exactly to the calculation whose results are being reported, and any modifications made during restarts should be included as a formal part of the input listing given. (It is not particularly useful or sufficient to be told in a footnote that "the standard LOFT input model Version 117 was used as the basis for the Experiment L2-5 input deck" without an accompanying listing.)

With the recent capability of including microfiche in reports, this does not require much additional room, although care must be taken, when formally or informally copying the report, to provide copies of any attached microfiche. We know of least one case where a published Experimental Data Report was put on microfiche by DOE and distributed to libraries with no copy made of the microfiche in the back cover of the printed report; that microfiche just happened to contain all the data plots. Also, in the example given in the previous paragraph, we were sent a Xerox copy of the report without copies of the microfiche attached, which fiche consisted of a number of appendices giving input listings and plotted results for this L2-5 calculation.

Besides a listing of the input used, reports should normally explain where any unobvious input numbers came from (i.e., what

assumptions were made, what informal unpublished information was used, etc.); for example, it is often difficult for the outside observer to determine why a particular junction loss coefficient was chosen. Also, some geometric input in published reports is in disagreement with published facility descriptions, but usually no explanation of the discrepancies is given. While one tends to assume that the input decks then represent either more accurate or more current facility information, they may simply be wrong.

Although input decks should always be provided to facilitate comparisons between different calculations, in no sense should they be used as substitutes for accurate and current facility descriptions and/or experimental operating specifications, although this is often done. The difficulty is that at least one analyst has already edited and simplified the actual physical data (if any), making assumptions with which another analyst may not agree, and that models and assumptions appropriate for one code or code version may not be valid for another. (A good example is attempting to develop a 3-D TRAC vessel nodalization from a 1-D RELAP4 or RELAP5 input deck.) If the data being taken from another input deck is based on some real information, that original information should be available to all analysts; if the required number was simply made up in the earlier deck or arrived at through tuning of that deck and code, it should not be used.

AI.3.2 Code Updates

In order to understand someone else's analysis results and compare them to one's own results, differences in code versions must be as well known as differences in input models. Although most reports now identify what particular cycle was used to generate a reported calculation, occasionally nonstandard code updates are tried in an attempt to improve calculated behavior and agreement with data. Such code updates should also be given as part of the report documentation, together with the background basis for the update and results showing the effect of the update. It would also help the reader to know whether such a nonstandard update has been used for several previous or other calculations (and with what results), or only for the calculation in question, and whether it is expected to be useful (or even applicable) to other and future analyses.

The major difficulty in determining exact code configuration for any given calculation lies with those analysts running on computers at laboratories such as Los Alamos or INEL, where ongoing code (TRAC and RELAP, respectively) development efforts create rapid turnaround of code versions available for execution. On the other hand, getting up-to-date code mods and bringing up each cycle on outside computers can be a substantial task, and analyses then tend to be run with a few standardized release versions (as we have done in this assessment program).

Another problem with nonstandard code versions is commonly found when attempting to interpret LOFT and/or Semiscale analyses from INEL. Both these experimental programs maintain large analysis efforts and often make their own code modifications, independent of the code development group. These updates are often used for only one or a few analyses and never become part of the formal code. An example here is the code updates (such as an extended interphase mass transfer model) listed in the post-test analysis report for LOFT test L9-1; it is not clear if these updates were used in future analyses or adopted by the code developers, or abandoned after this one calculation, but it is clear that we are not running the same code and should not expect the same results. If the INEL report had given the results with and without the code updates, we would have been able to make a better judgement on their possible effect.

The above discussion presupposes that the code developers are providing a clear description of each particular code cycle as it is formalized, whether that cycle is formally released or not. While listings of updates in any particular cycle are usually available, the reasons for the updates and their observed effects on calculated results are seldom documented in any detail.

AI.3.3 Calculational Results

One of the potentially most useful portion of analyses performed is seldom or never documented; this is the preliminary analyses, which may or may not have given reasonable results, and which may have led to the final choice of various parameters in the input model used for the final reported calculation. In many cases, these "failed" calculations will contain as much or more information as the "official" analysis. We have tried to present some documentation on our preliminary analyses in our topical reports, and would like to see more of this in all future reports.

One example already mentioned above is the desirability of presenting code results both before and after nonstandard code updates, such as the extended interfacial mass transfer model mentioned in the LOFT L9-1/L3-3 posttest analysis report [36] (apparently used only for the L9-1 portion of the analyses). More complete documentation would allow outside readers to evaluate for themselves the relative impact and appropriateness of a given code model change.

Another area needing more documentation is the observed difference in calculated results before and after some nonstandard input model changes. The final LOFT L2-5 pretest analysis report [33] gave the vessel downcomer crossflow junction loss coefficients as K ~100 in the forward direction and K ~20 in the reverse direction with no discussion or justification; conversations with one of the authors revealed that the

forward K was chosen from (unreported) sensitivity studies as giving better agreement with expected results, while the reverse K was simply the K-value of the previous sensitivity study, which had not been properly updated for the next run. Meanwhile, the reader is left wondering if some subtle point is being missed.

APPENDIX II CODE PORTABILITY

RELAP5/MOD1 is a very computer-dependent code. It was written to take advantage of the hardware architecture of the CDC CYBER-176 and the NOS-BE operating system. Thus, the code requires extensive changes to run on any other computer, even the CDC CYBER-76 or the CDC 7600. Although the software of both of those computers is very similar to that of the CYBER-176, the CYBER-176 has about two times as much small core memory (SCM) as the CYBER-76 or 7600. Because RELAP5 needs this additional memory in order to run large problems on the CYBER-176, reasonably sized problems cannot be run on either the CYBER-76 or 7600 without major rework of the code storage algorithms. Based on our experience, we have estimated that approximately two or three man months of an experienced programmer's time is required to convert and check out the code on a different CDC computer.

The conversion of RELAP5 to run on non-CDC computers is even more difficult because of the use of many non-standard programming techniques. Conversion to more modern hardware, such as a CRAY-1 or CDC CYBER-205, is estimated to take about six man months and each new set of updates to the code would require additional time for conversion. This fact is of some importance to the NRC since no group which does NRC calculations has a CYBER-176 except INEL. The other laboratories have 7600s, CYBER-76s, and CRAY-1s. In a few years, as obsolete hardware is phased out, only more modern systems such as the CRAY-1 and CYBER-205 will be available.

AII.1 CYBER 76 Conversion

Although the compilation sequence for RELAP5/MOD1 allows the user to choose options which attempt to select certain FORTRAN statements needed for the CYBER-76 (or the older 7600), not all system-dependent code is changed correctly. This is partly due to the fact that INEL does not have ready access to a CDC 7600 or CYBER-76 with which to check out those options. In particular, one of the memory management routines, written in assembly language, did not work under the SCOPE 2 operating system we use on our CYBER-76, and that routine had to be modified. The DISSPLA plot package which RELAP5 uses for in-line plotting also needed different initialization calls on our system.

A major part of the conversion effort to the CYBER-76 at Sandia involved the segmentation directives, which determine how the code is loaded into memory. Because RELAP5 is such a large code, for the CDC machines the code must be split up so that only those parts of the compiled code that are actually

needed at any given time are resident in fast memory. The segmentation directives needed for the CYBER-176 using the NOS-BE operating system are significantly different from those for the CYBER-76 using the SCOPE2 operating system because of the much larger fast memory or SCM available on the CYBER-176.

The segmentation process used with RELAP5/MOD1 requires common blocks used as pointers to be loaded at the end of the various segments so that the end of the segments can be located. This allows RELAP5 to know where its code ends and where it can find work space. Under NOS-BE, a dummy segment must be declared for each of those common blocks, and then the common block must be assigned to that segment. For SCOPE 2, all of those special declarations must be taken out, and each pointer block must be assigned to the segment whose end it is marking. Also, under NOS-BE, if a common block occurs in several different code segments and no segmentation directive is given for that block, it will only be loaded at one memory address. However, under SCOPE 2, copies of it will be loaded at different addresses in each segment. Therefore, during the conversion process, these duplicate common blocks must be identified and a segmentation directive generated to force that block to load at a point in memory where it is accessible to all the segments which need it.

NOS-BE also allows a variable in a common block to be defined by a data statement in a segment other than the segment to which the common block is assigned. Since SCOPE 2 does not allow this, several data statements had to be moved to different segments.

The most serious difficulty we had with putting RELAP5/MOD1 on our CYBER-76 and 7600 machines was the severe limitation on the size of SCM. No problems of significant size could be run without a major effort to change the code so that less SCM would be needed.

Since it was found that for some large problems there was not enough SCM, even during the input phase, several changes were made to input routines. The large buffer used to write the plot headers detailing each plot variable was moved from SCM to large core memory (LCM). The segmentation directives were modified so that not all the input routines were in memory at the same time.

RELAP5 dynamically allocates a large amount of SCM for work space needed to solve the hydrodynamic equations. We moved this dynamic file from SCM to LCM, which involved changing the calls to reserve space for the file, and also changing the equivalence statements for all the variables which are stored in this file. These variables also included some reactor kinetics and

heat transfer work space variables, thus all subroutines to which these work space variables were passed as parameters had to have statements inserted which declared those passed variables to be in LCM.

Even with the above described changes, the RELAP5 code still took up far too much SCM to run large problems. Therefore, the large transient segment was further broken up into 25 independent segments which could share the same memory addresses. In order to do this, we had to decide which routines were independent of others and which routines had to go in each segment. Code was then moved around through the use of new segmentation directives so that the amount of SCM needed was minimized. The routines calling these 25 segments were put into a transient root segment.

We soon found that the use of this new transient segmentation caused a large increase in the amount of input/output (I/O) time needed for execution because each one of the new segments had to be moved from disk into SCM every time step. Therefore, instead of letting the operating system move the segments from disk to SCM, RELAP5 was modified so that the code itself moved the segments, and the swapping was done from LCM to SCM, not from disk to SCM. At the end of the input processing phase, RELAP5 uses pointer common blocks to determine the lengths of each of the 25 segments and decides whether there is enough room in a special fixed length LCM common block to hold all of the segments. If there is sufficient room, the transient commences. The calls to the 25 routines through which the segments are entered have been changed to calls to a single managing routine. On the first call to this manager for each of the 25 segments, the segment is loaded by the system and executed. Then the manager copies the segment into the LCM block. On subsequent calls, the manager moves the segment from LCM into the correct SCM addresses. By calling a dummy routine which the system "thinks" is always at that SCM address, the manager causes the system to do no loading from disk and to execute the segment which RELAP5 has loaded. With this method, the CPU time needed for problem execution increases by only about 10%. If this segmentation is used, some common blocks must be moved from the overlapped segments into the transient root segment. Also, a new common block must be created in order to pass parameters to the segments.

AII.2 CRAY-1 Conversion

We received special updates from INEL which were intended to help create a CRAY version of RELAP5 from the CDC version. Most of these preliminary updates were developed at Los Alamos National Laboratory (LANL) for use on their CRAY running under

the CTSS operating system. Since the Sandia CRAY runs under the COS operating system, many changes to the LANL updates had to be made to get our version to run. Also, LANL had apparently not completed the code changes to convert RELAP5 to the CRAY on a production basis, since some routines were not totally converted.

Since most of the complicated memory management routines and random disk I/O routines were written in CDC assembly language, substitutes for them had to be found. A considerable number of CRAY-1 memory management routines were obtained from Sandia-Livermore to do these tasks and our ability to use these FORTRAN language routines saved a great deal of time and effort on our part.

Most of the CRAY updates result from the fact that RELAP5 is highly dependent on the CDC computer word length of 60 bits while the CRAY word length is 64 bits. Several data fields are packed into one word throughout the RELAP5 code, and both putting the fields into the appropriate bits and getting the field back out of the word are dependent on the number of bits in the word. There are about 2000 lines of code in which these operations are done; each of these lines had to be changed for the program to run correctly on the CRAY. During the conversion process, we followed the LANL procedure of making each update in such a fashion as to allow the user to continue having the ability to select either the CDC or CRAY versions of the code.

Since the CRAY memory is much greater than that of the CYBER 76 or the 176, all of the RELAP5 routines may be loaded at once. However, since the RELAP5 logic uses common block addresses to find the end of the code in memory, changes to the addressing scheme had to be made. A blank common was loaded at the end of the code and addressing of the work space was done from there. Also, because the CRAY does not treat array indices the same way the CDC does, and because RELAP5 uses these indices to determine common block locations, some rearrangement of common block locations was done.

Many of the print lines in RELAP5 were 134 characters long. Since the CRAY only allows 133 characters per line, those coding lines had to be changed.

Many times in RELAP5, the high order bit in a word is set in order to set a flag, and then the flag is checked by testing for a negative integer. Since the CRAY does not consider a word with only the high order bit set to be a valid integer, the RELAP5 tests on that word do not work properly. Therefore, the places in the code where this can be a problem had to be found and changed. Also, in many places in the code, an address is stored in a word along with other data, and then the word is used as an array index, with the assumption that "hardware

masking" will allow only the address to be seen as an index and the rest of the word is disregarded; the number of bits which are hardware masked is different on the CRAY and CDC computers, so those cases had to be found and the coding changed.

Since division of one number by itself does not always give a result of exactly one, and since RELAP5 can be sensitive in certain areas as to whether a number is exactly one or not, several places in the code were changed so that the division was not done if the divisor and dividend were equal, with the result being directly set to one.

Another big source of conversion effort was due to the CRAY having only 8 characters per word, while the CDC has 10. This meant that all of the alphanumeric fields stored in data statements in the code had to be changed. Also, the input processor was changed so that it would not flag a 10 character component name as being in error. The change caused only the first eight characters to be accepted for the name. This was done so that input decks set up for the CDC would run on the CRAY.

Even though the memory on the CRAY is considerably larger than that of the CDC machines, the full memory of the CRAY cannot be utilized to run significantly larger problems than can be run on the CYBER-176 or CYBER-76. This is because RELAP5 packs certain array addresses into one computer word, as already mentioned, and the length of those addresses has been restricted to 18 bits. This restriction was not addressed in our CRAY conversion effort and would have to be fixed to allow use of all the CRAY memory for a single problem.

AII.3 Summary

We believe that RELAP5 should be converted to a hardware independent form as quickly as possible. We recognize that there was no particular need for it to be machine independent when it was primarily intended for LOFT and Semiscale experiment analyses at INEL, with only limited use by other national laboratories, but its intended role has changed considerably in the last few years. It now appears to have a wide base of users throughout the national laboratories and the general public.

ANSI-standard FORTRAN 77 is the currently accepted language for scientific programming. Using this standard language, we believe that RELAP5 can be made to run efficiently on many different computers, ranging from a VAX 11/780 to a CRAY-1. Use of FORTRAN 77 would automatically discourage, if not disallow, address packing and bit packing, such as is currently done in RELAP5, but we believe that the amount of storage saved using these programming techniques is fairly minimal and is more detrimental than helpful in the overall sense.

DISTRIBUTION:

Division of Technical Information
and Document Control
NRC Distribution Contractor
U. S. Nuclear Regulatory Commission
15700 Crabbs Branch Way
Rockville, MD 20850
300 copies for R4

U. S. Nuclear Regulatory Commission (4)
Reactor Systems Research Branch
Division of Accident Evaluation
Office of Nuclear Regulatory Research
7915 Eastern Avenue
Silver Spring, MD 20910
Attn: Louis M. Shotkin
Fuat Odar
Richard Lee
H. S. Tovmassian

U. S. Nuclear Regulatory Commission (3)
Reactor Systems Branch
Division of Systems Integration
Office of Nuclear Reactor Regulation
Washington, DC 20555
Attn: Brian Sheron
G. Norman Lauben
Ledyard Marsh

Ruby Cochrell, 6400 (15)
Sandia National Laboratories
P. O. Box 5800
Albuquerque, NM 87185

EG&G Idaho (6)
Idaho National Engineering Laboratory
P. O. Box 1625
Idaho Falls, ID 83415
Attn: T. R. Charlton
G. W. Johnsen
Edna Johnson
L. Feinauer
V. H. Ransom
R. J. Wagner

Thad D. Knight
Dennis R. Liles
Los Alamos National Laboratory (2)
K553 Q-9
Los Alamos, NM 87545

Argonne National Laboratory (2)
Reactor Analysis and Safety Division
9700 South Cass Avenue
Argonne, IL 60439
Attn: Tom A. McDonald
Heide Komoriya

P. Saha, 130
Department of Nuclear Energy
Brookhaven National Laboratory
Associated Universities, Inc.
Upton, New York 11973

Babcock & Wilcox Co. (NPGD) (2)
P. O. Box 1260
Lynchburg, VA 24505
Attn: N. H. Shah
R. A. Turner

Jesse Fell (5)
Deputy Director, Water Reactor Programs
Atomic Energy Establishment
Winfrith
Dorchester, Dorset DT28DH
ENGLAND

Dr. K. H. Krewer, Head
Nuclear Safety Research Section
Der Bundesminister Fuer Forschung
und Technologie
Postfach 20 07 06
5300 Bonn 2
FEDERAL REPUBLIC OF GERMANY

Dr. M. Banaschik
Nuclear Safety Research Section
Der Bundesminister Fuer Forschung
und Technologie
Postfach 20 07 06
5300 Bonn 2
FEDERAL REPUBLIC OF GERMANY

Dr. Helmut Schnurer, Dipl.-Ing.
Regulation and Licensing of Nuclear Reactors
Der Bundesminister des Innern
Referat RS I 2
Postfach 170 290
5300 Bonn 1
FEDERAL REPUBLIC OF GERMANY

Prof. Dr.-Ing. Habil. E. F. Hicken
Gesellschaft fur Reaktorsicherheit (GRS) mbH
Forschungsgeland
8046 Garching
FEDERAL REPUBLIC OF GERMANY

R. G. Mas
Commission of European Communities
Joint Research Center
21020 Ispra (Varese)
ITALY

Dr. Helmut Holtbecker
Commission of European Communities
Joint Research Center
21020 Ispra (Varese)
ITALY

Dr. E. Burck
Reactor Safety Programme
Ispra Establishment
Joint Research Center
21020 Ispra (Varese)
ITALY

Dr. Raymond Klersy
Reactor Safety Programme
Ispra Establishment
Joint Research Center
Commission of the European Communities
21020 Ispra (Varese)
ITALY

Mr. Tom Doyle
Reactor Safety Programme
Ispra Establishment
Joint Research Center
Commission of the European Communities
21020 Ispra (Varese)
ITALY

Dr. Sergio Finzi
Commission of the European Communities
Directorate General XII-J[illegible]
Directorate Nuclear Research and
Development
Square de Meeus, n° 8
Brussels
BELGIUM

Mr. Jean-Pierre Contzen
Director of Programmes
of the Joint Research Centre
Commission of European Communities
Rue De La L 01 200
B 1040 Brussels
BELGIUM

Mr. Mitsugu Ishizuka, Director
Reactor Regulation Division
Nuclear Safety Bureau
Science and Technology Agency
2-1, Kasumigaseki 2-chome
Chiyoda-ku, Tokyo
JAPAN 100

Dr. Satoru Iijima, Secretary General
Nuclear Safety Research Association
2-2, 1-chome, Uchisaiwai-cho
Chiyoda-ku, Tokyo
JAPAN

Dr. Hiroei Nakamura, Head
Division of Power Reactor Projects
Japan Atomic Energy Research Institute
Tokai Research Establishment
Tokai-mura, Naka-gun
Ibaraki-ken, JAPAN

Dr. Franz Winkler
Kraftwerk Union Aktiengesellschaft
Reaktortechnik
Hammerbacherstrasse 12 u. 14
Postfach 3220
D-8520 Erlangen
FEDERAL REPUBLIC OF GERMANY

Prof. Dr. H. Karwat
Technische Universitat Munchen
c/o Gesellschaft fur Reaktorsicherheit mbH
Forschungsgelande
D-8046 Garching
FEDERAL REPUBLIC OF GERMANY

Professor F. Mayinger
Lehrstuhl und Institut fur Verfahrenstechnik
der Technischen
Universitat Hannover
3 Hannover
FEDERAL REPUBLIC OF GERMANY

Dr. D. Lummerzheim
Gesellschaft fur Reaktorsicherheit
(GRS) mbh
Postfach 101650
6000 Koeln 1
FEDERAL REPUBLIC OF GERMANY

Kerforschungzentrum Karlsruhe
Weuerstrasse 5
75 Karlsruhe 1
FEDERAL REPUBLIC OF GERMANY

1531 S. L. Thompson
6400 A. W. Snyder
6410 J. W. Hickman
6411 A. C. Peterson
6417 D. C. Carlson
6420 J. V. Walker
6421 T. R. Schmidt
6422 D. A. Powers
6423 P. S. Pickard
6425 W. J. Camp
6427 M. Berman
6427 C. C. Wong
6440 D. A. Dahlgren
6442 W. A. von Riesemann
6444 D. A. Dahlgren, Actg (15)
6444 L. D. Buxton
6444 R. K. Byers
6444 R. K. Cole, Jr.
6444 P. N. Demmie
6444 D. Dobranich
6444 M. G. Elrick
6444 L. N. Kmetyk
6444 R. Knight
6444 J. M. McGlaun
6444 J. Orman
6444 W. H. Schmidt
6444 R. M. Summers
6444 S. W. Webb
6449 K. D. Bergeron
3141 C. M. Ostrander (5)
3151 W. L. Garner
8024 M. A. Pound

NRC FORM 335 (2.84) NRCM 1102, 3201, 3202

U.S. NUCLEAR REGULATORY COMMISSION

BIBLIOGRAPHIC DATA SHEET

SEE INSTRUCTIONS ON THE REVERSE

1. REPORT NUMBER (Assigned by TIDC, add Vol. No., if any)
NUREG/CR-3936
SAND84-1122

2. TITLE AND SUBTITLE
RELAP5 Assessment: Conclusions and User Guidelines

3. LEAVE BLANK

4. DATE REPORT COMPLETED
MONTH: October | YEAR: 1984

5. AUTHOR(S)
L. N. Kmetyk

6. DATE REPORT ISSUED
MONTH: October | YEAR: 1984

7. PERFORMING ORGANIZATION NAME AND MAILING ADDRESS (Include Zip Code)
Division 6444
Sandia National Laboratories
P. O. Box 5800
Albuquerque, NM 87185

8. PROJECT/TASK/WORK UNIT NUMBER

9. FIN OR GRANT NUMBER
A-1205

10. SPONSORING ORGANIZATION NAME AND MAILING ADDRESS (Include Zip Code)
Reactor Systems Research Branch
Division of Accident Evaluation
Office of Nuclear Regulatory Research
U. S. Nuclear Regulatory Commission
Washington, DC 20555

11a. TYPE OF REPORT
Technical

b. PERIOD COVERED (Inclusive dates)
--

12. SUPPLEMENTARY NOTES

13. ABSTRACT

The RELAP5 independent assessment project at Sandia National Laboratories is part of an overall effort funded by the NRC to determine the ability of various systems codes to predict the detailed thermal/hydraulic response of LWRs during accident and off-normal conditions. The RELAP5/MOD1 code has been assessed at Sandia against a variety of test data from both integral and separate effects test facilities. All these analyses have been documented in detail in individual topical reports; in this paper we attempt to evaluate the overall code performance by comparing results from many different calculations, and to offer other users some guidelines based on our experience to date.

All results show that good primary side steady state initial and/or operating conditions are readily obtained, given adequate facility descriptions and some user experience or guidelines, although problems are usually encountered in the steam generator secondary sides.

Results from a large number of integral test analyses show that the primary system response (e.g., pressure and break flow) is well-predicted in a wide variety of transients; most observed discrepancies can be attributed to known problems already being addressed by the code developers. Core heatup response (e.g., dryout and PCT) is generally also well-predicted, particularly during the blowdown phase of large break LOCAs. Given the lack of specific reflood algorithms in MOD1, it is not surprising that core quench is sometimes not calculated accurately; we have, however, seen a number of problems with the accumulator injection which would preclude calculating reflood correctly even when such a reflood package is implemented in later versions of RELAP5. The secondary system response (e.g., steam generator pressure and temperatures) is usually not correctly calculated in either integral or separate effects test analyses.

14. DOCUMENT ANALYSIS - a. KEYWORDS/DESCRIPTORS

15. AVAILABILITY STATEMENT

16. SECURITY CLASSIFICATION
(This page) Uncl
(This report) Uncl

17. NUMBER OF PAGES
177

18. PRICE

b. IDENTIFIERS/OPEN-ENDED TERMS